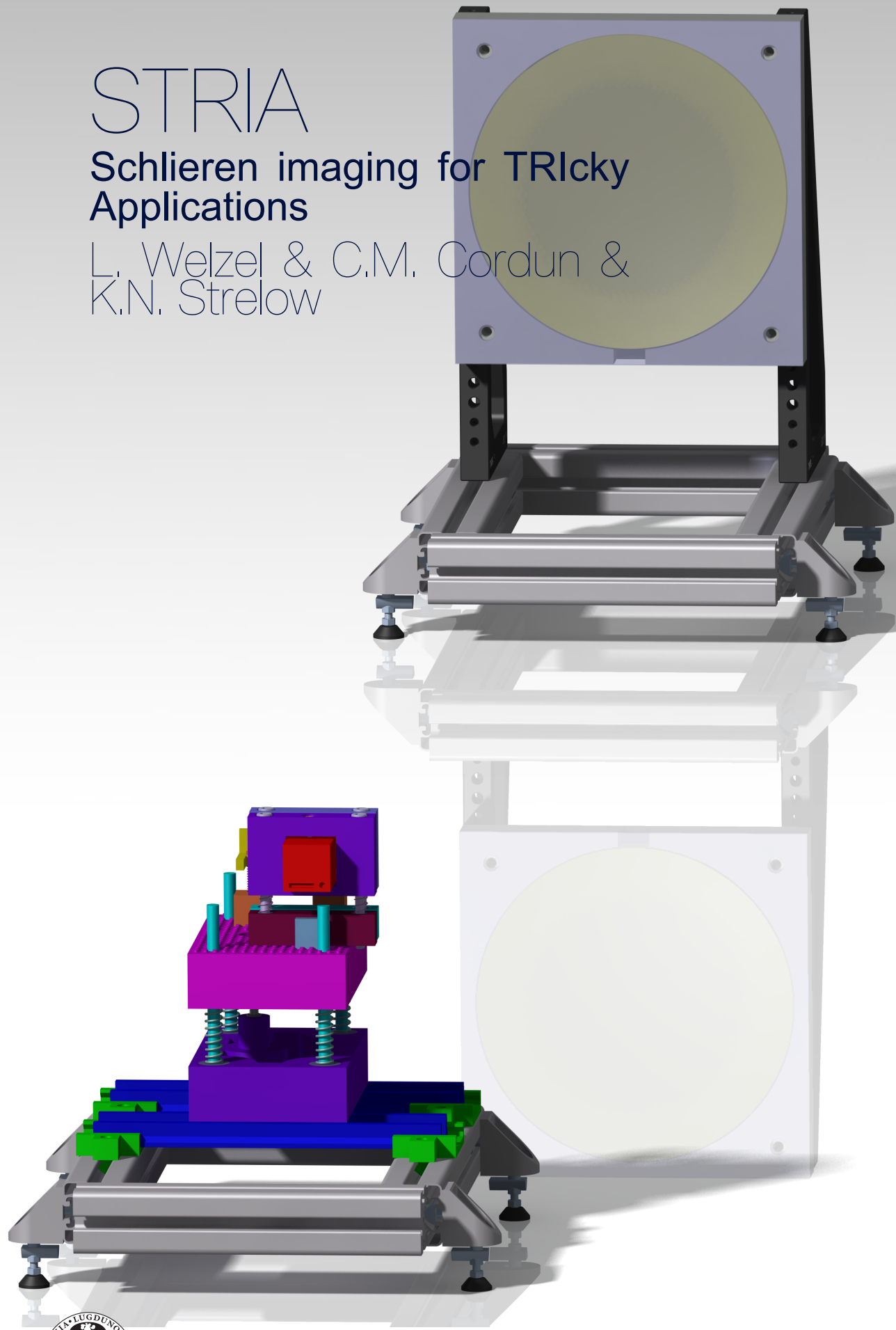


STRIA

Schlieren imaging for TRicky Applications

L. Welzel & C.M. Cordin &
K.N. Strelow



Universiteit
Leiden
Observatory

This page left intentionally blank.

STRIA

Schlieren imaging for TRicky Applications

by

L. Welzel & C.M. Cordun & K.N. Strelow

Design of Optical Systems

Leiden, The Netherlands, May 30, 2022



Universiteit
Leiden
Observatory

Contents

1	Introduction	2
2	Mission Analysis	5
2.0.1	Schlieren for Propellant Ignition	5
2.0.2	Solid Rocket Motor (SRM) Grains	5
2.1	Project Definition	8
2.1.1	Stakeholders	8
2.1.2	Problem statement and NGOs	9
2.2	Requirements	10
2.2.1	Traceability matrix	10
3	Design space	14
3.1	Design space	14
3.1.1	List of possible components and their properties	14
3.1.2	Trade-off	21
4	Detailed design	27
4.1	Product breakdown structure	27
4.2	Optical design	33
4.3	Mechanical design	38
4.3.1	Optics Assembly	45
4.3.2	Mirror Assembly	52
4.4	Electrical design	53
4.5	Software design	53
5	MAIT	54
5.1	Manufacturing/Implementation plan	54
5.2	Assembly	54
5.2.1	Ordering parts	55
5.2.2	Preparations	55
5.2.3	Putting components together	56
5.3	Integration	56
5.3.1	Alignment of the optical system	56
5.3.2	Integration of electronics and software	57
5.3.3	Safety	57
5.3.4	Facilities and support equipment	58
5.4	Test plan	59
5.4.1	For every component:	59
5.4.2	Platform	59
5.4.3	LEGO component mount	59
5.4.4	Light Source	59
5.4.5	Sample System	59
5.4.6	Parabolic Mirror Assembly	59
5.4.7	Beam Cutter System	60
5.4.8	Collimating System	60
5.4.9	Detecting System	60
5.4.10	Electronics	60
5.4.11	Software/Computer	60
5.4.12	System tests	60
5.5	Reusability	61
6	Building	62
7	Calibration	63
7.1	System calibration	63
7.2	Extra step for better imaging	64

8 Test Plan	65
8.1 For every component:	65
8.2 Platform	65
8.3 LEGO component mount	65
8.4 Light Source	66
8.5 Sample System	66
8.6 Parabolic Mirror Assembly	66
8.7 Beam Cutter System	66
8.8 Collimating System	66
8.9 Detecting System	66
8.10 Electronics	67
8.11 Software/Computer	67
8.12 System tests	67
9 Results	68
9.1 Image Analysis	68
9.2 Cover vs. no cover for the primary mirror	68
9.3 Spray Up	68
9.4 Spray Down	76
9.5 Candles	77
9.5.1 Standard white candle	77
9.5.2 Scented candle	77
9.5.3 Comparison between candles	81
9.6 Results Summary	81
10 Future work	82
A Appendix	84
A.1 Photon budget calculations	84
A.2 Wave front error (WFE)	85
A.3 BOM	86
A.4 BOM	87
A.5 BOM	88
A.6 BOM	89
A.7 BOM	90
A.8 BOM	91
B Design Changes & Iterations	91
B.1 Platform dimensions	92

0 Abstract

Schlieren imaging for TRicky Applications is a low-cost, easy-to use solution for the purpose of doing on site imaging of ignition tests of slow-burning propellant test grains for TU Delft students. Outside day-time conditions as well as portability are properties that makes this a particularly tricky application for Schlieren imaging. With this Schlieren imager, students will potentially have a new tool to analyze spatial and temporal features of grain ignition, like presence of turbulent flow and heat transfer, boosting both science and safety in the workspace. We designed the system according to our requirements, which were met to our satisfaction. The system is compact, easy to set up and to calibrate (<30mins), and produces high framerate, high resolution images. Due to a shortage of time, however, we were not able to test the system in the field, but only confirm requirements in the lab by testing heat flow from candles, and gas flow and droplet formation from a compressed-gas dust-remover. The results are promising, and we believe that only a few alterations are needed to be able to use the system in the field.

1 Introduction

Schlieren imaging is a method to make the invisible visible: imaging gradients in refractive index of a transparent medium. Gradients in refractive index can be caused by gradients of temperature or density, or by inhomogeneous mixing of different substances. The underlying principles are very basic: light rays travel through a medium and are refracted depending on its refractive properties. This results in angular differentiation, which can be translated to differences in intensity or color, that can be observed. Naturally occurring phenomena that rely on the same physics are the fata morgana, heat haze, and mirage. Scientific descriptions of Schlieren-like methods date back to the 17th century, when Robert Hooke wrote down his observations on inhomogeneous media in *Micrographia*, (Hooke, 1665), Observation LVIII. He explained a number of phenomena like the twinkling of stars, chromatic aberration and convection in fluids, in the context of variations in density, key to this was his observation of veins in glass, or *Schlieren* in German and *striae* in Latin. He observed these density variations with a basic Schlieren setup, with a candle as a light source of which the light is refracted by the medium (e.g. the heat disturbances of the second candle in [Figure 1.1](#)),

a telescope lens and an observer. Some of the refracted light will fall outside the eye pupil (as depicted in the image), causing the observer to see a shadow in that particular part of the image. It took some time before Schlieren imaging really took off, probably because there was no immediate need for it,. Not until it became crucial for ballistics in Victorian times, and high-speed flight after World War I for example (G. Settles, 2001a). Not long after Hooke's findings, Christiaan Huygens used Schlieren-like methods for optical shop testing. Schlieren imaging how we know it now, however, stems from the 19th century, with both Leon Foucault and August Toepler contributing to the field. The former is considered the first to add an explicit cut off to the setup, the role of which used to be played by the eye pupil itself. This simple and sensitive setup allowed for many amateur telescope-builders to test their mirrors with sub-micron accuracy (see [Figure 1.2](#)). Toepler's setup included a lantern as a light source, an adjustable knife-edge and a telescope for observing (G. Settles, 2001a).

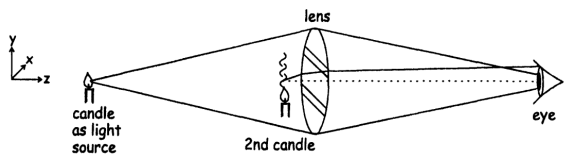


Figure 1.1: Hooke's original schlieren system, using two candles, a lens, and the human eye. Taken from Schlieren and Shadowgraph Techniques by G.S. Settles.G. Settles, 2001a

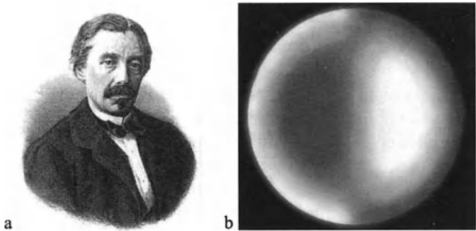


Figure 1.2: a J. B. Leon Foucault, b "shadow" pattern of a parabolic mirror observed by Foucault's knife-edge test (photo by G.S. Settles). Taken from Schlieren and Shadowgraph Techniques by G.S. Settles.G. Settles, 2001a

the medium, so that the image does not depend on where exactly between the two lenses the medium is crossed by the light beam. In the third example, a single mirror is used to reflect the light from the light source, so that it will pass twice through the medium ("test area"). In this way, the light will be twice refracted, doubling the sensitivity of the system. Many variations exist, with one or multiple lenses or mirrors, placed on- or off-axis. Furthermore, instead of a knife-edge, some other way of distinguishing between different angles may be used, like a two-colored filter. Some more advanced examples include large-field Schlieren, and Focusing Schlieren (with use of a grid, rather than one light source).

As shown in [Figure 1.3](#) Schlieren systems detect changes in the third degree gradient of the refractive index of a fluid. Hence, they allow for much more sensitive imaging than shadowgraphs.

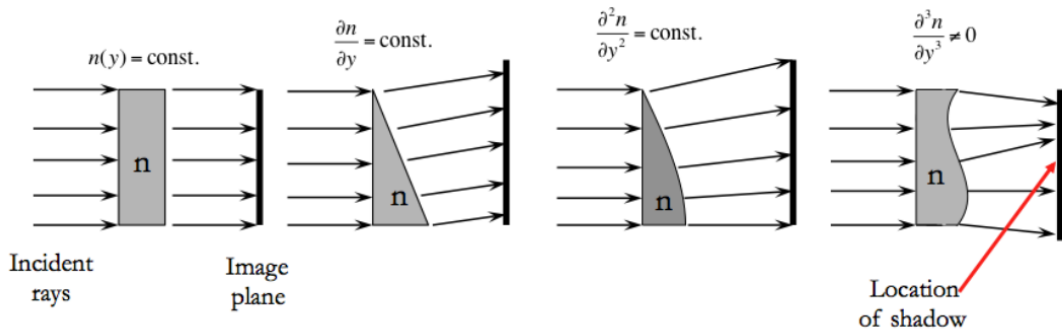


Figure 1.3: Schlieren systems image third degree gradient of the refractive index along a direction. Schmidt, 2014

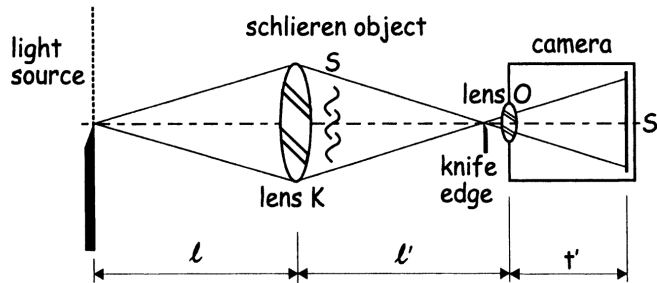


Figure 1.4: Toepler's single-field-lens schlieren arrangement. (Schlieren and Shadowgraph Techniques, G.S. G. Settles, 2001a).

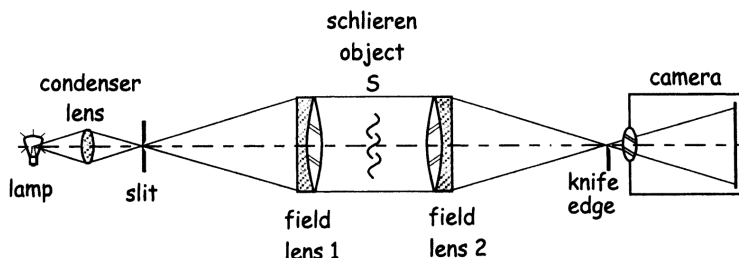


Figure 1.5: Dual-field-lens schlieren arrangement. Taken from Schlieren and Shadowgraph Techniques by G.S. G. Settles, 2001a.

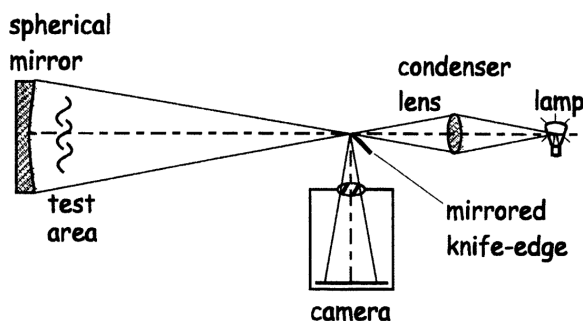


Figure 1.6: Diagram of the single-mirror coincident schlieren system. Taken from Schlieren and Shadowgraph Techniques by G.S. G. Settles, 2001a.

State of the Art: Modern developments in the ways of Schlieren imaging rely more on the developments in software than on the development of more advanced optical systems: background-oriented Schlieren (BOS) methods

are now state of the art (e.g. Raffel, 2015, Gojani, Ardian B., Kamishi, Burim, and Obayashi, Shigeru, 2013). In BOS, the light source is usually replaced by a known background pattern, which for example can be made up of a pattern with dots, stripes, or a checkerboard. Images with and without a medium in between the background and the detector are compared, and image correlation software is used to extract the information of the medium that is to be imaged. It is even possible to use a natural background for this use, as for example NASA did to image the shockwaves of one of their supersonic jets above desert ground (see Figure 1.7).

Schlieren in Astronomy: In astronomy, an important factor to take into account for Earth-based observations is the atmosphere, as turbulence and density variations will alter observational images, due to changing refractive index over time and location.

Analyzing and counteracting these effects relies in its basis on the very same principles as Schlieren imaging. Specifically Zernike wavefront sensing is in method very close to traditional Schlieren imaging, but instead of a traditional knife-edge, a phase plate is used (see G. Settles, 2001b for a general introduction of Zernike's phase contrast method and its relation to Schlieren imaging, see e.g. and Wallace et al., 2011 and Neil, Booth, and Wilson, 2000 for readings on more recent Zernike wavefront sensing methods). Another area in which Schlieren methods are used, is that of phase-apodised-pupil Lyot coronagraphs (PAP LC), where a knife-edge or multiple darkzones are used (Por, 2020). As discussed before, Schlieren methods can also be used for testing optical components for homogeneity and general shape.

Science case: A related field of study, in which Schlieren imaging is widely used, is aerospace engineering. It is the perfect method to analyse rocket exhaust plumes (e.g. Kirchheck, Saile, and Gühan, 2019, Morales, Peguero, and M. Hargather, 2017, Coulas-McKenney, Winter, and M. Hargather, 2016), shock waves in air (e.g. Kleine and Grönig, 1991, even shockwaves from trumpets: Pandya, G. S. Settles, and Miller, 2003), turbulence (e.g. TAYLOR and THOMPSON, 1969), and heat flow (e.g. Tanda, Fossa, and Misale, 2014).

For example, aerospace engineering students in Delft sometimes use Schlieren imaging to analyze the performance of a new rocket engine design. However, Schlieren imagers at the TU Delft are not readily available for use, especially not at different locations, where tests might be performed. For this reason, there might still be a lot to gain from a more simple Schlieren imager, that is easy to transport and set up at a new location. In this way, Schlieren imaging could be applied more often, adding a valuable tool to an aerospace engineer's toolbox.

Our goal is to show that Schlieren imaging of rocket propellant ignition is possible for amateur rocketry groups, that ignition and combustion relevant phenomena, specifically mixing and droplet production, ejection and/or evaporation, are clearly visible in our images. We aim to encourage amateur rocketry groups to make use of our design to improve the safety of their rocket engines and better understand the most critical stage of a rocket launch.

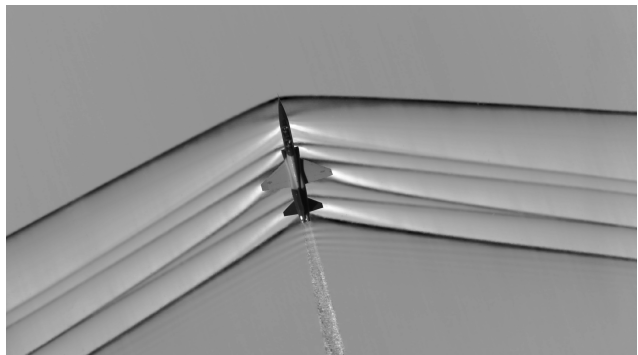


Figure 1.7: This Schlieren image dramatically displays the shock wave of a supersonic jet flying over the Mojave Desert. Researchers used NASA-developed image processing software to remove the desert background, then combined and averaged multiple frames to produce a clear picture of the shock waves. **Credits: NASA Photo.**

2 Mission Analysis

2.0.1 Schlieren for Propellant Ignition

The ignition of solid rocket motors is the most critical phase of their operations. If part of a rocket the engine is close to the launch pad and hence the severity of a critical failure is extremely high. For amateur rocketry the ignition is equally important as a large initial thrust is necessary to clear the launch site and guide with sufficient speed to be self-stabilizing. In the past the analysis of solid propellant grains has relied on numerical investigation supported by Schlieren imaging. Nevertheless, the results of these tests are rarely published since especially solid rocket motor technology is often classified. Ciucci, FOSTER, and JENKINS, 1992; Toscano et al., 2022 The systems that can be used to image the ignition of solid rocket motors are typically inaccessible and not reproducible for amateur rocketry. Still, the investigation of ignition of propellant ignition can help improve the safety of amateur rocketry.

Clearly, a low cost system is needed to image ignition that can be used by students as well as amateur rocketry societies.

2.0.2 Solid Rocket Motor (SRM) Grains

The phenomenon we specifically want to investigate is the ignition and initial burn of a solid rocket propellant (sub) grain. The Safety Board (SB) of DARE will provide the propellant. The SB will require a test plan, test procedures and a risk management strategy prior to providing the propellant grains. The propellant is wax-like mixture of Sorbitol and Potassium Nitrate (KNSB), which is a common low-powered amateur rocketry propellant. The propellant does not spontaneously ignite, is non-toxic, and is shock-resistant. The grains can be provided coated with a 4:1 mixture of nitro cellulose and black powder dissolved in acetone for accelerated ignition or provided as-is. This makes it a very safe option as a baseline test. Nevertheless, the SB has stressed that the grains are DARE-internally handled as explosives, and thus reserves the right to withdraw their approval at any point. Higher-powered solid rocket propellant grains are available, specifically APCP, if the system has been tested and the procedures have been validated. Testing these high energy composite (HEC) propellants might pose an additional challenge to the system as sputtering can occur and the propellant can be ignited spontaneously.

Both grains can be ignited using dry or wet heat, both electrically and using burning material. The SB recommends to ignite the grain either remotely or manually using a punk (smoldering stick), with the test operator and test conductor wearing the appropriate PPE. The SB will not provide black-powder ignition plugs (squibs), unless a safety officer transports and handles them and the test is performed on the "Fellowship field" near the Aerospace Engineering faculty of the TU Delft. The SB recommends against using squibs for this test.



Figure 2.1: Batch of propellant grains from the most recent casting. The red line is ca 100 mm. Figure courtesy of DARE.

The grains themselves are cylinders with a diameter of roughly 44 mm with a central hole with a diameter

varying between 12 and 16 mm. The grains have a maximum length of 200 mm when cast and are typically cut into 50 mm pieces. Its flame front speed is between 5-7 mm/s depending on temperature, at atmospheric pressure. The combustion of KNSB, is given by [Equation 2.1](#) for the oxidizer/fuel ratio used in DARE. Two images of grains are shown in [Figure 2.1](#) and [Figure 2.2](#), where the first one is from the cast we will be able to use and the second one shows a better view into the grain itself. We will use much shorter grains that have been cut down to a height of around 20 mm.

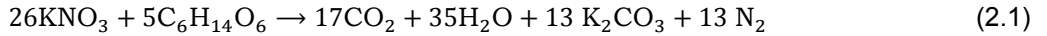


Figure 2.2: Batch of casted and cut propellant grains for high-power amateur rocketry. The outer grain diameter is roughly 150 mm. Figure courtesy of DARE.

The flame temperature is non-trivial to estimate and depends on local pressure as well as grain temperature and specific make-up which can vary strongly between samples. DARE has observed as much as 20% variance between samples from a single batch depending on environment conditions of the test. From previous experience we can expect the following events during ignition ([Olde, 2019](#)).

- melting point of sorbitol: $100 - 110^\circ\text{C}$,
- boiling point of sorbitol: 295°C ,
- melting temperature of KNO_3 : 337°C
- decomposition of $\text{KNO}_3 \rightarrow \text{KNO}_2 + \text{O}$: 400°C

Adiabatic flame temperature at ambient pressure will be between 700-1440 K and thermal runaway starts around $350 - 400^\circ\text{C}$. The grains can produce soot and smoke during burn. Hence, appropriate ventilation needs to be provided. [Figure 2.3](#) shows an example ignition sequence of a KNSB pallet.



Figure 2.3: Ignition and burn of KNSB pallet. Figure courtesy of DARE, [Olde, 2019](#).

In order to capture interesting phenomena, we need to be able to observe events happening on the scale of 100-1000 ms. In order to observe sputter and non-flow phenomena we need to be able to observe events happening on the scale of 1-100 ms. Hu, Wang, and Tian, 2016

We then estimate the minimum deflections for the combustion products as given in Figure 2.4.

The estimate was computed using Equation 2.3 to Equation 2.5, which in combination give the deflection as a function of the gas temperature T and Gladstone–Dale constant k .

For an ideal gas the Gladstone–Dale equation and Equation 2.3 below hold so that the refractive index n can be computed as a function of the gas temperature.

$$n = k\rho + 1 \quad (2.2)$$

, where ρ is the gas density.

$$p = \rho RT, \quad (2.3)$$

where p is the gas pressure, assumed to be ambient since the fluid velocities are small and the fluid hence incompressible, and the specific gas constant R .

For a schlieren system the deflection is then given as Equation 2.5, where Equation 2.4 is simplified assuming instant refractive index changes.

$$\varepsilon_y = \frac{1}{n} \int \frac{\partial n}{\partial y} dz \approx \varepsilon_y = \frac{Z}{n_\infty} \frac{\partial n}{\partial y} \quad (2.4)$$

$$\varepsilon_y = \frac{a}{f_2} \quad (2.5)$$

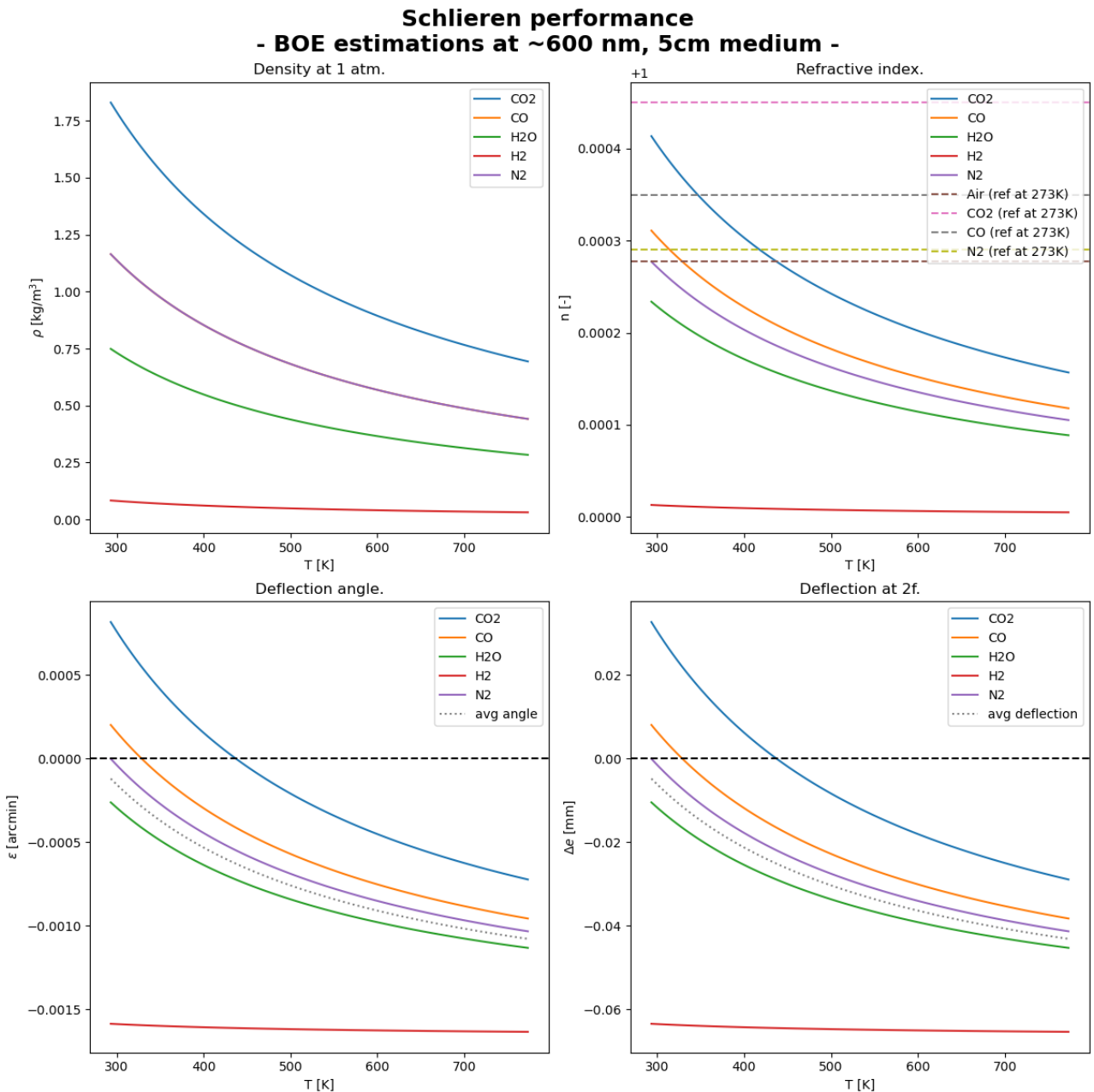


Figure 2.4: Expected deflections for samples in a 2f system.

2.1 Project Definition

In the previous section, it was described what the typical conditions are of SRM grains, that we want to observe. The grains themselves are approximately four centimeters in diameter. From [Figure 2.3](#) it is obvious that the full burning phase reaches a larger size, but the first steps of ignition will occur close to the surface of the grain. With framerate imaging (100-1000 ms) interesting changes in airflow velocity and shape can be observed, and regions of laminar and turbulent flow can be characterized. With even higher framerate (1-100 ms), sputter and non-flow phenomena could be observed.

Due to the short time we have for the course, we identify back up goals and/or optical lab test observations as observing similar phenomena in candle flames, anti-dust spray can, small droplets.

2.1.1 Stakeholders

For this project, there are multiple active or passive stakeholders, each with its own specific requirements, and they are presented below:

- SH1: Lecturer/TA (active)

- They set the boundaries, state the resources and evaluate the design. If everything is in order, they accept the design.
- They expect that the system is relatively simple, possible to make in 2 weeks and within the budget of €500. The mechanical system must be made mostly from LEGO, with some 3D printed pieces, if necessary. The designed optical system needs to be stable, reusable, and to disassemble easily.
- SH2: Instrumentation department/Laboratory of Leiden University (active)
 - They affect the system with specific regulations and existing resources.
 - Their expectations are regulations related: The system should not use lasers because an extra laser instruction course is not desired. Moreover, the system should fit on an optical bench in the laboratory because the available space is limited.
- SH3: External customer (Delft Aerospace Rocket Engineering - DARE)
 - They impose extra conditions on the system.
 - They expect that the optical system can observe the thrust of a small rocket or at least be able to image the heat flow during ignition from a SRM grain.
- SH4: Team
 - They set the mission, needs, requirements, and build components, integrate the system and validates it. They are also affected by the system in terms of resources and final grade.
 - They expect that the system works properly in the given time span and that it satisfies the expectations of the other stakeholders.

2.1.2 Problem statement and NGOs

Problem: the flame front spread and speed uniquely determine the start-up characteristics and potential grain production problems not visible otherwise. Map the occurrences of turbulent and non-turbulent flow, formation of droplets, speeds and directions of these phenomena. There is no such existing device at Leiden University or TU Delft that can image these things.

Need: We need to design and build a system for Leiden University and TU Delft to image the optical transient flame and flow properties during ignition of a SRM grain to determine possible production problems. The framerate needs to be high enough to image turbulence and potentially sputter during ignition.

Next, we present the **goals** and **objectives** of this project in the following list, where the main items are the goals and the secondary items are the objectives for each goal. The goals are listed in order of their priority:

Primary (science) goals:

- Produce a system that can image heat and mass transport using a schlieren imaging system in the optical **(A1)**
 - store digital images or videos of heat/mass transport made visible with a schlieren system **A1.1**
- Image the ignition of solid rocket motor propellant grains **(A2)**
 - determine if and by how much a surface coating of a 4:1 mixture of nitro cellulose and black powder dissolved in acetone accelerates the flame front spread **(A2.1)**
 - find the rate at which a solid rocket motor propellant ignites, at which rate changes in visible phenomena (shape, type of flow) are visible **(A2.2)**
 - track heat and mass transport around the ignition site (spatial mapping) **(A2.3)**
 - determine if a surface coating of a 4:1 mixture of nitro cellulose and black powder dissolved in acetone improves gasification of the propellant measured by the presence of droplets **(A2.4)**

Secondary (technology) goals:

From SH3 and SH4:

- The system should be able to produce science images for the time and conditions of a typical TU Delft solid rocket motor propellant grains test burn (~ 2 minutes), with clearly visible phenomena on the images (**B1.1**)
 - Alignment and focusing of the system should be stable on this timescale
 - Features that are visible at the beginning of this timescale, should still be observable at the end.
 - Observations can be checked directly after observations (or live)
- The system should be usable for a number of experiments over the next few years, allowing for set-up and realignment within a reasonable time (30 – 45 minutes) (**B1.2**)
 - Use should not damage the system, items that wear quickly should be cheap and easy to replace
- The system should be transportable to other locations, so that experiments can be conducted in Leiden as well as in Delft (**B1.3**)
 - The system should be compact
 - The system should be light-weight enough to carry it to another location without the need of special equipment

From SH1

- within the limits of the DOS course (**B2.1**)
 - Clear time limit of nine weeks
 - Keep costs within budget: €500
 - P(ass the requirements of the course)
- Use creative/low cost solutions (**B2.2**)

Tertiary (EOL) goals:

- Exhibit the system on open-door days (primary/high-school) for the instrumentation department (**C1**)

After the preliminary design review the team decided that it was unfeasible to build and test the system for imaging solid rocket motor grain ignitions. This was because the added effort of making the system secure and testing outside of the optical lab would have taken too much time. Instead the project scope was narrowed on the optical table and verification of the systems function for the imaging of solid rocket motor grain ignitions. The production and testing of the support structure of the optics and sample were hence no longer part of the project. Furthermore, the grain ignition tests were replaced by others tests intended to verify that the system meets the requirements for imaging grain ignition.

2.2 Requirements

In this section, the system level requirements are stated, and their verification method is explained. In the Traceability matrix, it is shown how the requirements flow down from the NGOs from Subsection 2.1.2. In this matrix, information on verification of the requirements is also presented.

2.2.1 Traceability matrix

ID	NGO	Description	Verification	Compliance
SH REQUIREMENTS				
SH-PM-SCHED-01	B2.1	The design shall be frozen by 29.5.2022	Inspection: Was the design frozen by the date?	Y
SH-PM-SCHED-01.01	B2.1	The design shall pass PDR by 25.4.2022	Inspection: Was the design preliminarily accepted by the date?	Y
SH-PM-SCHED-01.02	B2.1	The team shall deliver a Design Report by 29.5.2022	Inspection: Was the design report delivered by the date?	N
SH-PM-SCHED-02	B2.1	The design shall be production ready by 25.4.2022.	Inspection: Was the team able to produce the design by the date?	Y
SH-PM-SCHED-03	B2.1	The system shall be fully assembled by 29.5.2022	Inspection: Has the system been assembled by the date?	Y
SH-PM-SCHED-04	B2.1	The system shall be operational by 22.5.2022	Inspection: Was the team able to operate the system by the date?	Y
SH-PM-SCHED-05	C1	The system shall be maintained until by [TBD: 1.7.2022].	Inspection: Was the system supported until the date by the team?	NA
SH-PM-COST-01	B2.1	The total project cost shall not exceed 500 Euro (FY2022)	Inspection: Were the project costs, as tracked by the BOM/cost sheet below the amount?	Y
SH-PM-COST-02	B2.1	All project costs shall be traceable.	Inspection: Were the project costs tracked?	Y
SH-PM-COST-03	B2.1	All significant expenses shall be approved by lecturer.	Inspection: Were all significant expenses approved?	Y
SH-PM-LEG-01	B2.1	The project shall comply with all local laws and regulations.	NA	
SH-PM-SAFE-02	B2.1	The project shall comply with all LU regulations.	NA	
SH-FUN-PERF-01	A1	The system shall detect optical light.	Test: Does the system work using light sources in the optical?	Y
SH-FUN-PERF-02	A1	The system shall translate refractive index gradients in its optical path to a 2D image.	Test: After calibration put a candle, or an object which creates large changes in the environment density and verify that fluid movements (e.g. hot air and gas) are visible on the output system.	Y
SH-FUN-PERF-03	A2	The system shall accept a DARE-SRM propellant grain in the optical path.	Demonstration: Put a representative sample with the proper dimensions in the systems optical path and verify that it fits.	Y
SH-FUN-PERF-03.01	A2	The system shall accept a DARE-SRP-SRM2020-BD propellant grain in the optical path.	Demonstration: Put a representative sample with the proper dimensions in the systems optical path and verify that it fits.	Y
SH-FUN-PERF-03.02	A2	The system shall accept a DARE-SRM-[TBD] propellant grain in the optical path.	NA	
SH-FUN-PERF-04		The team shall be able to operate the system.	Demonstration: Practice operating the system (without voltage) in the Lab and show that the distance can be kept.	Y
SH-FUN-STRUCT-01	B2.2	The system shall prominently feature LEGO components.	Inspection: Is Lego featured in the design?	Y
SH-FUN-STRUCT-01.02	B2.2	The mechanic sub-systems shall be based on LEGO components.	Inspection: Are the mechanic sub-systems lego based?	Y/N

SH-FUN-STRUCT-02	The system shall not be destroyed during nominal operation.			Inspection: Is the system operational after tests?	Y
FUNCTIONAL REQUIREMENTS					
FUN-PERF-01	A1	The system shall detect visual light, roughly from 400 nm - 700 nm		Analysis/Test: verify that the response curves of the individual components (lightsource and detector) meet the requirement.	Y/N
FUN-PERF-02	A2	The system shall be able to capture at least 100 images per second.		Test: Record a video before mounting the camera on the final optical system and during test conditions and verify that the framerate is met.	Y
FUN-PERF-02.01	A2	The system shall be able to scan its FOV at least 100 times per second.		Analysis: Verify that the camera specifications meet the requirement.	Y
FUN-PERF-02.02	A2	The system shall be able to save a full image at least 100 times per second.		Analysis: Verify that the camera specifications meet the requirement.	Y/N (Saves to memory, not to disk. Bugs were encountered sometimes)
FUN-PERF-03	B1.1	The team shall be able to access the footage at most 2 minutes after taking it.		Demonstration: Show that the resulting images/videos are accessible in the prescribed time.	Y
FUN-PERF-04	B1.1	The system shall meet all functional requirements in ambient daylight.		Test: Verify meeting other requirements in the lab with the lights switched on. The Michelson contrast in the resulting image shall still be at least 0.5.	Y
FUN-PERF-05	A2.3	The FOW shall be of the order of 10cm		Test: Image an object of the desired : Y	
FUN-PERF-06	A1.1	The system shall produce 2D images.		Demonstration: Take test image of the detecting system before mounting it on the designed optical system and verify it is an 2D image.	Y
FUN-PERF-07	A1.1	The system shall produce 3D image cubes (video).		Demonstration: Take test images of the detecting system before mounting it on the designed optical system, process them and verify it is a video or image cube.	Y
FUN-PERF-08	A1.1	The team shall be able to access the recorded data from the system digitally.		Demonstration: Verify that we can access the recorded data from our laptop.	Y
FUN-STRUCT-01	B1.1	The system shall be able to withstand 0.01 N constant force in X,Y,Z direction without movement.		Demonstration: Verify that the system does not move when lightly pressing against the components in the lab.	Y
FUN-STRUCT-01.01	B1.1	The system shall be able to withstand shocks of the order of people walking next to the setup		Demonstration: Verify that the system does not shake when lightly hitting the support with a finger.	Y
FUN-STRUCT-01.02	B1.1	The system shall be able to withstand vibrations on the order of a car driving at least 15 m from the setup.		Demonstration: Verify that the system does not shake when lightly shaking the support with a finger.	Y
FUN-STRUCT-02	B1.3	The system shall weigh no more than 20 kg.		Inspection: Verify that the system is less than 20 kg by inspection or weighing the setup.	Y

FUN-STRUCT-03	B1.3	The system shall fit in a 2mx2mx1m space in its system-level disassembled state.	Inspection: Verify that the system fits in the volume by inspection or weighing the setup. Analysis/Inspection/Test: Verify that the requirement is met by testing components close to heat sources, inspecting it after operation in the lab and verifying the materials can withstand these temperatures.	Y
FUN-STRUCT-04	B1.1	The system shall remain functional for ambient temperatures between 5 and 40 degrees C.	Inspection: Verify that the system looks that it can be transported in a car or train.	Y
FUN-STRUCT-05	B1.3	The team shall be able to transport the system by car or train.	Test: Test the system by performing a normal test and show that the system produces images of the quality required by the other requirements.	Y
FUN-STRUCT-06	B1.1	The system shall keep the optical components stable within displacements of no more than 1 mm during operation.	Inspection: Show that no system is supported by a translation stage with more than 3 axis translation.	Y
FUN-STRUCT-07	B1.2	The optical components shall be maximum 3-axis translateable, if necessary.	Demonstrations: Adjust the focal plane with an accuracy of at least 1mm.	Y
FUN-OPT-01	B1.2	The team shall be able to adjust the systems focal plane within 1 mm	Demonstartion: Show that the LED is imaged at the knife edge.	Y
FUN-OPT-02	B1.1	The light source shall remain at the focal point of the system.		

3 Design space

3.1 Design space

A Schlieren imager can have multiple designs, but is always composed of more main components: a point light source, a primary optical system, a possible secondary optical system, a device to cut the light beam, a light detector, and the support system. The possible options for each component are presented in [Table 3.1](#).

Light source	Automotive tail light bulb
	LED
	Fiber optic cable
	Laser
Main optical device	Spherical mirror
	Parabolic mirror
	Fresnel Lenses
	Nothing
Secondary optical device	Nothing
	Plane mirror
Device to cut the beam	Razor blade
	Filter
	Beam splitter
Collimating system	Collimating lens
	Parabolic mirror
Detecting system (includes a collimating lens)	DSLR camera
	SBIG
	PointGrey
	Andor EMCCD
	FLIR blackfly
	Raspberry pi v2
Mount system	LEGO
	3D prints
	Wood
	Metal

Table 3.1: Required main components and possible devices that can be used for them.

3.1.1 List of possible components and their properties

In this subsection, we present the different options for each component, how they function, their advantages, disadvantages, costs and risks.

Point light source

Type	How it works	Advantages	Disadvantages	Costs	Risks
Automotive tail light bulb	The thin, straight filament must align with the razor edge to work.	Easy to procure.	Needs precise alignment and the image is not very good.	< €10	Can prove hard to align. There is a high chance that it will not work.
LED	To make this a point like source, we have to sandpaper the dome of the LED until we almost reached the die. Then, we cover it in silver tape completely except the leads. We make a small pinhole in the front and we connect it to a power supply to turn it on.	Easy to make and produce a good image.	Needs a lot of tries to sand the LED perfectly, easy to burn.	30 of them for €15, €10 other instruments (like sandpaper and tape)	Trying to lower the entrance voltage can fail.
Fiber optic cable	We feed a very bright source into a fiber optic cable using a condensing lens.	Very bright point source light.	Larger and more complicated to make.	€10 the light source, €15 the condensing lens, €5 the fiber optic	The lens can damage. Creating the system in the allocated time can fail.
Laser	A laser is a good approximation for a point-like source.	Easy to mount.	Need of laser training. Can prove difficult to make it work and expensive.	€50	Can damage the eyes. Can prove too difficult to make it work. The laser training can take too long and we will remain with too little time to finish the system.

Table 3.2: Description of the possible light sources options, with their advantages, disadvantages, costs and risks.

Principal optical device

Type	How it works	Advantages	Disadvantages	Costs	Risks
Spherical mirror of 20 cm diameter and long focal distance	The mirror has the task to focus the divergent light beam into a single point. It must have a large focal distance to determine small variations in the refractive index. Its focal distance (f) must also not be too long because the detecting system is positioned at a distance $2f$ from the mirror. It must be of high quality, the same which is used for telescopes. It must be aligned such that the beam of light falls exactly in its center,	Produces more light for the image. Most common in use. Inclination of rays do not matter. Light passes thought the observed medium twice.	Delivery takes a lot of time if we damage it. Expensive. Hard to find online	€500 from ThorLabs	If broken or damaged, delivery will take too long (a few weeks) and it will be more than our budget.
Parabolic mirror of 20 cm diameter and long focal distance		Relatively easy to find online. Easy to use. Light passes thought the observed medium twice.	Produces less lightning across the image. Delivery takes a lot of time if we damage the mirror. Expensive. Focal point differs with the inclination of rays.		
Lenses	The lens is used to make the divergent beam of light parallel. Then, after the light passes through the medium, another lens is used to disperse the beam.	Cheap, easy to find and buy	It is only used for the most basic Schlieren cameras. Does not produce high-quality images because of coma abberation (Goldstein and Kuehn, 1996). Light only passes through the obsereveed medium once.	€100 from ThorLabs	The produced image can be of too low quality and nothing is observed.
Nothing	There needs to be a bright source behind the observed object. The background needs to be flat and uniformly illuminated.	No costs	Data needs to be processed a lot before visualizing. Very difficult to build.	None	It is a very complicated system. Construction and data processing can take significantly more than the required time.

Table 3.3: Description of the possible principal optical components, with their advantages, disadvantages, costs and risks.

Secondary optical device

Type	How it works	Advantages	Disadvantages	Costs	Risks
Nothing	We do not put anything in between the mirror and the knife edge.	Easy to use. No further alignment required	If the rocket splatter behaves unexpectedly and emits dirt further than we think, it can make the detector dirty	None	None
Plane mirror	Before cutting the beam, we deviate the incoming light from the parabolic mirror using a plane mirror.	Can protect the detector if something unexpected happens and the rocket grain emits particles much further than expected.	Makes the alignment harder. Produce more aberrations and optical errors.	None (if it comes with the telescope mirror), €40 if bought independently	Can make the alignment significantly longer, which can make the system not portable
Beam splitter	We put the light source and the detector in different position. The light first passes through the light beam and goes to the mirror. When it returns, part of it goes to the detector and can be analyzed.	The light source and the detector do not need to be too close together. Can make alignment easier.	75% of the light is lost in the beam splitter (if we use a 50-50 beam splitter). Another kind of beam splitter loses more of the light.	> €200 from ThorLabs	If too much of the incoming light is lost, the image becomes too dark to distinguish any details. If broken, can take too long to order and new one and since it is expensive, we can run out of budget for a new one.

Table 3.4: Description of the possible secondary optical components, with their advantages, disadvantages, costs and risks.

Cutting the optical beam

Type	How it works	Advantages	Disadvantages	Costs	Risks
Knife edge	The knife edge reflects part of the light and lets only a small fraction of it into the camera. This will reflect the rays that were deviated more due to a larger refractive index and they will not enter the detector, creating shadows. The ones least deviated will appear bright on the camera and we can distinguish between different refractive indices.	Cheap and easy to use.	More dangerous. Requires a lot of attention when used.	<€5	We can cut ourselves or damage the optics with it.
Filter	The filter absorbs part of the light. If it is more deviated from the original path, it will be absorbed and not enter the camera.	Can make colored images	More difficult to use and more expensive	€20	With the wrong filter, we will not be able to observe anything.

Table 3.5: Description of the possible beam cutting devices, with their advantages, disadvantages, costs and risks.

Collimating system

Type	How it works	Advantages	Disadvantages	Costs	Risks
Collimating lens	The lens is placed at a distance equal to its focal distance and the light, which is initially a point-like source, becomes collimated (the rays of light become parallel) after transmission	Relatively cheap. The detector can be placed on the same line as the lens, making alignment easier	The coating is very sensitive and it can damage if we do not use the lens according to the regulations	€60 from ThorLabs	If the platform has a small length, the detector might not fit due to its placement on the same line as the beam cutter and lens
Parabolic mirror	The mirror is placed at a distance equal to its focal distance and the light, which is initially a point-like source, becomes collimated (the rays of light become parallel) after reflection	The detector can be placed on a different axis, which is useful if the space is limited	The coating is very sensitive and it can damage if we do not use the mirror according to the regulations. The incoming rays are not parallel, producing coma aberration.	€140 from ThorLabs	The coma aberration can damage the image significantly, lowering its quality and making it impossible to use for sensitive observations

Detecting system

Type	How it works	Advantages	Disadvantages	Costs	Risks
DSLR	The light from the razor blade is collimated using a collimating system. Then, the parallel rays enter the camera, where they are detected.	Extremely large detecting area (22.3 mm x 14.9 mm). Between 30 and 60 frames per second reading speed	Very large and cannot be operated with a Python script	€200 -€400 for the camera second hand	Can prove too large to mount. Quite expensive if it breaks.
SBIG		Extremely large detecting area (18 mm x 13.5 mm)	Only one frame per second reading speed	€2000 for the camera from Andor	Can prove too large to mount. Extremely expensive if it breaks. With such a low reading speed we cannot detect important features in the fast burning grain.
PointGrey		Reasonable detecting area (7.11 mm x 5.34 mm)	Slow reading speed (13 fps)	€400 for the detector	With such a low reading speed we cannot detect important features in the fast burning grain.
Andor EMCCD		Very high reading speed (513 fps)	Very low detecting area (3 mm x 3 mm)	€1000 for the CCD	The detector size can prove too small and impossible to align properly.
FLIR blackfly		Both good reading speed (118 fps) and reasonable detecting area (7.07 mm x 5.30 mm)	None	€500 for the detector	The software required to read the data can be faulty. Extremely expensive if it brakes.
Raspberry pi v2		Good reading speed (90 fps max), easy to code, extremely cheap.	Very small detector (3.68 mm x 2.76 mm)	€30 for the Raspberry pi	The detector size can prove too small and impossible to align properly.

Table 3.6: Description of the possible detectors, with their advantages, disadvantages, costs and risks.

Support system

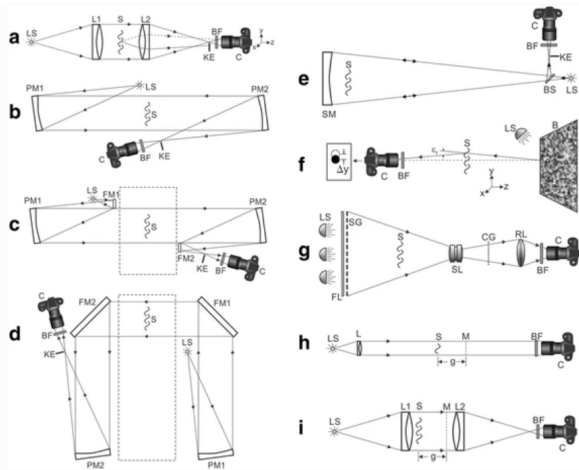
Type	How it works	Advantages	Disadvantages	Costs	Risks
LEGO	Lego pieces can be arranged in many different ways to create a support for the lenses and make them move on multiple axis.	Easy to build, cheap, can move on multiple axis, different designs possible, trial and error possible.	Can break from too much weight. Takes time to find the right design	€200 for different pieces that can rotate and translate.	Can separate by accident and damage the optical components.
3D prints	They are very light and can be printed in the exact shape of the optical components, holding them properly.	Light, can make any possible shape if the scheme is available.	Not easy to change something, takes a long time to print, not easy to translate and rotate.	€1000 for a 3D printer	It can stop working because of different errors. Delivery for a new one take too long time.
Wood	We can cut and shape wood such that it holds the lenses.	Relatively light.	Hard to model, needs extra tools and extra knowledge. Too time demanding	€200 for wood and tools	We can hurt ourselves since we do not have experience and the final product might not be usable.
Metal	We buy/built metal pieces and put them together. This works best if the system is already aligned to keep it stable.	Very stable: once the system is aligned and positioned on metal supports, it will not de-align easily.	The system needs to be aligned beforehand. Hard to use, heavy, expensive.	>€100	We might not have enough time to first align the system and then make a separate frame. It can also make the system too heavy and impossible to transport. Can make the necessary fine alignment impossible.

Table 3.7: Description of the possible mounting systems, with their advantages, disadvantages, costs and risks.

3.1.2 Trade-off

In this section, we present different design options and choose which one fits best with our requirements. After the design of the system is chosen, we look at the individual components, since there are more possible options for each components.

System set-up



Diagrams of different schlieren instruments: Toepler's lens-type system (**a**), simple "z-type" system (**b**), folded z-type systems with both non-parallel schlieren beams folded (**c**) and with the parallel beam folded twice (**d**), single-mirror, double-pass schlieren arrangement (**e**), Background-Oriented Schlieren (BOS) (**f**), focusing (lens-and-grid) schlieren system (**g**), direct shadowgraph system (**h**) and "focused shadowgraph" system (**i**). The individual components of these setups are described in detail in the text. List of the used abbreviations: B – background; BF - bandpass filter; BS – beamsplitter; C – camera; CG – cutoff grid; FL – Fresnel lens; FM1 – folding mirror 1; FM2 – folding mirror 2; g – defocusing distance; KE – knife-edge; L – lens; LS – light source; L1 –schlieren field lens 1; L2 – schlieren field lens 2; M – plane of camera focus; PM1 – parabolic mirror 1; PM2 – parabolic mirror 2; RL – relay lens; S – schlieren object (plasma); SG – source grid; SL – schlieren lens; SM – spherical mirror; x, y, z – Cartesian coordinates; Δy – ray displacement in y-direction; ϵ_y – refraction angle in y-direction

Figure 3.1: Different designs for a Schlieren imager, Traldi et al. (2018)

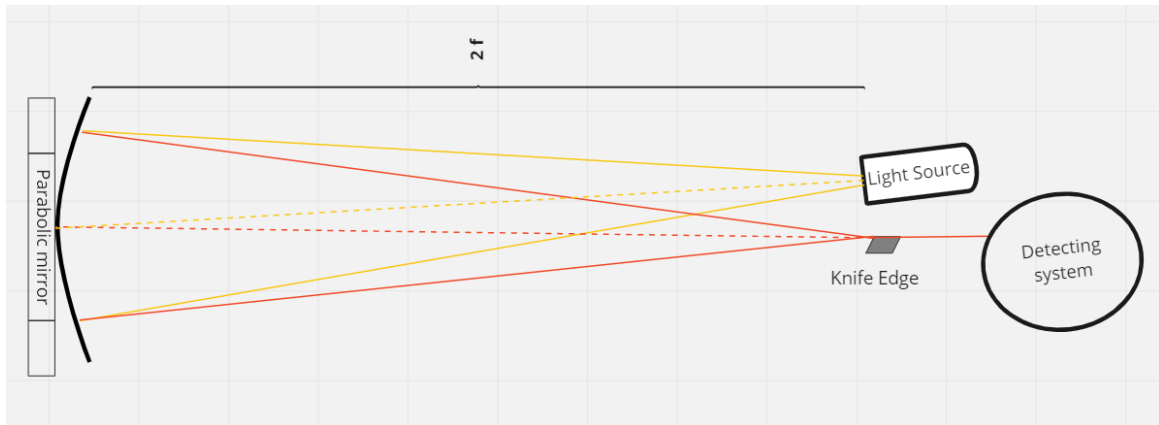


Figure 3.2: A basic Schlieren image design, from Andrew Davidhazy's website.

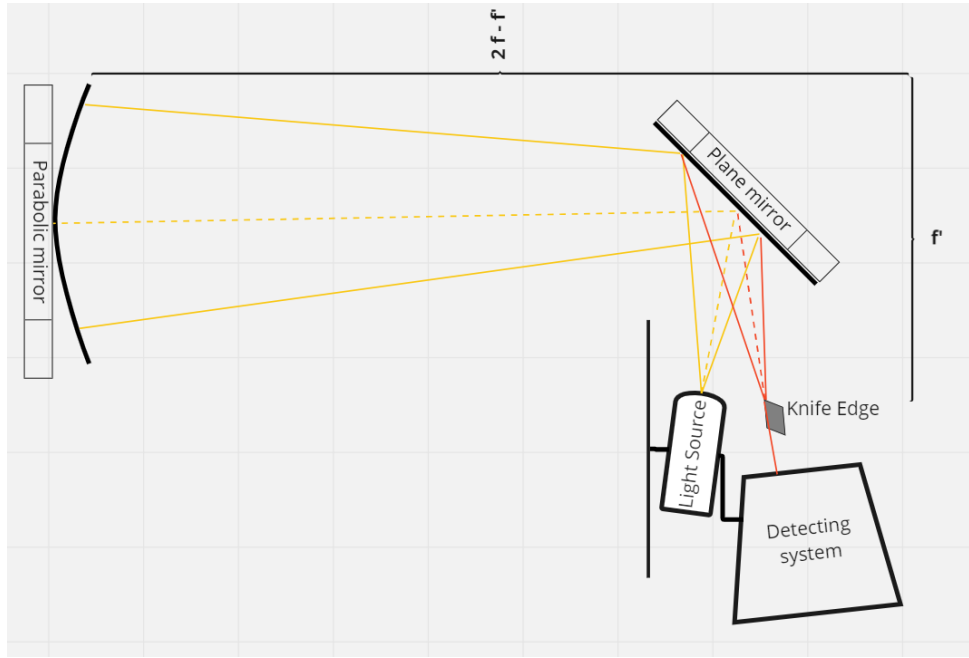


Figure 3.3: A basic Schlieren image design with a plane mirror.

Based on the [Figure 3.1](#), we got an overview of different design options. Here, we provide a short description of why some design options are or are not feasible for our optical system. We also add two other possible designs at the end, both based on the most basic design for a Schlieren camera ([Figure 3.2](#)). One of them is exactly the basic design, while the second one has an extra plane mirror which is used to deviate the beam initially, and before the light arrives at the razor blade ([Figure 3.3](#)).

- One large mirror has already been pre-ordered for use in this project. Because of budget and time constraints (SH-PM-COST-01, SH-PM-SCHED-03), it is not possible to have any design with more than one large mirror: design options b,c, and d are therefore rejected.
- BOS (design option f) together with design g are rejected because creating a large background screen that we can also easily transport to a new location is not possible with the available time and resources (FUN-STRUCT-03, FUN-STRUCT-05). Moreover, the software is complicated, time demanding, and out of our field of expertise.
- Designs h and i are shadowgraphs, not Schlieren cameras, so there is no need to consider them.
- System a is accepted as a possible solution since it is easy to make and has components within the price range.
- All the systems similar to the basic design (design e and the two extra designs) are accepted because they are easy to make and require a mirror, which have already been purchased.

After we reject the systems that clearly do not work for us, we remain with four possible systems, which are presented in more detail in

A	Basic Schlieren Imager	The design is the one presented in Figure 3.2 and it consists of: light source, mirror, knife edge, and detecting system.
B	Basic Schlieren Imager with plane mirror	The design is the one presented in Figure 3.3 and it consists of: light source, plane mirror, mirror, knife edge, and detecting system.
C	Basic Schlieren Imager with beam splitter	The design is the one presented in e in Figure 3.1 and it consists of: light source, beam splitter, mirror, knife edge, and detecting system.
D	Schlieren Imager with lenses	The design is the one presented in a in Figure 3.1 and it consists of: light source, two lenses, knife edge and detecting system.

Table 3.8: The four final possible designs which will be analyzed in detail.

Trade-off matrix

To compare the four possible designs, we define the criteria after which they will be scored. Each criterion has a weight and multiple categories which helps characterize the system better. The criteria and their sub-divisions are presented below:

- Risk:
 - System failure - shows how high the chances are that the system will fail to work in the end, because of time issues or because the rocket grain damages the system.
 - Personal safety - shows how safe it is to work with it
 - Components risk - shows how hard it is to replace components that can easily break
- Performance
 - Photon budget - shows what percentage of light reaches the detector
 - Wave front error - shows how large is the beam deformation
 - Field of view (FOV) - shows if the expected object can be fully imaged
- Ease of use
 - Calibration - shows how easily we can re-align the system after moving it to a new location
 - Size/mass - shows how easily we can move it to another location by train or car
- System complexity
 - Optical train - shows how complex is the optical train, how many components are needed
 - Required accuracy - shows how hard it is to reach the required accuracy for the system

After the four main criteria are clearly defined, we perform a AHP calculation to find their weights in the trade-off matrix. The resulted values are presented in [Table 3.9](#).

Risk	$54.9\% \pm 14.3\%$
Performance	$15.1\% \pm 2.4\%$
Ease of use	$9.4\% \pm 2.1\%$
System complexity	$20.7\% \pm 4.4\%$

Table 3.9: The analysing criteria and their weights.

Most of these characteristics for the different systems can be scored easily. However, for the photon budget and wavefront error of the systems, some calculations need to be done and are presented in [Appendix A](#). The resulted trade-off matrix with the filled values is presented in [Table 3.10](#). For the fields without exact numbers, the scores are given between 1 and 10, with 1 the worst value, and 10, the best. The sub-components are averaged and then, the resulted values for each criterion, are averaged with the weights defined before in [Table 3.9](#).

After performing the trade-off study for the different designs, we can clearly see that the one that fits best with our requirements is the basic setup of a Schlieren camera, with a light source, mirror, no secondary optics, knife edge or filter, and detector system. Thus, this is the system that we use for more detailed analysis.

Design	Risk (54.9%)			Performance (15.1%)			Easy to dissassemble/align (9.4%)		Complexity (20.7%)		Total score
	System failure	Personal safety	Components risk	Photon budget	WFE	FOV	Calibration	Size/mass	Optical train	Required accuracy	
A	9	9	8	48%	67nm - 117 nm	8	8	8	9	8	8.58
B	9	9	8	46%	95nm - 165 nm	8	7	7	8	7	8.13
C	6	9	7	12%	166nm - 291nm	8	7	7	8	7	7.04
D	10	9	10	35%	141nm - 248nm	5	8	8	9	7	8.55

Table 3.10: Trade-off matrix for the four designs.

Components trade-off

In the previous section, we selected a system design that fits best with our needs. For this design, there are still multiple options for specific components. In this section, we present the trade-off for each of the components.

Light source - There are four possible options for a light source in optical light, each with its own advantages and disadvantages. By taking into consideration their characteristics, and the fact that we aim for a simple, but qualitative device, we can give each of them a score from 1 to 10. All of this is summarized in [Table 3.11](#), and we see that an LED is the best option for the STRIA project.

Device	Advantages	Disadvantages	Score
Automotive tail light bulb	Cheap, easy to procure.	The resulted image is of very low quality.	6
LED	Cheap, easy to procure.	If we want to sandpaper it, it can take a few tries to make it right.	8
Fiber optic cable	Qualitative and bright light source	Large, vey complicated to make.	5
Laser	Already a point source	Lack of laser training.	3

Table 3.11: Different light sources with advantages, disadvantages and a score.

Primary optical component - Considering the chosen system design, the primary optical component must be either a spherical mirror or a parabolic one. Moreover, since the parabolic mirror has already been pre-acquired by the Stakeholders, we use a parabolic mirror as a primary optical component for our Schlieren imager.

Secondary optical component - The chosen system design constrains us in having no secondary optical component. This makes the system simpler, cheaper, and easier to align.

Cutting the optical beam - For cutting the beam, we have two possible options: a razor blade, and a filter. The filter is expensive when compared to the knife edge, and not necessary for our science goals. Thus, the best option for this optical system is to use the knife edge as a mean of cutting the light beam.

Collimating system - The parabolic mirror induces coma aberrations because the incoming rays are not parallel. Moreover, it is easier to align when all the components are on one axis. Thus, the collimating lens is a better option for our system.

Detector system - Lastly, we decide the best-suited detector, based on the size of the effective detection area and readout speed (all the candidate detectors are monochromatic). To decide on a specific detector, we look at their specifications, presented in [Table 3.12](#). Since we require a large detector size, fast readout speed, but small detector size and possibility to run it using Python, FLIR blackfly is the best option for our optical system.

Detector	Effective detecting area (mm)	Number of pixels	Framerate (fps = Hz)
DSLR	22.3 x 14.9	2816 x 2112	60
SBIG	18 x 13.5	3326 x 2504	1
PointGrey	7.11 x 5.34	1928 x 1448	13
Andor EMCCD	3.072 x 3.072	128 x 128	513
FLIR blackfly	7.07 x 5.3	2048 x 1536	118
Raspberry pi v2	3.68 x 2.76	3280 x 2464	30-90

Table 3.12: Possible detectors and their characteristics

4 Detailed design

In the previous sections we discussed possible designs for a Schlieren camera that meets our requirements, and we arrived at the conclusion that the design from [Figure 3.2](#) is best suited for our scope. In this section, we detail this design and present all of its characteristics.

4.1 Product breakdown structure

The STRIA project has multiple systems: light source, knife-edge, detector, collimating lens (all of them positioned on a platform), parabolic mirror, electronic, software, and sample support, all of which have their own subsystems. The product breakdown structure (PBS) is presented in [Figure 4.1](#), each system and its subsystems being described in this section. To make explanations easier, we define a three-axis for the system, presented in [Figure 4.2](#).

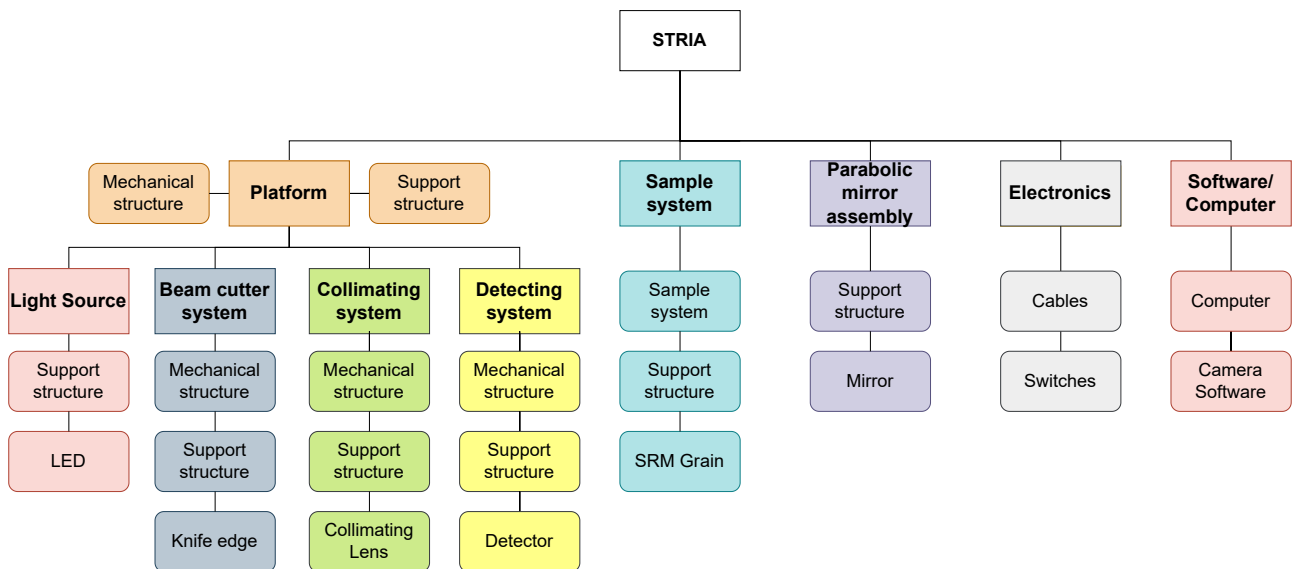


Figure 4.1: The PBS of the STRIA project.

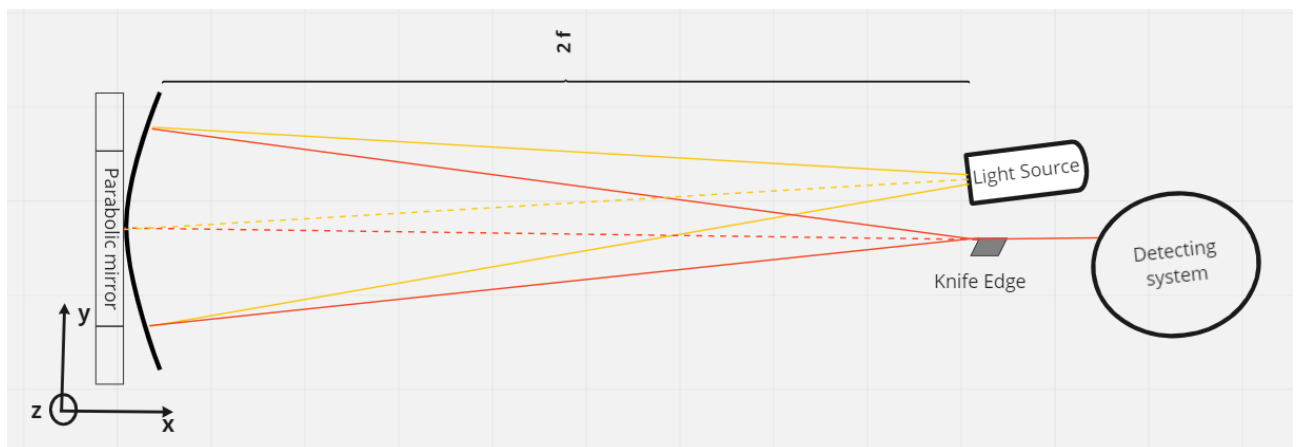


Figure 4.2: STRIA setup and coordinate system.

Platform

The platform supports the light source, beam cutter system, collimating system, and detecting system. It has two subsystems:

- Mechanical structure - It helps to translate the platform on two axes: y and z, with more than 3 cm on each axis. The required length originates from the fact we can align the mirror with an accuracy of 0.1 degrees, which corresponds to roughly 3 cm deviation of the beam from the center. The x-axis can be adjusted well enough by hand when positioning the system. The translation must be continuous, since high precision is needed, of below 2 mm.
- Support structure - It supports the platform. The platform needs to be as small as possible, but large enough to fit all the components. Considering that the collimating lens has a focal distance of 5 cm (and thus it needs to be 5 cm from the knife-edge) and that the detector is positioned 5 cm from the collimating lens, the platform must be longer than 15 cm. Moreover, the light and the knife-edge are on the same axis, so the platform needs to be wider than 10 cm. It must have roughly the same height on z as the other components, with an error less than the translation limit.

Light source

The light source consists of an LED and its support, which does not need to be adjustable.

- LED - The light source for the system. A simple LED can be turned into a good point source for the system. The LED must emit optical light, preferably in the range of 500 nm - 600 nm, which is the range in which the detector is the most sensitive (FUN-PERF-01). It is connected to the laptop via an Arduino.
- Support structure - It supports the LED. It needs to be small, to fit on the platform (max 5 cm x 5 cm in the xy plane) and the same z size as the other components, with a precision of 1 mm. It does not need to be adjustable because the movement of the platform is enough to align it with the mirror.

Sample System

This is the object that will be observed by the camera. Its subsystems are:

- SRM Grain - This is the observed object. It will be positioned 60 cm away from the mirror, so the observed object needs to be smaller than 15 cm (knowing that the mirror has 20 cm diameter and is positioned at 240 m from the light source $\Rightarrow \frac{20}{240} \cdot (240 - 60) = 15$). Thus, the SRM grain and its emission must be smaller than 15 cm. This is easily achievable because the SRM grain emission which is of interest to us is less than 5 cm.
- Support structure - It keeps the SRM grain in place. The support must be stable and withstand the incoming heat (above 50°C) from the grain (FUN-STRUCT-04). It must have the same height on z as the other components, with a precision of 1 mm.

Parabolic mirror assembly

The mirror is the only optical component that we prefer to keep stable, in the same place, because it is heavy and if it breaks, there is no quick replacement. Its subsystem is:

- Mirror: The mirror is the most important component of the system. It will be protected from the incoming dirt with a plastic screen.
- Support structure: The structure keeps the mirror in place and protects it from the incoming dust. It needs to fit the mirror well and keep it stable throughout the experiment. It must not be heavier than 5 kg because we have to align it by hand with a precision of 0.1 degrees in rotation, and less than 1 cm in translations on the x and y-axis (see technical requirements for details). Its z-axis has to be on the same level on the z-axis as the light source and the other optical components, with a precision of 1 mm.

Beam cutter system

This system cuts the focused light in half, and it has multiple subsystems:

- Mechanical structure - Helps to translate the knife-edge. The knife-edge needs to be able to translate along the x and z-axis. The mechanical system needs to translate within 2 cm in each direction and the transition needs to be continuous. The translation on the y-axis is not important because the knife-edge is wide (2 cm wide). On the x-axis, the knife-edge is positioned exactly where the focus of the mirror is, within an error of 1 mm, while on the z-axis it cuts the beam exactly in half, with a precision of less than 1 mm (see technical requirements for details).

- Support structure - Supports the knife-edge. It needs to be small, to fit on the platform (max 5 cm x 5 cm in the xy plane), and it must keep the knife-edge stable, such that small vibrations do not change its position. It must have roughly the same height on z as the other components, with an error less than the translation limit.
- knife-edge - Cuts the beam exactly in half at the focal point of the mirror. When unused, it is covered in a protective sheet for safety reasons.

Collimating system

This system collimates the light for the detector. It has multiple subsystems:

- Mechanical structure - It helps to translate the lens. The lens must translate on the z and y-axis, the x-axis not being important because, in this direction, it can tolerate errors of more than 2 cm. The translation on the z and y-axis is at least 2 cm so that the incoming light is centered on the lens. Small deviations (of a few mm) in the y and z direction can tilt the beam, making it miss parts of the detector (or miss it completely), so the translations must be continuous, and the required precision is 1 mm (see technical requirements for details).
- Support structure - It keeps the lens stable. It needs to be small, to fit on the platform (max 5 cm x 5 cm in the xy plane), to keep the lens stable and not scratch it. Small vibrations must not affect it, because that will change the mirror position more than the allowed error of a few mm. It must have roughly the same height on z as the other components, with an error less than the translation limit.
- Collimating lens - It collimates the light for the detector. It must not have many defects, like scratches or dirt, this ruining the image. Moreover, for our science goals, an achromatic lens is ideal.

Detecting system

This system records the burn of the SRM grain. Its subsystems are:

- Mechanical structure - It helps to translate the detector into three axes: x, y, and z. All the axis are equally important because the image must be centered on the detector, so it should translate at least 2 cm with a continuous translation, in all directions, within an error of 1 mm. The error comes from the fact that the size of the beam is approximately 4 mm in diameter, while the camera has a smaller detecting length of 5 mm.
- Support structure - It supports the system. It must be small enough to fit on the platform (max 5 cm x 5 cm in the xy plane) and it must keep the detector stable. Small hits on the support should not make the camera fall because the detector is very expensive and cannot be replaced. It must have roughly the same height on z as the other components, with an error less than the translation limit.
- Detector - It records the data on a 7 mm x 5 mm area, with a frame rate of 118.

Electronics

They connect the different devices and turn them on:

- Cables - They help to connect the camera to the laptop, and the LED to a power source. The one from the camera to the laptop needs to be longer than 1 m because the laptop will be used often and it should be at a safe distance from the system. The cables connecting the LED to the Arduino can be shorter, but the Arduino must be positioned in a stable. The distance from the Arduino to the laptop much be at least half a meter for an easy use.
- Switches - They help to turn the LED and the camera on and off. They must have delays less than a second because the SRM grain burns for less than 10 seconds.
- Lighter - This will help ignite the grain. The person can stand next to the grain when igniting it since its burn is predictable and in a limited space (of less than 5 cm)

Software/Computer

This is where the data is processed and analyzed:

- Computer - It helps to visualize the taken images and see whether the system works properly. It must have at least 2 GB of memory to store the data.
- Camera Software - It helps to transfer the data acquired by the camera to the computer and control the camera from a safe distance.

After the systems and subsystems are defined, we show how they interact with each other. The interfaces matrix is presented in [Table 4.1](#). The devices that help the light beam follow a specific part interact optically with the system next or previous to it in the light path. On the other hand, the systems that change position once another one's position is modified interact mechanically with each other. Moreover, the systems the LED and camera need electricity, so interact electrically with the electrical system. Lastly, the detector sends data to the computer with the help of connecting cables, so the interaction is both data-driven and electronic.

	Platform	Light source	Sample system	Parabolic Mirror Assembly	Beam cutter system	Collimating system	Detecting system	Electronics	Software/ Computer
Platform		M	-	M	M	M	-	-	
Light source			O	O	-	-	E	-	
Sample system				M	O	O	-	-	
Parabolic Mirror Assembly					O	O	-	-	
Beam cutter system						O	-	-	
Collimating system							O	-	
Detecting system								E	ED
Electronics									E
Software/Computer									

Table 4.1: Interface matrix where the interactions are the following: O-optical, M-mechanical, E-electronic, D-data

Now that the system is described in detail, with limitations and requirements for each subsystem, we trace the technical requirements back to the system requirements. This is presented in [Table 4.2](#)

ID	Technical requirement	System requirement ID
TECH-PERF-01	The platform needs to move more than 3 cm on z and y axis.	SH-FUN-PERF-02
TECH-PERF-02	The platform needs to move with 2 mm accuracy.	SH-FUN-PERF-02
TECH-PERF-03	The SRM grain needs to be shorter than 10 cm on z axis.	SH-FUN-PERF-03
TECH-PERF-04	The mechanical structure for the beam cutter system must translate with at least 2 cm on z and x axis.	SH-FUN-PERF-02
TECH-PERF-05	The mechanical structure for the collimating system must translate with at least 2 cm on z and y axis.	SH-FUN-PERF-02
TECH-PERF-06	The mechanical structure for the collimating system must have a 2 cm accuracy on x axis.	SH-FUN-PERF-02
TECH-PERF-07	The mechanical structure for the detector system must translate with at least 2 cm on z, y and x axis.	SH-FUN-PERF-02
TECH-PERF-08	The mechanical structure for the beam cutter system, collimating system, and detector system must have an accuracy of 1 mm.	SH-FUN-PERF-02
TECH-PERF-09	The mechanical structure for the beam cutter system, collimating system, and detector system must translate continuously, not in steps.	SH-FUN-PERF-02
TECH-PERF-10	The delays between the computer and detector system must be smaller than a second.	SH-FUN-PERF-02
TECH-PERF-11	All the components must have the same height on the z-axis.	SH-FUN-PERF-02
TECH-PERF-12	All the fixed components (light source, parabolic mirror assembly, sample system) must have an error on z-axis of less than 1 mm.	SH-FUN-PERF-02
TECH-PERF-13	All the components that have translations (platform, beam cutter system, collimating system, detecting system) must have the error on the z-axis less than the translation range.	SH-FUN-PERF-02
TECH-PERF-14	The parabolic mirror must be positioned with 2 mm accuracy on x and y axis.	SH-FUN-PERF-02
TECH-PERF-15	The parabolic mirror must be positioned with 0.1 degree accuracy on each rotation axis.	SH-FUN-PERF-02
TECH-PERF-16	The LED must emit in optical light, between 400 nm and 700 nm	FUN-PERF-01
TECH-PERF-17	The computer must have at least 2 GB of free memory.	FUN-PERF-08
TECH-STRUCT-01	The platform support structure needs to be larger than 10 cm x 15 cm, but as small as possible.	FUN-STRUCT-03, FUN-STRUCT-05
TECH-STRUCT-02	The platform support structure needs to be stable and not move with small vibrations	FUN-STRUCT-01
TECH-STRUCT-03	The support structure for the light source, collimating system, beam cutter system, and detector system needs to be smaller than 5 cm x 5 cm (the size on z axis is not critical).	FUN-STRUCT-03, FUN-STRUCT-05
TECH-STRUCT-04	The support structure for light source, collimating system, beam cutter system, and detector system needs to be stable and not move with small vibrations.	FUN-STRUCT-01, FUN-STRUCT-06
TECH-STRUCT-05	The sample support structure needs to withstand heat above 110°C.	SH-FUN-PERF-03
TECH-STRUCT-06	The cable connecting the detector system with the computer needs to be at least 1 m.	SH-FUN-STRUCT-02, FUN-PERF-08

Table 4.2: The traceability matrix from technical requirements to system level requirements.

4.2 Optical design

After all the technical requirements have been defined, we make the detailed optical design and check whether it meets the said requirements. We use Zemax OpticStudio to simulate the optical design and do the optimizations. A full representation of the set-up, to scale, is presented in [Figure 4.3](#), where all the main components can be seen: the light source, parabolic mirror (for this study we ignore the plastic cover), knife-edge, (achromatic) collimating lens, and the detector. After optimizing the system in Zemax, we obtained the best distances between the objects. For this process, we keep most of the parameters specified, with the exception of the distance from the razor blade to the lens, and from the lens to the detector, which are optimized. The distance between the light source and the parabolic mirror is equal to the distance from the mirror to the knife-edge and it is 2.4 m (2 times the focal distance of the mirror, which is 1.2 m). Moreover, the distance between the collimating lens and the knife-edge is almost equal to the focal length of the lens (which is 5 cm), 5.20 cm, while the distance between the lens and the detector is slightly larger, at 5.22 cm. We decided to use a lens with a focal distance of 5 cm because it gives a beam of 4 mm diameter, which is ideal for our camera with one dimension of 5 mm. A zoomed-in image of the beam cutter and collimating system is presented in [Figure 4.4](#), and we can easily see that the beam is cut in half after the knife-edge.

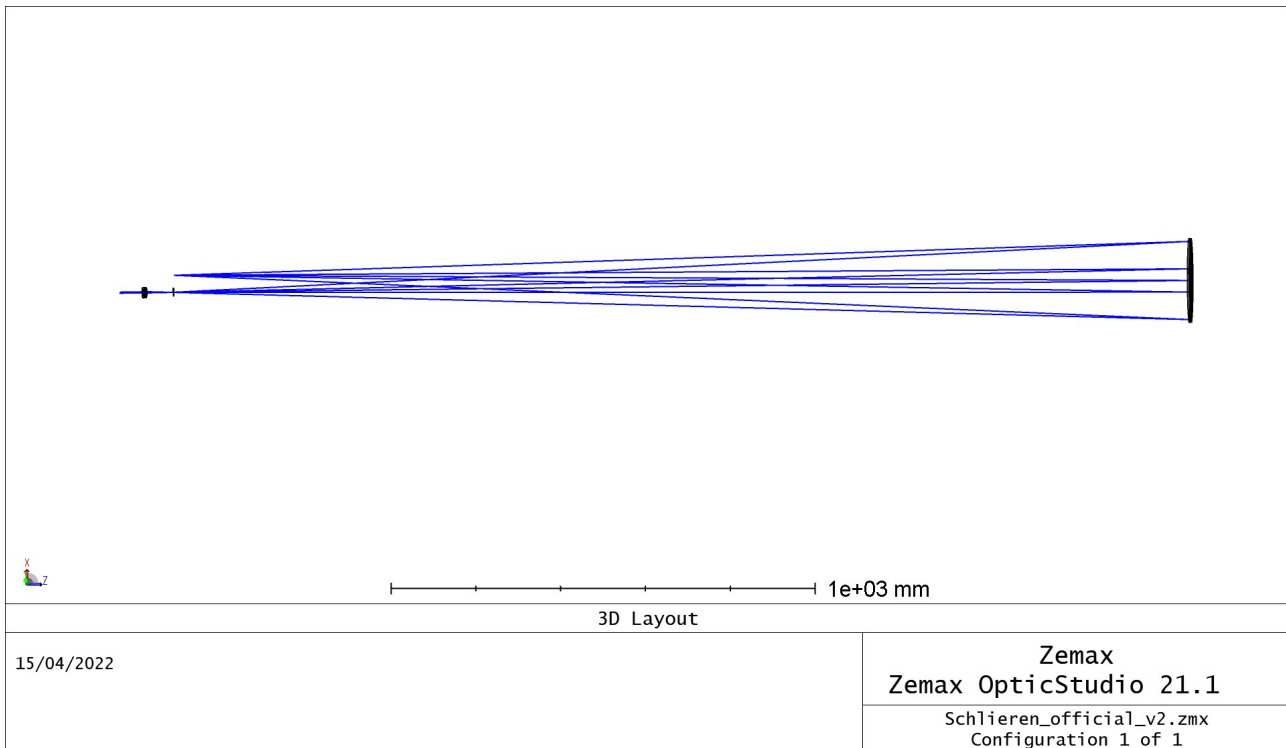


Figure 4.3: The full optical setup of STRIA.

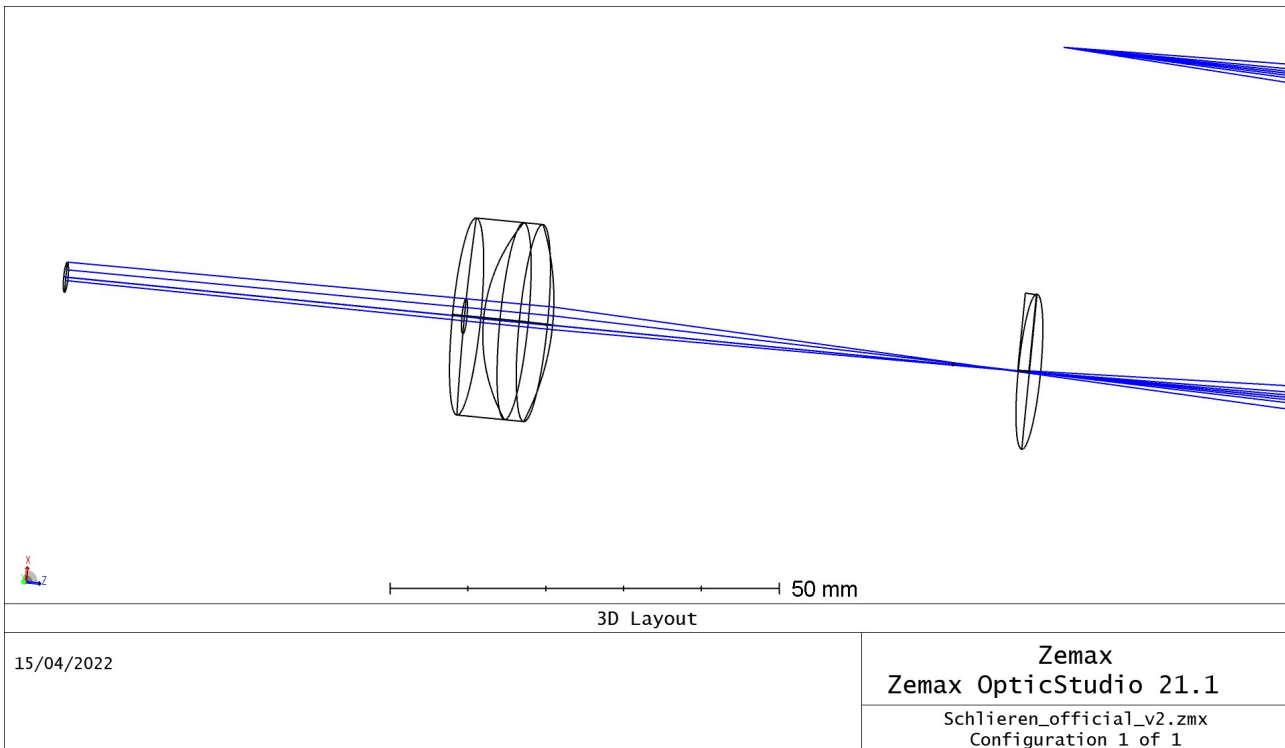


Figure 4.4: The optical setup of STRIA zoomed in to the knife-edge and collimating mirror.

After the system is simulated and optimized, we check the errors that are tolerated by the components that can move: parabolic mirror, collimating lens, and knife-edge.

Parabolic mirror: The mirror's alignment is crucial for a functioning system. If the mirror has an error of more than 2 mm on each of the three axes (x, y, or z), the focus changes position significantly and the knife-edge cannot cut the beam exactly at the focus, its translation range not being large enough. Tilting the mirror is also a possible error in alignment and its effects are significant. A tilt of more than 0.5° rotates the direction of the resulted beam, and it arrives more than 4 cm away from the knife-edge. The maximum tilt of the mirror is 0.1°, which can be corrected by translating the platform for less than 3 cm.

Collimating lens: Moving the lens on the z or y-axis tilts the parallel rays which exit the lens. If the lens is miss-aligned by more than 1 mm, the rays are tilted and not all of them reach the detector area. Moreover, an error of more than 2 cm on the x-axis makes the resulted rays not parallel anymore (which results in a much smaller/larger beam on the detector) and increases the chromatic aberration significantly.

Knife-edge: The knife-edge controls how much light passes further to the collimating lens. If the z-axis translation has an error larger than 1 mm, then there will be more/less light than needed arriving on the lens and the resulted image will be saturated/very dark, making the detection of the changes in density impossible. The translation on the x-axis is just as sensitive, but for another reason. Because the mirror is parabolic, it does not have a single focus, and rays with different inclinations have different focuses. However, we are mainly interested in the paraxial rays because we image close to the center of the mirror, so that is the focus that needs to be found. In [Figure 4.5](#), we can see how the beam spot diagram changes with slight changes in the knife-edge distance from the perfect focus. For a parabolic mirror, the knife-edge is perfectly at the focus of the paraxial rays if the beam spot looks like in [Figure 4.5b](#), and it has a diameter of 1.5 mm on the n=knife edge. For reference, [Figure 4.5a](#) is when the knife-edge is 1 mm before the focus, while [Figure 4.5c](#), is when the knife-edge is half a mm after the focus. In case of a larger distance, of 2 mm after the focus, the resulted beam is presented in [Figure 4.5d](#). From these simulations, it is clear that we must place the knife-edge with 1 mm accuracy on the x-axis.

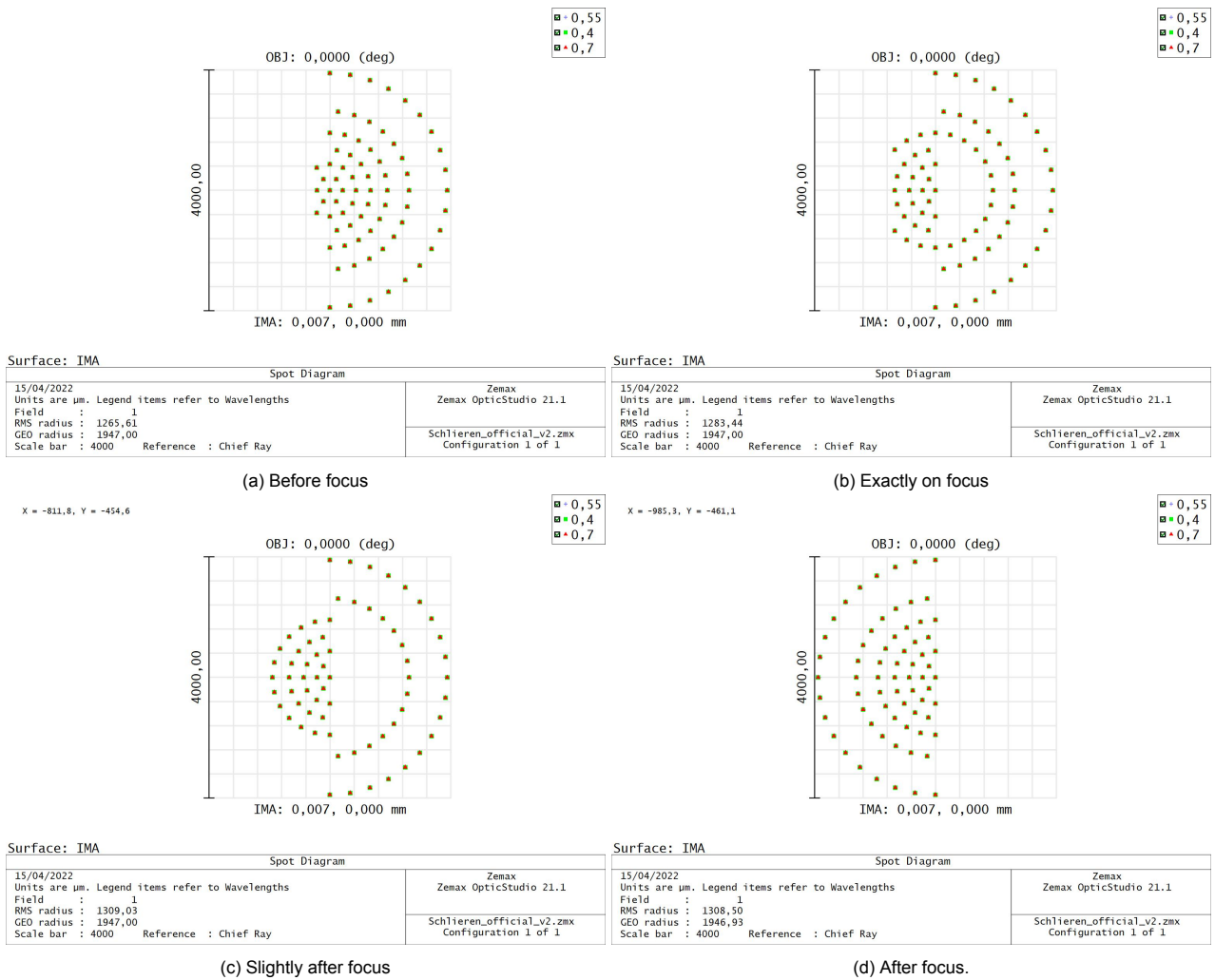


Figure 4.5: The shape of the beam when the knife is at different distances from the focus of the paraxial rays of the mirror.

A summary of all the tolerances is presented in [Table 4.3](#). As an observation, rotation for the other optical components is not considered because, with the help of LEGO, once the platform is aligned, the components cannot be rotated around any axis.

Optical element	Tolerances
Parabolic mirror	2 mm for translation on all axis 0.1° for rotation around all axis
Collimating mirror	2 cm for translation on x axis 1 mm for translation on y and z axis
knife-edge	1 mm for translation on z and x axis 3 cm (its width) for translation on y axis

Table 4.3: A summary of all the tolerances for the main optical components.

Photon Budget

To ensure that the a common LED as a light source is bright enough to get a strong signal, and not too bright and oversaturating the detector, the photon budget was calculated. Because the brightness of a LED depends on the resistor that is added to the system, we will first go through all the steps of the photon budget, and then work our way back to get an estimate for the needed resistance.

Since a common LED is the light source, we know that it emits mainly green light, so at around 550 nm. Thus, we calculate the photon budget at this wavelength. A LED has an opening angle of about 15° (information on LEDs was mainly found on a webpage of LED Supply ([Scully, 2019](#))). At a distance of 240 cm, this results in a radius of $r = 240 \cdot \tan 15^\circ \approx 64.31$ cm. The percentage of emitted light that illuminates the mirror is therefore ~ 2.4%.

The reflective curve, for the parabolic mirror and the (achromatic) lens are presented in [Figure 4.6](#), and [Figure 4.7](#), respectively. Moreover, we assume that the knife-edge blocks exactly half of the light, so 50% and that the detector (FLIR blackfly) has the quantum efficiency from [Figure 4.8](#).

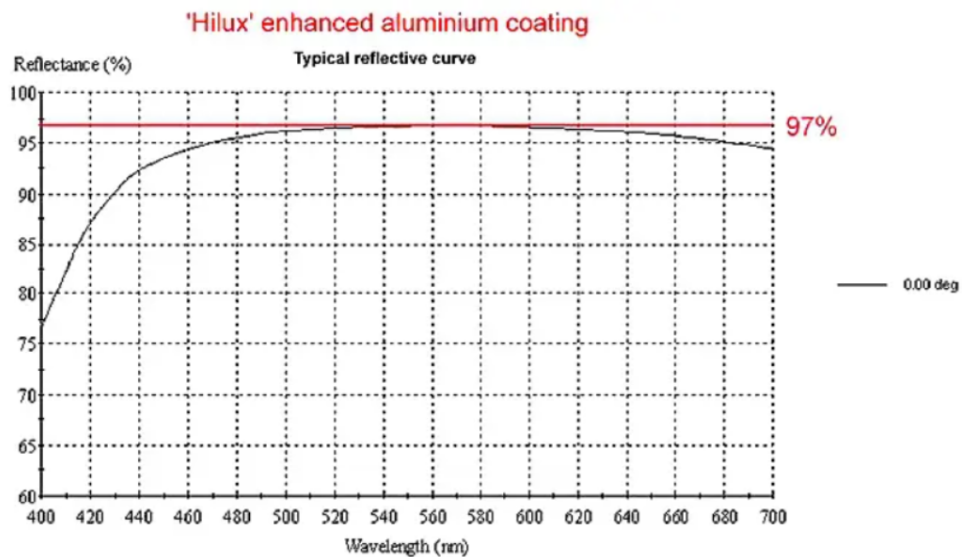


Figure 4.6: The reflective efficiency of the ThorLabs parabolic mirror.

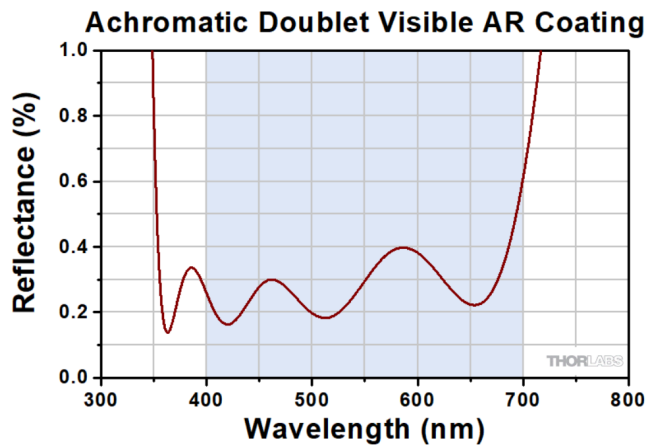


Figure 4.7: The reflective efficiency of the ThorLabs collimating lens.

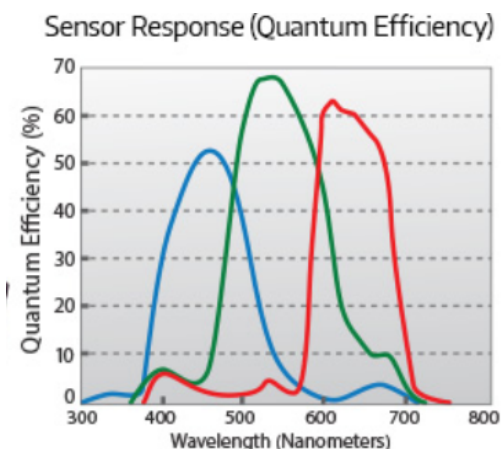


Figure 4.8: The quantum efficiency of the FLIR blackfly detector.

Considering all of the above, the throughput of the optics and detector together is:

$$\text{system throughput} = 0.97(\text{mirror}) \cdot 0.5(\text{knife edge}) \cdot 0.82(\text{lens}) \cdot 0.68(\text{detector}) = 27\% \quad (4.1)$$

So, after the initial light passes through all the optical components, 27% of it can be detected by the FLIR blackfly. Remember, however, that only 2.4% of the light emitted by the LED enters the system.

The beam that falls on the detector is assumed to be circular, with a diameter of 2 mm, on a 5×7 mm detector. This means that $(\pi \cdot 2^2)/(5 \cdot 7) \rightarrow 36\%$ of the detector is illuminated. Of a total of 1500×1500 pixels, that results in the illumination of 810000 pixels. The number of photons arriving per second is assumed to distribute evenly over these pixels, and can be divided by the maximum framerate of 118 s^{-1} to get the number of photons per pixel per image.

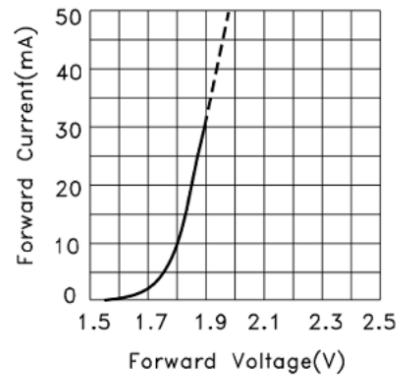
Now we have enough information to reverse engineer the needed properties of the LED. We start with the information that can be stored on a 8-bit camera: $2^8 = 256$ photons per pixel for every frame, with a maximum of 118 per second. In the beam as it arrives at the detector, this corresponds to the following number of photons per second (ignoring the quantum efficiency, as it was incorporated in the system throughput):

$$\begin{aligned} \text{photons per second} &= 256(\text{photons per pixel}) \cdot 118(\text{frames per second}) \\ &\cdot 810000(\text{pixels per beam})/0.36(\text{fraction illuminated pixels}) \approx 6.1 \cdot 10^{10}(\text{photons/s}) \end{aligned} \quad (4.2)$$

The number of photons per second that is needed from the LED is then $N_p = 6.1 \cdot 10^{10}/0.27/0.024$, and the power is $P = hcN_p/\lambda \approx 3.4 \cdot 10^{-6} \text{ W}$ at 550 nm. Figuring out the details is a bit more tricky, because the current

through the system depends on the resistance of the resistor, and the forward voltage depends on the current through the system. To get an idea, we assume that the forward voltage is equal to $V_F = 2\text{V}$. From $P = V \cdot I$, with the desired power, we can already see that the current needs to be incredibly small, which reduces the forward voltage too a number that cannot be retrieved from [Figure 4.9](#). On the other hand, if no resistor is used at all, the voltage over the LED is 5 V, and the resistance can be estimated to be $\sim 15\Omega$ in the high-current regime ([anonymous, 2019](#)), resulting in a current of $I \sim 0.33 \text{ A}$. The power produced by the LED in that case would be of order $P_{max} \sim 1.65 \text{ W}$, causing extreme oversaturation of the detector.

In conclusion, a common LED will be too bright for the detector to use without a resistor, and will likely burn out because of high current. However, because we enter the non-linear regime for LED properties, it is hard to predict which resistor will be needed to get the best result. In the end, a process of trial and error was used to find the best resistor present as to not oversaturate the background of our test-images. A $4.7 \text{ k}\Omega$ resistor turned out to be the best fit.



Kingbright Super Bright Red LED (APT2012SRCPRV)

Figure 4.9: Forward voltage and current of an LED, taken from CircuitBread ([Crowell, 2019](#))

Wavefront Budget

Another important calculation for the system is the wavefront budget, ignoring the plastic cover of the mirror, whose specifications are unknown. However, for a Schlieren camera, a rough approximation is enough because the system is not sensitive to small wavefront errors. Knowing this, calculating the wavefront error only for the optical components is a good approximation. For this, setup, we only use ThorLabs components and they have a WFE of $\lambda/6$. The beam cutter and the camera can be ignored. Thus, the resulted wavefront error is $\sqrt{2} \cdot \lambda/6 = 130 \text{ nm}$. In all this calculations, we did not consider the plastic cover, which induces a significant amount of aberrations, being the component that damages the wavefront the most. However, the plastic cover is known to induce a pattern on the obtained image, which can be cleaned in post-processing.

Lastly, we make sure that the tolerances and errors met the requirements. The tolerances determined with the help of the Zemax code match well with the technical requirements. All the tolerances are larger or equal to the precision required by the technical requirements. A summary of this is presented in [Table 4.4](#).

Optical system specification	Requirement
The total distance between the razor blade and the detector is less than 15 cm	TECH-STRUCT-01
The distance between the light source and the razor blade is less than 10 cm	TECH-STRUCT-01
The parabolic mirror can have a tolerance of 0.1° in rotation	TECH-STRUCT-15
The parabolic mirror can have a tolerance of 2 mm on each translation axis	TECH-STRUCT-14, TECH-STRUCT-12
The collimating lens can have a tolerance of 2 cm on x axis	TECH-STRUCT-06
The collimating lens can have a tolerance of 1 mm on z and y axis	TECH-STRUCT-08
The knife-edge can have a tolerance of 1 mm on z and x axis	TECH-STRUCT-08
The system can detect best at 550 nm	TECH-STRUCT-16

Table 4.4: The optical system specifications and the requirements that it meets.

4.3 Mechanical design

The mechanical design consists of two main assemblies, as discussed previously. The optics assembly is shown in [Figure 4.11](#), [Figure 4.13](#), [Figure 4.14](#), [Figure 4.14](#), [Figure 4.15](#), and the mirror assembly is shown in [Figure 4.16](#), and [Figure 4.25](#). The two assemblies can be placed separately from each other. They have a maximum foot-print of 380x320 mm, when disassembled into their subsystems.

Generally, we make use of springs to resist gravity. All non 3D printed parts are commercial off-the-shelf (COTS). The spring constants have been chosen by trading of fine control (high spring constant), easy adjustment (low spring constant) total travel and un-/compressed length, generally between 0.1 and 0.5 lbs./mm. The springs have been chosen in such a way that the central bolt or guides prevent excessive buckling. The springs push against washers and bolts holding high loads also have washers. Bolts into 3D printed plastic make use of COTS heat-set threaded inserts which can easily hold the highest compression load of the springs. Bolts have been sunk where needed or convenient. Bolts travel through the threaded inserts and generally have no additional backstop. Washers and other press-fitted parts make use of crush ribs. We make use of LEGO patterning as a rough adjustment and optical table surface. We use LEGO 1 and 2 axis translation stages (TS) and have indicated their positions. The LEGO mounts have been built on a trial and error basis and are presented in [Figure 4.17](#), together with the 3D printed mounts for the small components. The translation in LEGO works with the help of the small wheels. Rotating the wheel translates the component on one specific axis. Besides the platforms for the components there is a support for the detector's cable because without it, the detector support is bending due to the large weight of the cable.

We generally use metric and ISO/DIN COTS manufactured and/or sold in the EU, specifically the Netherlands and Germany. No component has a lead time of longer than 1 week. The 3D prints will be a major bottleneck for the schedule since we do not expect to get everything right in the first try.

As a starting point for the design we estimated the pointing accuracy and translation accuracy of the system:

Pointing accuracy: Assuming 1cm CCD/detector width and simplest setup, the pointing angle is given by:

$$\alpha_{M1, max} = \arctan\left(\frac{0.5 \cdot l_{CCD}}{2f}\right) = \arctan\left(\frac{5 \text{ mm}}{2400 \text{ mm}}\right) < 0.1194^\circ \quad (4.3)$$

Assuming that the pointing error must be less than 5-10% of CCD/detector width, the required pointing accuracy becomes:

$$5\%: \alpha_{M1, REQUIREMENT} < 0.01^\circ \quad (4.4)$$

$$10\%: \alpha_{M1, REQUIREMENT} < 0.02^\circ \quad (4.5)$$

$$(4.6)$$

Translation accuracy: Assuming 1cm CCD/detector width and simple setup and that the translation error must be less than 5-10% of CCD/detector width, the translation accuracy must be:

$$5\%: \Delta E < 0.05 \text{ mm} \quad (4.7)$$

$$10\%: \Delta E < 0.1 \text{ mm} \quad (4.8)$$

The cost breakdown of the physical systems is currently still incomplete, however the estimate is shown in [Figure 4.10](#).

Priority	ID	Procurement (External/Internal)	Supplier	Total Part Quantity	Package Quantity	Name	Description	Subsystem	Cost Estimate	Cost pp [EUR]	Total cost [EUR]
1	External	Amatec		25	25	C0300-022-1250M	Medium compression spring	-	1.86	46.5	
2	External	Amatec		10	10	C0180-026-0750S	Small compression spring	-	3	30	
2	External	Amatec		4	4	A-RDF1515	Large compression spring	Vertical TS	2.93	11.72	
3	External	123D.nl		40	2	M8x9 heat set inserts	-	-	8.95	17.9	
4	External	123D.nl		20	1	M3 5x5 heat set inserts	-	-	3.95	3.95	
5	Internal (WS)	Faculty Workshop		1	5	M3 Stainless Steel Socket Head Screw, L30mm, partially threaded, min thread length: 18.0mm	KE/LED	5 euro /50		2	
6	Internal (WS)	Faculty Workshop		1	5	M3 Stainless Steel Washer OD 6mm, T 0.6mm	KE/LED	3 euro /100		2	
7	Internal (WS)	Faculty Workshop		1	5	M6 Stainless Steel Socket Head Screw, L80mm, fully threaded	TS Vertical (base)	7 euro /10		5	
8	Internal (WS)	Faculty Workshop		1	50	M6 Stainless Steel Washer, OD 11mm, T 1.4 mm	TS Vertical (base)	5 euro / 100		3	
9	Internal (WS)	Faculty Workshop		1	10	M6 Stainless Steel Socket Head Screw, L70mm, partially threaded, min thread length: 24.0mm	LENS/CAMERA	7 euro /10		7	
10	Internal (WS)	Faculty Workshop		1	5	M3 Stainless Steel Socket Head Screw, L12mm	LENS/CAMERA	5 euro /50		2	
11	Internal (David)	-		1	1	Camera	CAMERA	-	0	0	
12	internal (David)	-		1	1	LED/Arduino	LED	-	0	0	
13	internal (Lukes)	-		1	1	Razor blade	KE	-	0	0	
14	internal (David)	-		1	1	PLA	-	-	10	10	
15	internal (David)	-		1	1	Lens	LENS	-	75.62	75.62	
											Total 216.69
											Margin (20%) 43.34
											Delivery (10%) 21.67
											Total incl. Margi 281.70

Figure 4.10: System cost overview.

As mentioned above, the system scope was reduced to only include the mirror assembly and optical platform as produced subsystems. Hence, the support structure and sample holder was not produced and the z-translation stage (table) was replaced by a Lego plate.

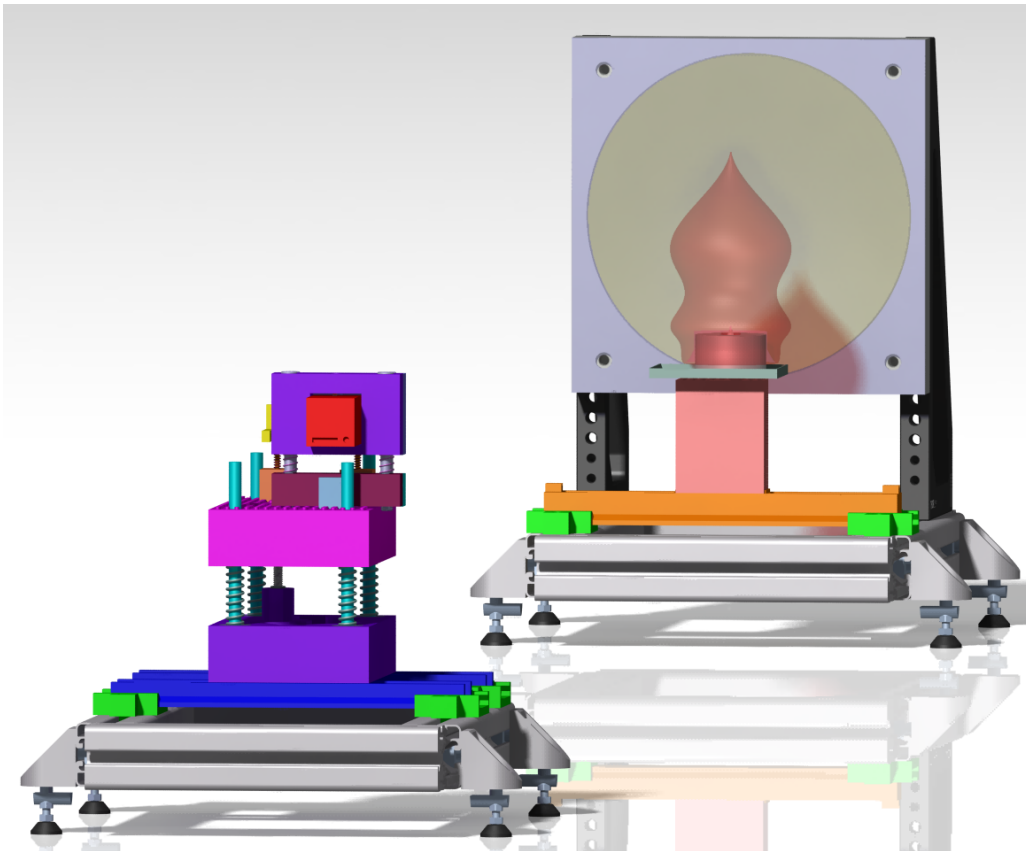


Figure 4.11: System render in artificial colors.

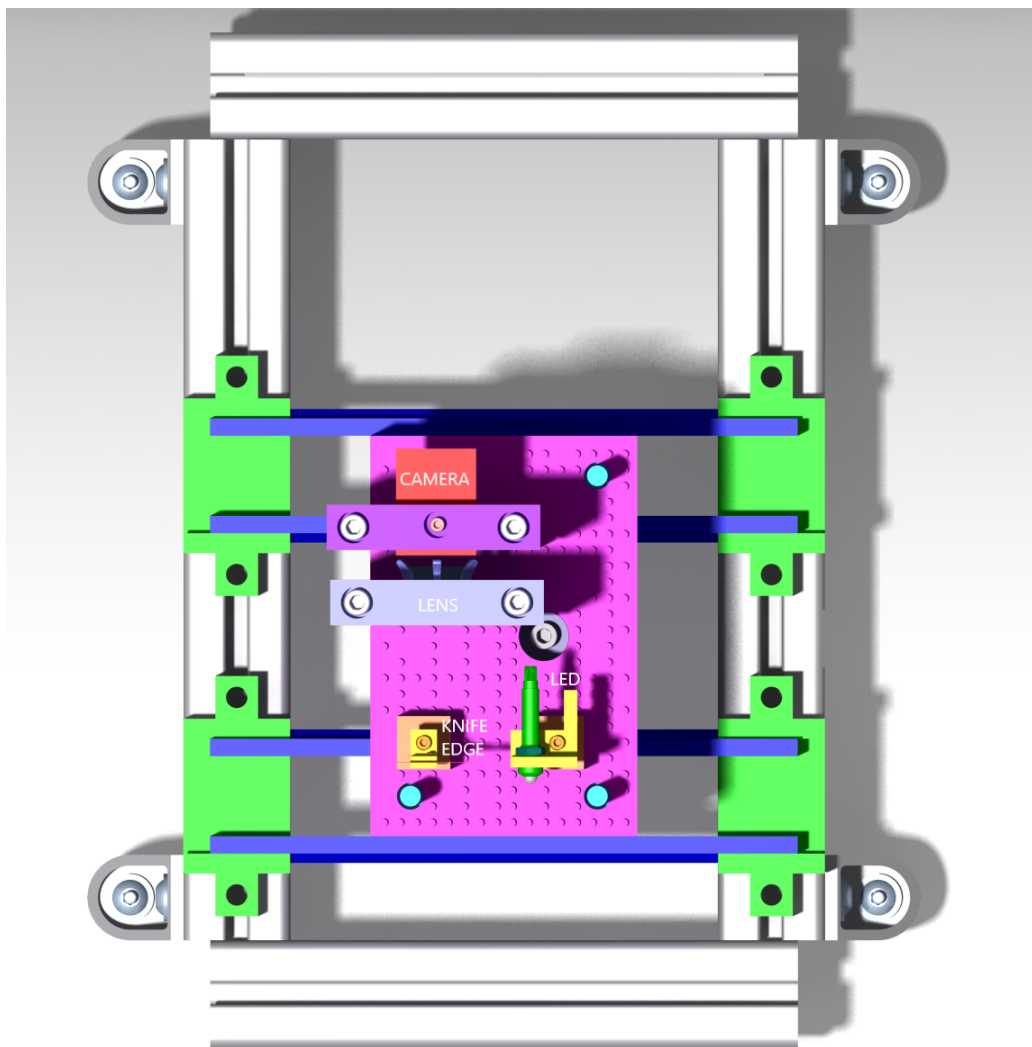


Figure 4.12: Top-view of the optical system (no main mirror) with the main elements indicated.

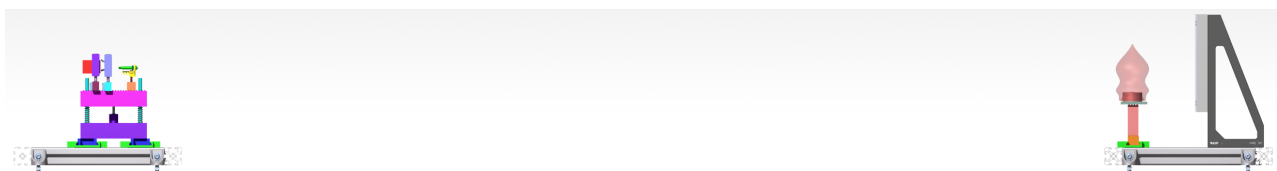


Figure 4.13: Side-view of the optical system (to scale).

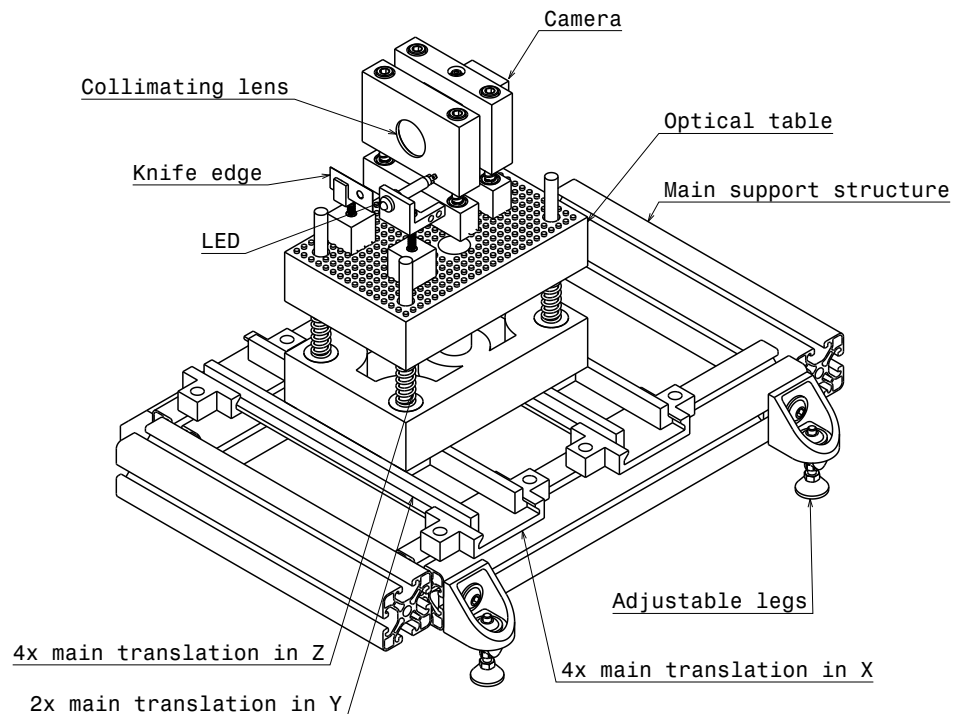


Figure 4.14: Iso-schematic of the main elements from the optics assembly.

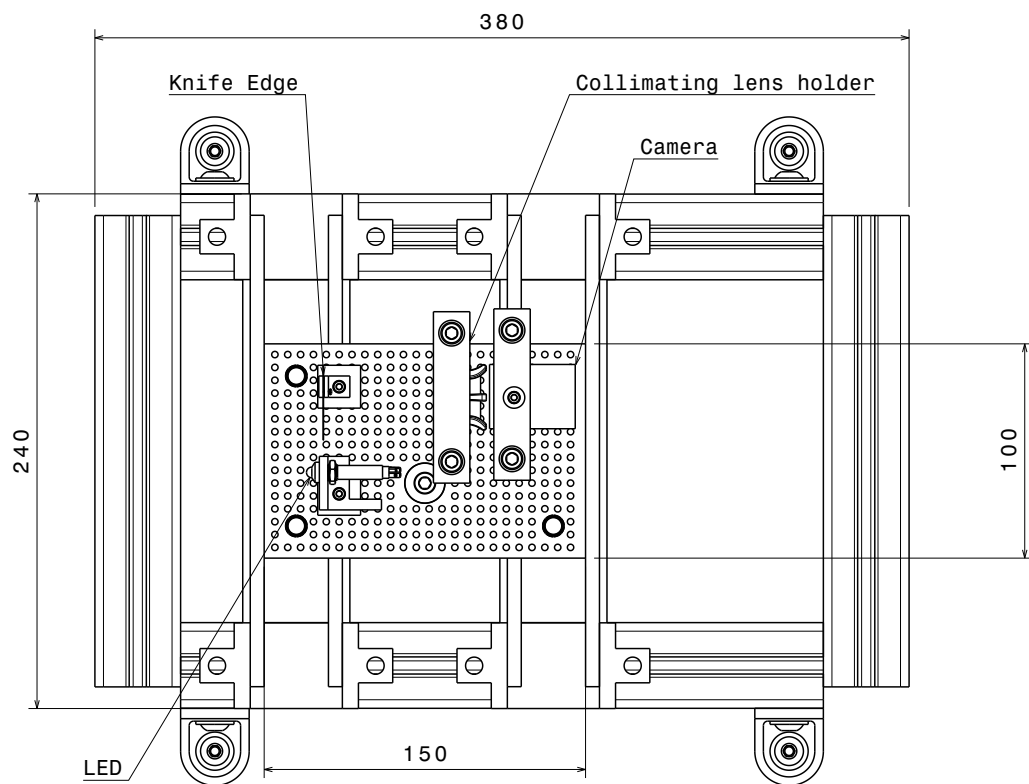


Figure 4.15: Top-schematic of the main elements from the optics assembly.

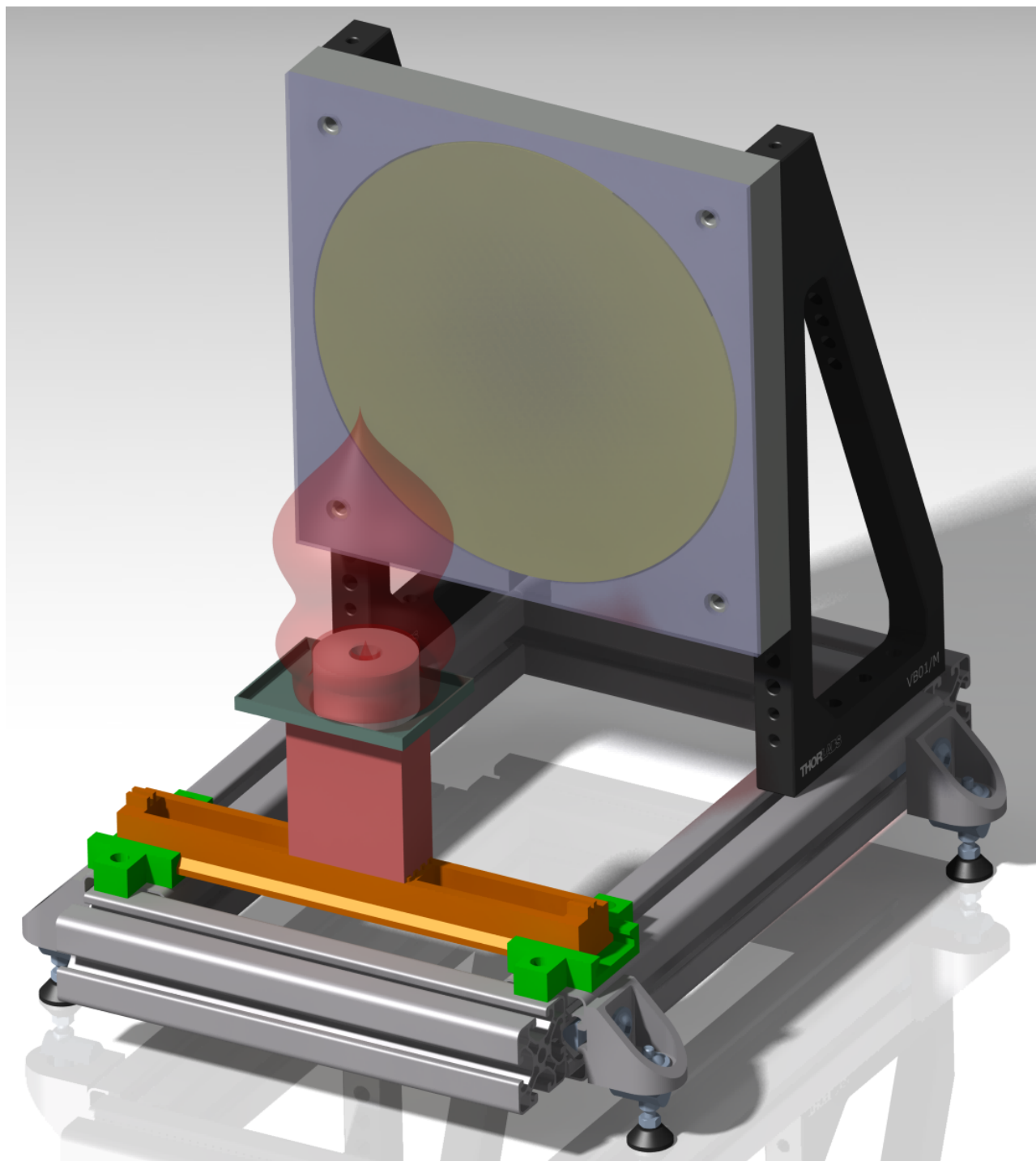


Figure 4.16: Render of the mirror assembly with a burning sample placed in the container.

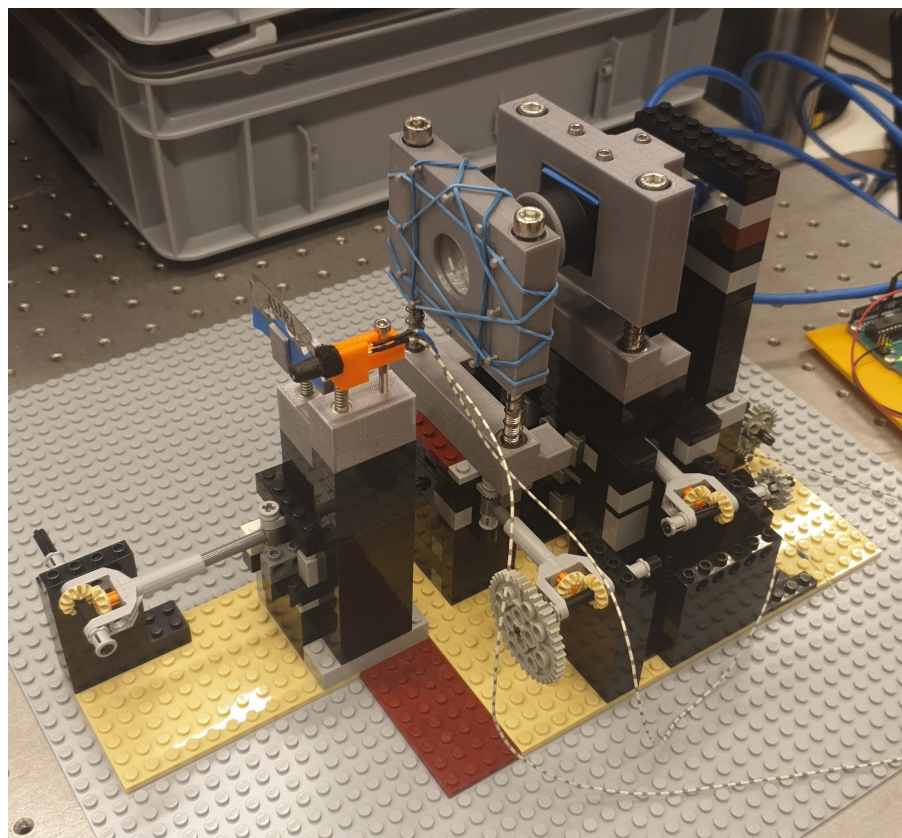


Figure 4.17: The LEGO mount used for 2-axis translation together with the 3D printed supports for the LED, lens, detector and knife edge.

4.3.1 Optics Assembly

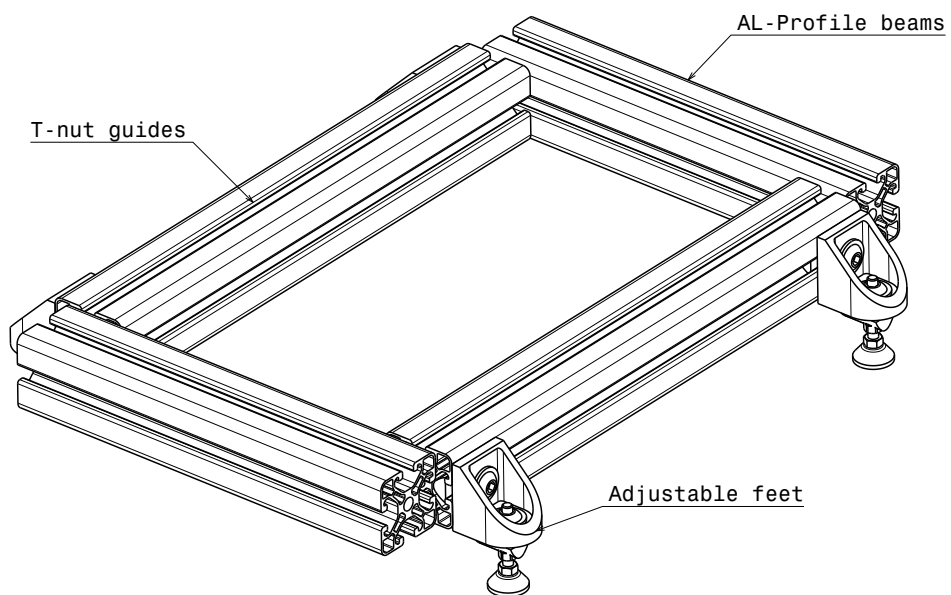


Figure 4.18: Iso-schematic of the support. Made from COTS AL-profiles. The guides allow us to slide inserts and fixate them. This is only usable for rough alignment since the guides do not tightly constrain movement until the inserts are pinned in.

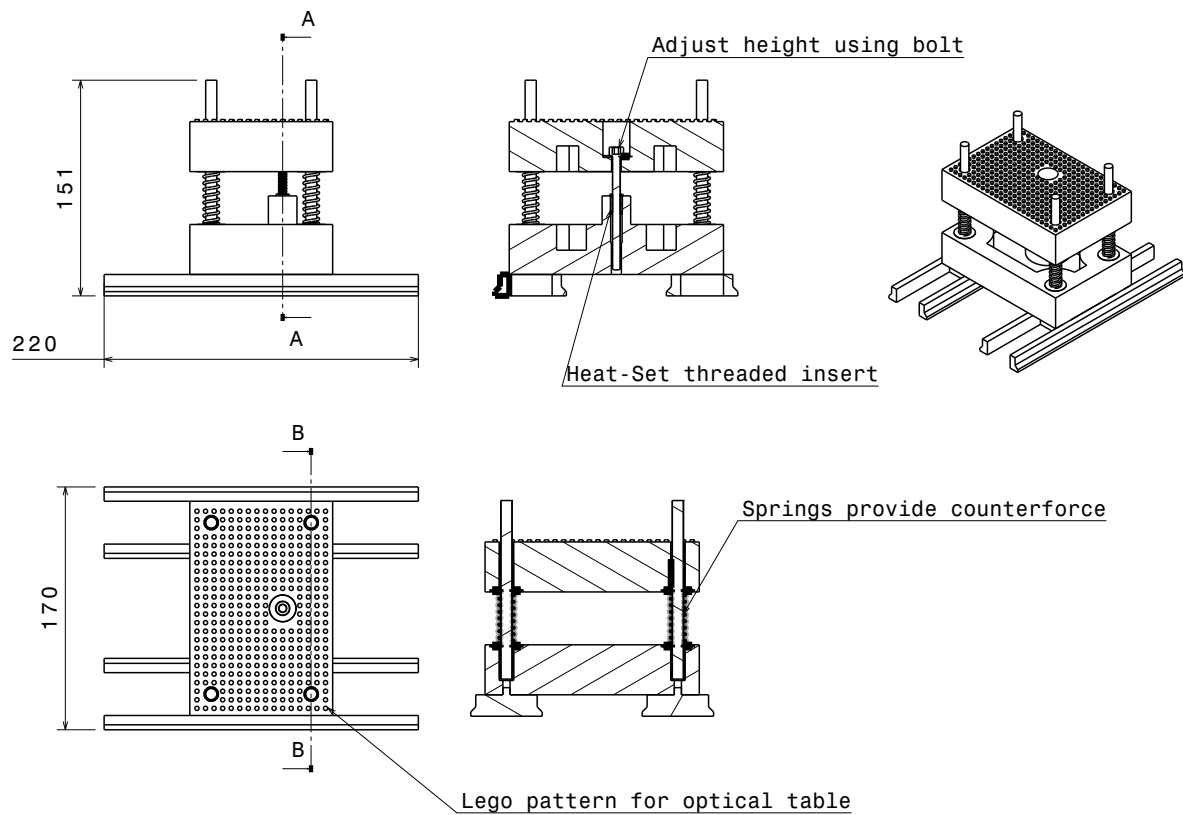


Figure 4.19: Iso-schematic of the main optical table. It can translate in all three dimensions and it can finely translate in the Z dimension. The movement is guided by 4 rods and adjusted using a bolt. The bolt is placed off-axis to not block valuable space on the table. The top of the table has LEGO patterning to allow rough and flexible placement of other optical components.

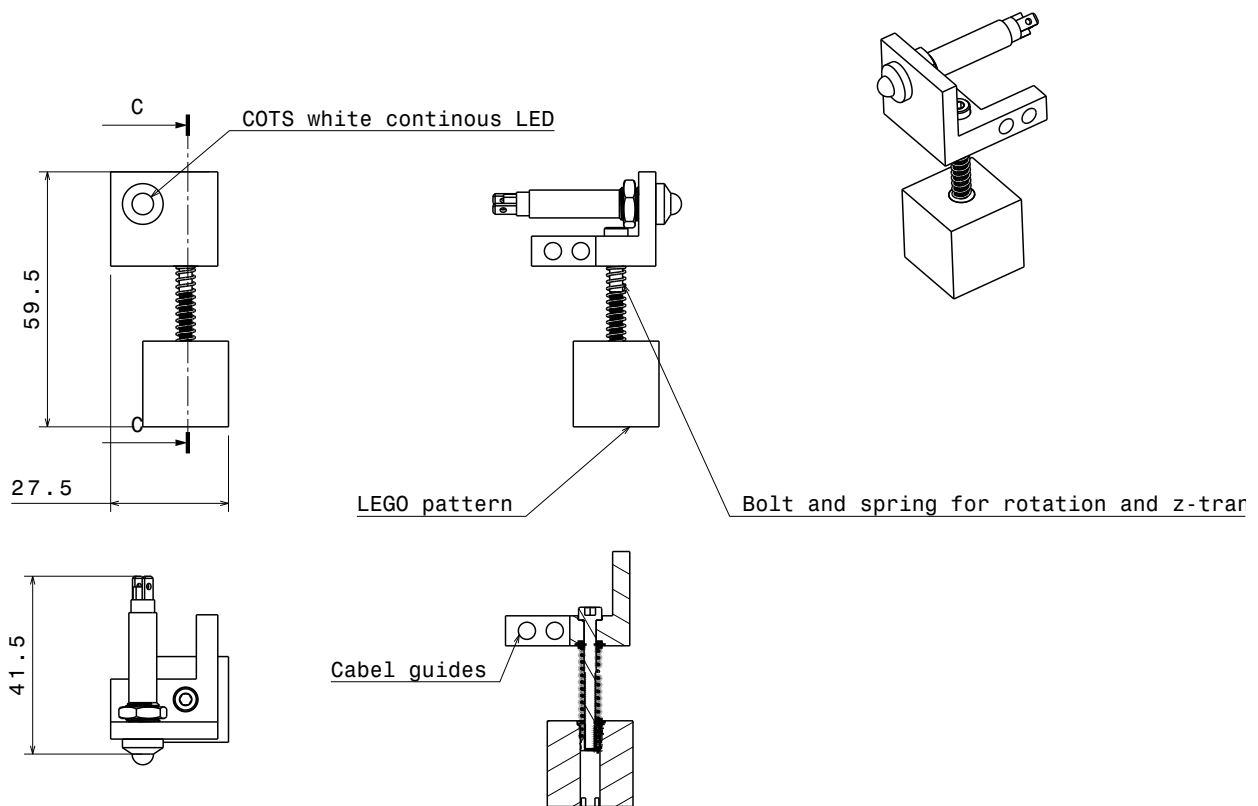


Figure 4.20: Iso-schematic of the LED holder. We use a COTS LED here which is rated for outside use. The LED produces white continues light. The holder has guides for the LED cables. The holder itself can rotate around the bolt axis and translate in Z-direction using the bolt. The bottom of the assembly has LEGO patterning to allow flexible placement.

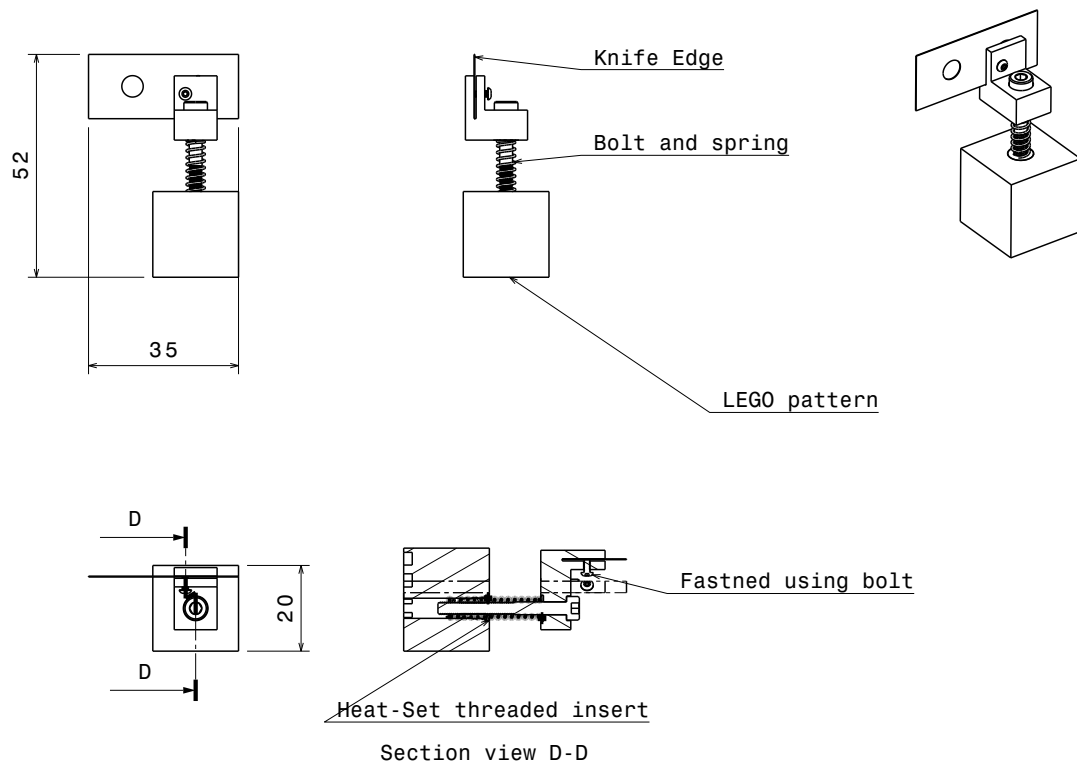


Figure 4.21: Iso-schematic of the knife edge holder. The knife edge is wide enough to not need translation in the Y-direction. The holder itself can rotate around the bolt axis and translate in Z-direction using the bolt. The bottom of the assembly has LEGO patterning to allow flexible placement. If necessary the knife edge can be supported against rotation using a pin.

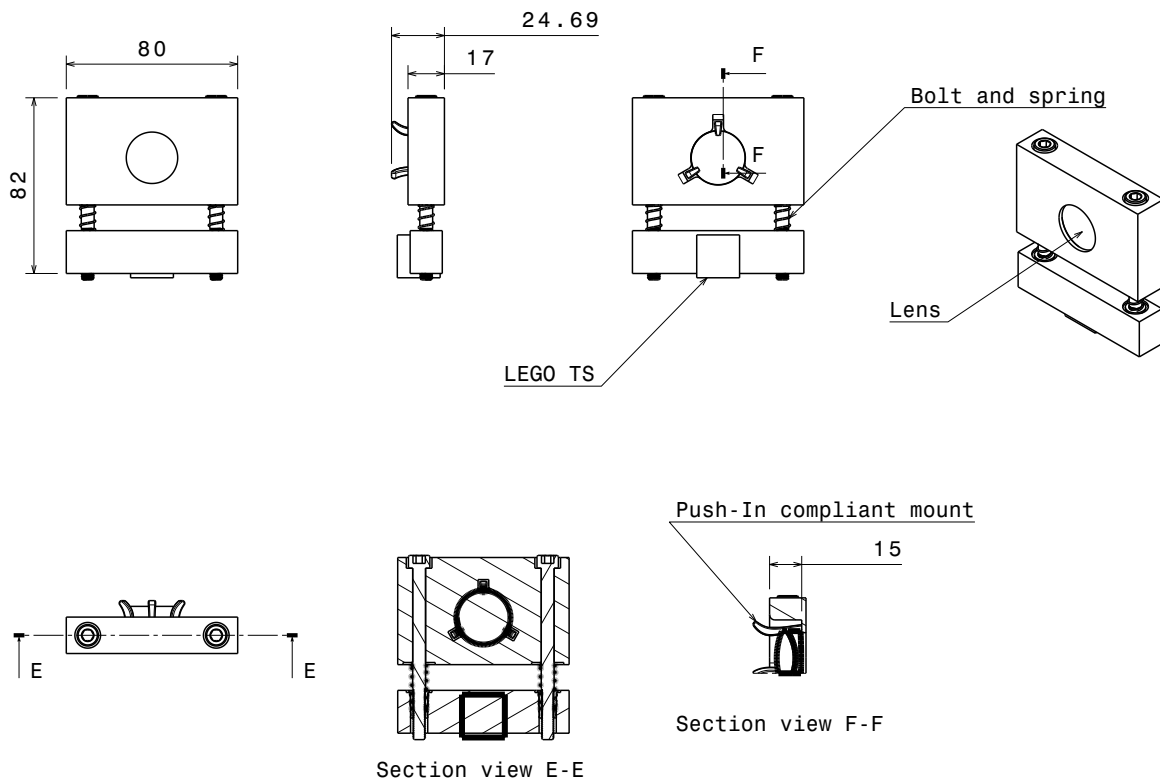


Figure 4.22: Iso-schematic of the collimating lens mount. The mount translates in z-direction and is placed on a LEGO 1-axis (Y) translation stage. The lens is constrained by two bolts and springs (of which either both or one can be actuated). The lens is fixated in three spots using a guiding compliant mechanism which can hold lenses with a smaller depth than 15mm for the 1 inch and >30 mm for the 2 inch version. Here shown is the old, 1 inch version.

The lens holder, shown in [Figure 4.22](#), was the only part that had to be significantly changed after the preliminary design review. When testing it using a 3D printed lens the compliant holders broke along the printed planes. A new design was made which uses rubber bands and two interlocking plates to hold the lens. This design was sufficient for the tests that were performed, however still has issues that can be best addressed by a redesign. These issues are:

- The clamping force on the lens is not sufficient to secure it if the system is shook.
- The pin-hole design is relatively large and wastes space.
- The two printed parts are large and too complex for their purpose, resulting in an inappropriately high failure probability print
- The rubbers will quickly degrade and no longer securely hold the lens.

A new iteration should be based on a screw tightened compliant mechanism that clamps the lens between two C-shapes, a sketch is shown in [Figure 4.23](#).

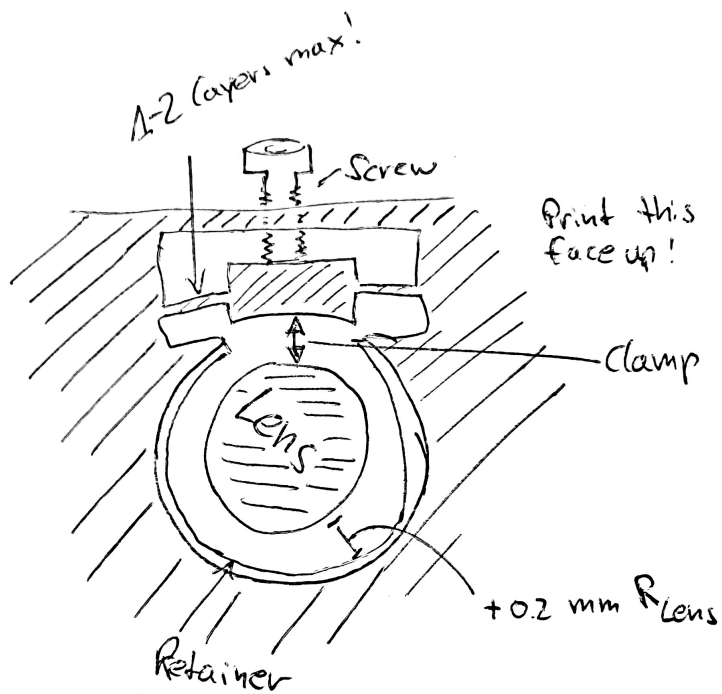


Figure 4.23: Sketch for the next (3rd) iteration of the lens holder. A screw actuated C-clamp holds the lens in place when fastened. The small plastic connections flex allowing pressure on the lens to be exerted over a large area and avoids metal-lens contact. The lens is initially placed in the center and supported by a lip/retainer. The translation mechanisms can be the same as for the older designs.

For testing the lens mount a 3D printed equivalent was used to not damage the actual lens.

The camera holder (Figure 4.24) was changed to allow for three screws to hold the camera. When testing the camera it was found that the cable exerts a significant moment on the camera. Hence the single screw was replaced by three screws in a triangle configuration to better counteract the moment.

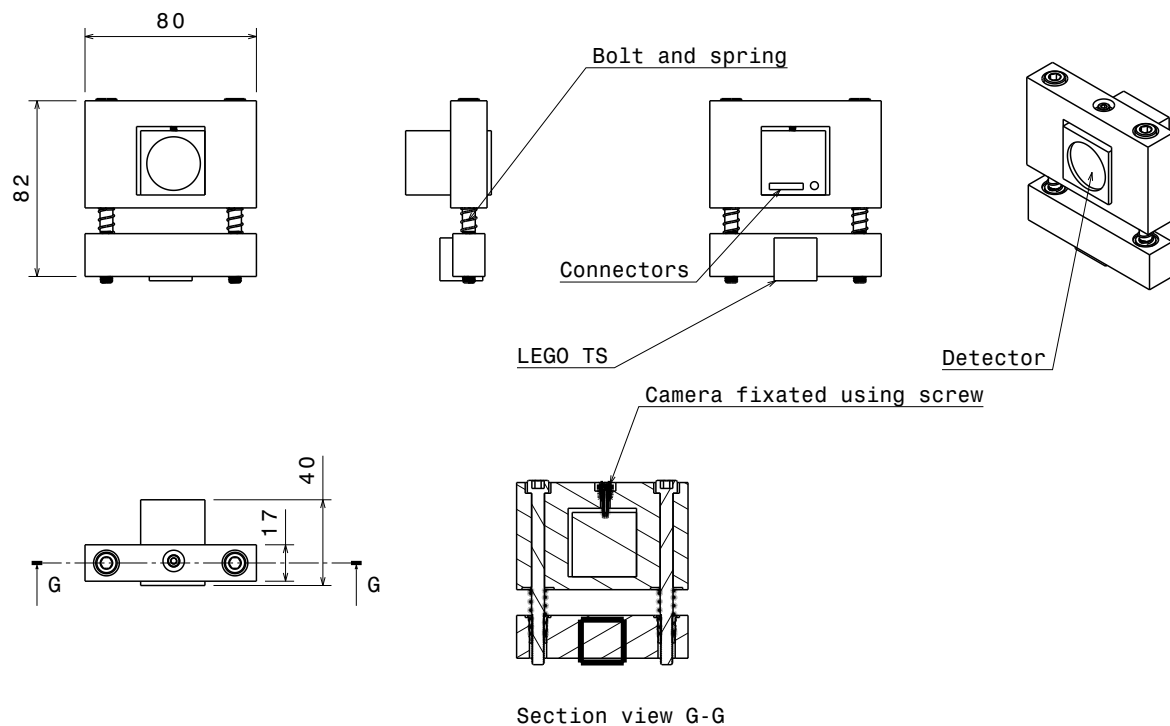


Figure 4.24: Iso-schematic of the camera mount. The mount translates in z-direction and is placed on a LEGO 2-axis (X, Y) translation stage. The lens is constrained by two bolts and springs (of which either both or one can be actuated).

4.3.2 Mirror Assembly

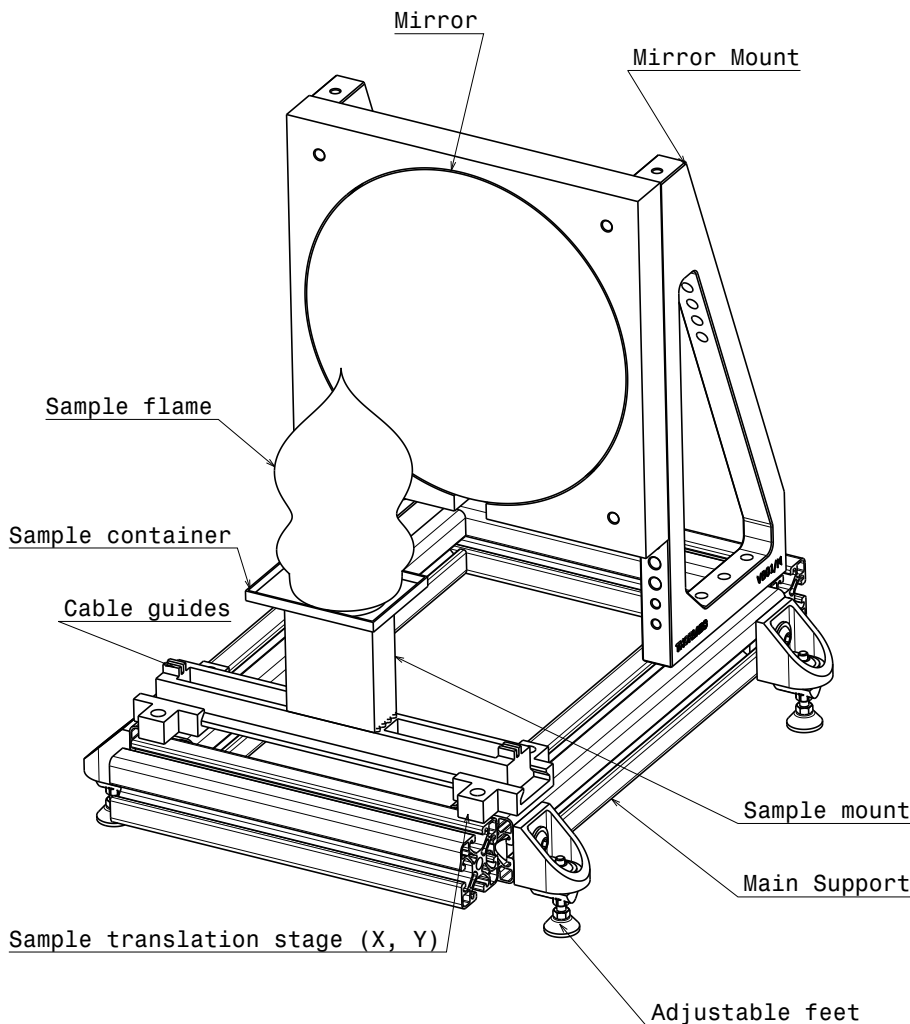


Figure 4.25: Iso-schematic of the main elements from the mirror assembly. The screen is not shown and normally placed in front of the mirror, see [Figure 4.16](#). The support accepts a X, Y translation stage which carries the sample. The sample sits in a metal support cage which is mounted on a LEGO tower. If the samples is electronically ignited the cables can be secured in guides. The mirror mount is fastened to the support using the standard slot nuts.

4.4 Electrical design

The electrical design for our system is relatively simple. As can be seen in [Figure 7.1](#), only the light source and the detector are connected to other components electrically. The light only needs a small cable that connects it to a power source and a switch. Since the light will be turned on before the alignment procedure, its cable can be anywhere, as long as it does not affect negatively other systems. An Arduino will be used to manipulate the light source because it can be easily accessed using a computer. The detector is connected directly to the computer (using a USB type C to USB type A or a USC type C to USC C connector), which is both the power source and the switch for the camera. The cable connecting these two components must be longer than 1 m because we need access to the laptop throughout the experiment without changing anything in the alignment of the system. Thus, even small vibrations caused by walking must be minimized.

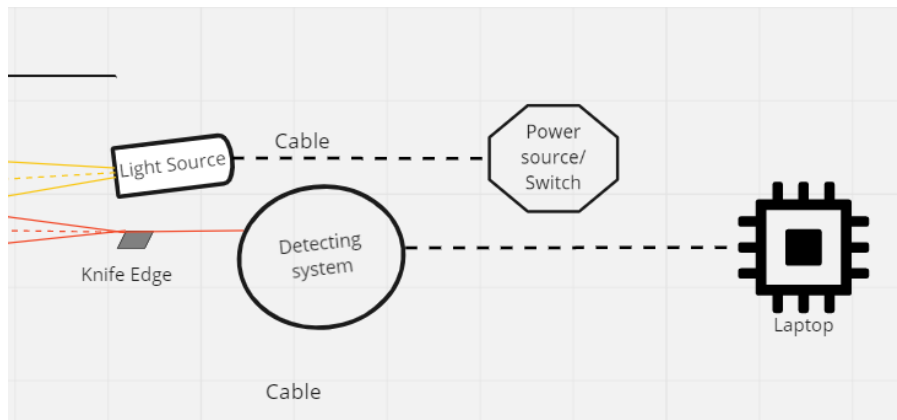


Figure 4.26: Diagram of the required electric system.

The electrical specifications for these components are:

- LED - 8.5 Watts power usage, and an input voltage being between 1.2 to 3.6 V DC. To lower its intensity, it is connected in series with a $220\ \Omega$ resistance for calibrating, and a $4\ k\Omega$ resistance, for imaging.
- FLIR blackfly - 3 W maximum power usage, and an input voltage of 5 V DC.
- Computer - a common laptop has a 65 W power usage, and an input voltage of 100-240 V DC.

Other specifications, like heating and shielding are not important for our simple system.

4.5 Software design

The STRIA system does not use complicated software, its principal science task being to image the burn of an SRM grain. Thus, a crucial software is for reading the output of the FLIR blackfly at different speeds and using different types of files. This software is open source: <https://flir.app.boxcn.net/v/SpinnakerSDK> and it is used for visualizing the camera image in real time. For saving the images, however, we use a designated Python code that is developed by the same company and that can record the science images in bitmap files, at 118 fps.

Another required Python software is for operating the LED using an Arduino board. This short code uses a command to turn the LED on and off.

Lastly, we use Python for data processing. First, we convert all the bmp files from one observation into one large fits file. Then, before analyzing the data, we divide each image with the flat field which is taken at the beginning of each day of observations. We collect 100 images for the flat field and average them to obtain a single file which is used for data processing. When averaging, we only consider the area of the detector which is illuminated by the LED, ignoring the unused region. For more detailed analysis of the velocity distributions and other characteristics of the flow, we use the OpenFlow open-source code.

5 MAIT

In this chapter, we will discuss the following things: Manufacturing, Assembly, Integration and Test plan - in that order.

5.1 Manufacturing/Implementation plan

Optical design:

- **Parabolic mirror:** we use the mirror that the Stakeholders purchased in advance. Thus, there is no lead time. Moreover, if the mirror breaks, we will try to make the Schlieren imager using lenses because they are cheaper and delivered faster.
- **Collimating lens:** we will first check if an appropriate lens is available in the lab on the 5th of April, and otherwise we buy a new one from THORLABS. In the case that it breaks, we order a new one, the lead time being approximately a week.
- **knife-edge:** we will buy a cheap razor blade. In case one breaks or has defects, we can buy another one, the lead time being a day.
- **Mirror cover:** use the cover that is already present. If the cover is damaged, we procure a new one, this process taking approximately one week. If we notice that the cover material is of low quality, we will change the material of the covers, its lead time remaining approximately one week.

Mechanic design:

- See Appendix [Section A.3](#)
- Make/code/Buy/Reuse. Think about lead times, support equipment and contingency.
- **LEGO mounts** - reuse/borrow LEGO bricks that are present in the lab, and buy a number of (used) LEGO bricks that are specifically needed for building the mounts. In case some break, we can buy other pieces, the lead time being a few days.

Electrical design:

- **Light source:** Use the LED from the Arduino box that was already ordered by the Stakeholders. If the LED is damaged, we order a new one, the delivery time being one day. A power source is required and will most likely be another laptop.
- **Camera:** Borrow the FLIR blackfly that is present in the lab. In case of any defects, we will use the PointGrey, because it is the only detector with the same detecting area, so we do not need a new collimating lens.
- **Laptop:** Borrow the laptop from one of our team members to use in the project (future users will have to provide their own laptop). In case of failure, another laptop shall be used.

Software design:

- Detector: we use open source software that works with the FLIR blackfly camera. The lead time for this is a week because a team member needs to install it and test it.
- LED: we use Python to code the Arduino and operate the LED from a laptop. The lead time is one week because of installation and testing.
- Data processing: we use a Python code to visualize and analyze the raw data from the detector. The lead time is two weeks for coding and testing.

5.2 Assembly

In general, we start by assembling smaller subsystems, and adding them together after that. Some things can be done at the same time, while some are dependent on each other. These steps are presented in the order in which they will be conducted in the laboratory.

5.2.1 Ordering parts

We first order the parts that are still needed:

- Aluminium structures
- Bolts, inserts, and other small metal pieces used for connecting different elements
- Lens (possibly)

And buy some small parts from local shops: knife-edge.

5.2.2 Preparations

Detection subsystem:

Install the software, make sure we have all the right cables, and make test images with the camera. We make sure that the software works, and that we can easily access the images/videos right after recording.

LED

Make the LED circuit with the Arduino and the computer. We connect the LED to a resistor in series, and to the laptop, which acts as a switch and power source. As described in [Section 4.2](#), some trial and error was needed to find the right resistor. The final design has a $4.7\text{ k}\Omega$ resistor, which gives enough LED power to observe in daylight, and does not saturate the detector.

Subsystem mounts (LEGO)

When all the LEGO pieces are complete, we prepare the following mounts on top of 5cm x 5cm flat LEGO pieces:

- Mount for the camera
- Mount for the razor blade
- Mount for the LED
- Mount for the lens

For all the mounts, a 3D-printed holder for the lens is needed, which connects the different components with the LEGO mount. This needs to be designed, adapted from some tests that David did, and we need to test for size, and stability when connected to a LEGO surface. Each component will have its own specially designed 3D printed mount.

Before using the expensive components, we make sure that each one of the components can be safely fixed on the mount. For safe testing we can use 3D printed props with the appropriate dimensions instead of using the real camera and lens for testing stability. Most importantly: use a 3D-printed lens to test designs for a 3D-printed lens holder.

Mirror mount

The mirror mount was kindly prepared for us by Robin Schrama, with the courtesy of Remko Stuik from the 'fijn mechanische dienst'.

Preparing the platforms that will carry the mirror assembly and the optical assembly

These steps are the same for the mirror platform and for the platform that carries the lens, knife-edge, light source, and camera.

1. We order the aluminium parts
2. We design the 3D printed connecting surface (partly done)
3. We 3D print the connecting surface
 - (a) Add the translation system for the x- and y-direction

4. We assemble the aluminium parts to our design
5. We attach the 3D printed surface to the aluminium structure
6. We test the movement of the degrees of freedom and fixing them (see [Table 4.4](#))

5.2.3 Putting components together

After the subsystems have been put together, it is time to assemble the complete system.

1. Attach the component mounts of the camera, LED, collimating lens, and knife edge to the components platform
2. Test the degrees of freedom and the stability of the system.
3. Attach the mirror mount to the mirror platform
4. Test for stability
5. Measure the appropriate distance between the platforms, and put them at the positions in which they will be used.
6. Attach the components to their mounts, starting with the cheaper ones: knife-edge, LED, lens, camera.
7. Double check that everything is fixed safely.
8. Safely attach the mirror to the mirror mount.
9. Attach the mirror cover.
10. Begin alignment.

5.3 Integration

In this sections, we explain everything that is we need to do after we assemble the system and before we use it for science experiments.

5.3.1 Alignment of the optical system

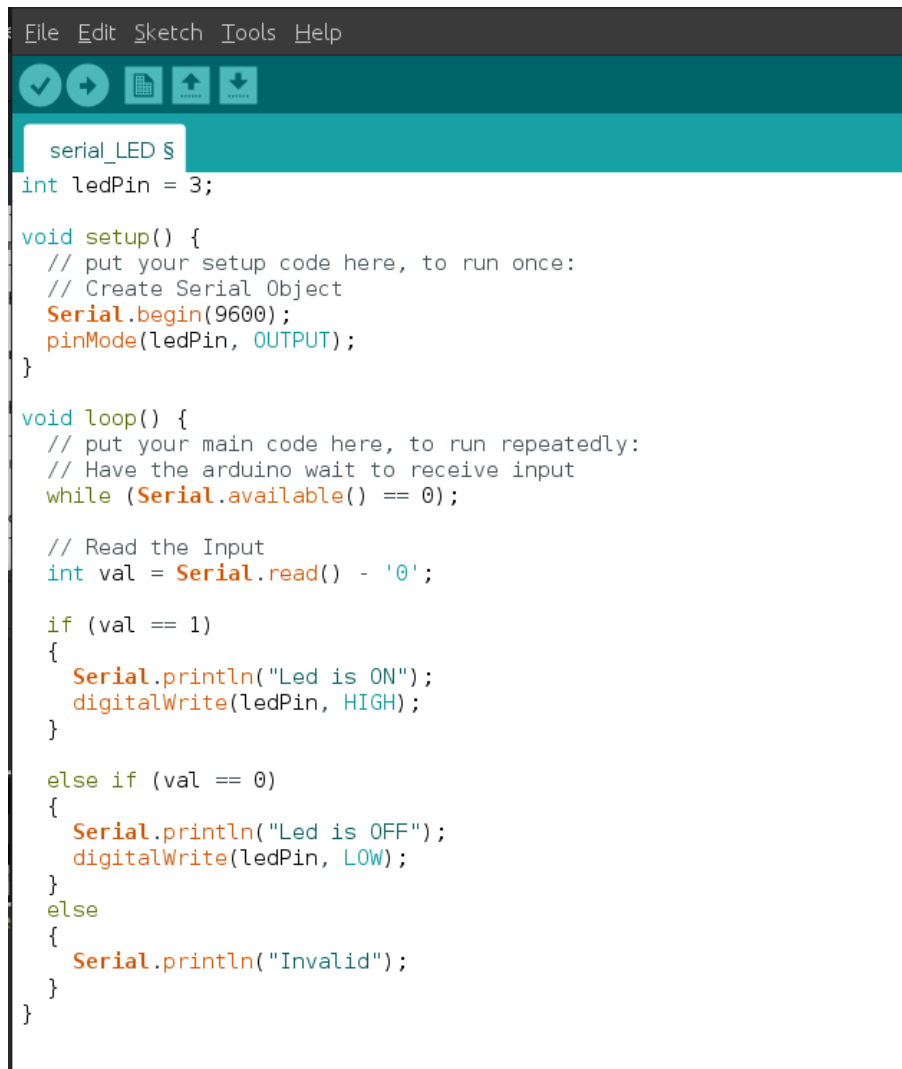
For aligning the optical system, we will use a number of steps:

1. Place the mirror assembly and the optical assembly at their pre-established positions as accurately as possible, by moving them over the tabletop or other surface.
2. Make sure the optics platform is at such a level that the components are aligned within 3 cm on the z-axis with the center of the mirror.
3. First, make sure the LED properly illuminates the full mirror - a white sheet of paper can help to see where light passes the mirror edge.
4. Remove all the covers from the knife edge, camera and lens.
5. Make sure the LED and knife edge are at the right position. They should be as close together in y-direction as possible, at $2f$ distance from the mirror, at equal distance from the optical axis of the mirror.
 - Use the degrees of freedom of the mounts, and a white sheet of paper to fine tune the positions. The LED and the knife edge should be at the same y-coordinate, and the spot size at the knife edge should be as small as possible (~ 3 mm diameter, which is the same size as the opening diameter of the LED).
 - If the knife edge is at the focus, the image should look like a half-illuminated circle - if not, the inner part of the circle will be illuminated on one side, while the outer side is illuminated on the other.
6. Put the lens in line with the point where the light beam is focused at the knife edge, and at a distance of 52 mm in x-direction of it. This step needs the least precision because moving the lens on x-axis with as much as 1 cm does not affect the image on the detector, as we found in the Zemax simulation and optimization.

7. Put the detector at 52 mm behind the lens, but be aware that some fine tuning will be needed to find the best focus. Do this by using SpinView to see the live feed from the camera and by putting an object with small details on the grain's platform. Move the camera until the image centered on the detector and it is as sharp as possible for the human eye.

5.3.2 Integration of electronics and software

- The software for the detector needs to be compatible with the laptop we use: look up the documentation, and test it on the laptop.
- The camera needs to be compatible with the laptop: connect it, and test it. See if we can easily access the data right after the observations.
- Make sure the LED works when connected to the Arduino and the laptop. For the final design, additional electric wires were soldered to the LED, and to pins to connect it to a breadboard. The LED could be switched on and off per laptop-keyboard with the Arduino code presented in [Figure 5.1](#)
- Always make sure we have a power source, and enough cables with the right length, presented in the electrical system before.



```

File Edit Sketch Tools Help
  ↗ ↘ ⌂ ⌃ ⌄ ⌅ ⌆
serial_LED §
int ledPin = 3;

void setup() {
    // put your setup code here, to run once:
    // Create Serial Object
    Serial.begin(9600);
    pinMode(ledPin, OUTPUT);
}

void loop() {
    // put your main code here, to run repeatedly:
    // Have the arduino wait to receive input
    while (Serial.available() == 0);

    // Read the Input
    int val = Serial.read() - '0';

    if (val == 1)
    {
        Serial.println("Led is ON");
        digitalWrite(ledPin, HIGH);
    }

    else if (val == 0)
    {
        Serial.println("Led is OFF");
        digitalWrite(ledPin, LOW);
    }
    else
    {
        Serial.println("Invalid");
    }
}

```

Figure 5.1: Arduino code used to switch the LED on and off from a laptop keyboard.

5.3.3 Safety

Because of the type of experiments we plan to perform, involving burning propellant grains, safety measurements are of particular importance. We discuss both safety to the system and safety for the users of the system.

Safety for users

Once everything is set up, and the experiment is about to start, a few things need to be taken care of:

- Before setting up: getting safety instructions from the appropriate person in Delft about using the propellant grains, and instructions for the (lab)space that we will use.
- Before setting up: check if we need safety goggles for the experiment with the propellant grain
- The laptop is placed at a distance of at least 2 m from the test grain.
- All people involved in the experiment and any spectators need to keep a distance of at least 2 m to the grain. The person igniting the grain is the exception, but he/she needs to wear protective glasses.
- Other people in the area need to be made aware about the experiment and safety measurements.
- Depending on safety instructions, we will decide on how to light the propellant grain on fire, and who will do that.
- There will be a fire extinguisher on site, and at least one person that knows how to use it.
- We wait the appropriate time to be sure that the grain is safe, before we get closer.
- We remove the remains of the grains after they cool down and put them in an area suited for their disposal.
- Use removable cover for the razor blade when it is unused.
- Using the LED does not require glasses or any other kind of protection, but the user should not look directly into it. It is not dangerous long term, but it can cause blindness for a few seconds.

Component safety:

- Check: the burning grain will be close to the mirror cover and the 3D printed platform: how hot will they get? Can they withstand that heat? We check this by putting a flame next to a small piece of the same material used to make the mirror and check how it behaves
- The mirror will be covered with a plastic cover that protects it from splatter and ash. It can be cleaned after use.
- The distance between the burning grain and the optics assembly is large enough as to keep the components in this assembly safe.
- The most expensive component, the camera, will additionally be covered by the components in front of it, and can be covered from the top.
- Stability of all mounts and assemblies will be checked before adding the real components, to make sure assembly is safe.
- The mirror and lens will only be handled while wearing special gloves.

5.3.4 Facilities and support equipment

Most of the testing will be done in the optics lab in the Huygens Laboratory. The actual measurements will be done at a test facility at the TU Delft, that will be specified later.

List of support equipment:

- Extension cord/power strip (borrow/buy)
- Tools (borrow/use own tools)
- Bolts and nuts (optics lab)
- Ruler (3m)
- White sheet of paper to focus light on
- Stockpile of gloves, to carefully handle the mirror and lens with
- Level

5.4 Test plan

In this section we will discuss the tests that will be performed to analyze the performance of the system and the subsystems.

5.4.1 For every component:

- FUN-STRUCT-02: weigh the platform and add it to the calculation of the total weight.
- FUN-STRUCT-03: measure the dimensions with a ruler.
- FUN-STRUCT-06: measure how precise the mechanical remain after perturbations.

5.4.2 Platform

- FUN-STRUCT-01: we place some objects on it, weighing up to a few kg: it might change some z-position, but otherwise it should be stable.
- FUN-STRUCT-01.01: put a ruler next to the platform, and observe what happens if we softly hit the platform
- FUN-STRUCT-01.02: put a ruler next to the platform, and observe what happens if someone walks past, or if something heavy is dropped nearby.
- FUN-STRUCT-03, FUN-STRUCT-05: measure the platform. It should not be larger than 10 cm x 15 cm because of the size of the 3D printer (it can print maximum 18 cm x 18 cm).

5.4.3 LEGO component mount

For the LED, detector, knife edge and collimating lens.

- FUN-STRUCT-01: we place some objects on it, weighing up to a few 100g: it might change some z-position, but otherwise it should be stable.
- FUN-STRUCT-01.01: put a ruler next to the platform, and observe what happens if we softly hit the platform
- FUN-STRUCT-01.02: put a ruler next to the platform, and observe what happens if someone walks past, or if something heavy is dropped nearby.
- FUN-OPT-01: put a ruler next to it and see if it can be adjusted with the required precision.
- FUN-STRUCT-07: check if every mount has the required degrees of freedom, by trying to move it.

5.4.4 Light Source

- FUN-OPT-02: when in place in the complete system: test if it stays in focus by checking if the knife edge is still in focus after some perturbation.

5.4.5 Sample System

- SH-FUN-PERF-03: test this by putting the propellant grain in position.
- FUN-STRUCT-01.01: it should not fall or move when a small shock is applied
- FUN-STRUCT-01.02: it should not fall or move when a small vibration is applied

5.4.6 Parabolic Mirror Assembly

- FUN-STRUCT-01.01: put a ruler next to the mirror, and observe what happens if we softly hit the platform on which it stands
- FUN-STRUCT-01.02: put a ruler next to the mirror, and observe what happens if someone walks past, or if something heavy is dropped nearby.

5.4.7 Beam Cutter System

- FUN-STRUCT-01.01: put a ruler next to the knife edge, and observe what happens if we softly hit the platform on which it stands
- FUN-STRUCT-01.02: put a ruler next to the knife edge, and observe what happens if someone walks past, or if something heavy is dropped nearby.

5.4.8 Collimating System

- FUN-STRUCT-01.01: put a ruler next to the lens, and observe what happens if we softly hit the platform on which it stands
- FUN-STRUCT-01.02: put a ruler next to the lens, and observe what happens if someone walks past, or if something heavy is dropped nearby.

5.4.9 Detecting System

- FUN-STRUCT-01.01: put a ruler next to the detector, and observe what happens if we softly hit the platform on which it stands
- FUN-STRUCT-01.02: put a ruler next to the detector, and observe what happens if someone walks past, or if something heavy is dropped nearby.

5.4.10 Electronics

- FUN-PERF-05: we measure the distance from the grain to the laptop used to record the data.

5.4.11 Software/Computer

- FUN-PERF-02: observe for 10 seconds and calculate the mean number of images per second that were taken.
- FUN-PERF-03: do test observations and measure the time it takes before they can be viewed with the software. It should be < 2 minutes.

5.4.12 System tests

- SH-FUN-PERF-02: a candle or some other source of air disturbance will be placed in the optical path, close to the mirror, and some test images will be taken to see if the disturbances are visible.
- FUN-PERF-01: an image of the LED, which is known to emit optical light, is taken and checked if it is detected by the detector. We check if there is any stray light in the system from the LED due to other unexpected reflections.
- FUN-PERF-04: performance with lights on will be compared to the performance with the lights off (compare the contrast in both images)
- FUN-PERF-06, FUN-PERF-07, FUN-PERF-08: look at the output data on a laptop.
- FUN-STRUCT-01, FUN-STRUCT-06: Observe what happens to the spot on the detector when individual components or groups of components are disturbed, or if someone walks by.
- FUN-STRUCT-02: calculate the sum of the weights of the individual components, it should be less than 20kg.
- FUN-STRUCT-03: calculate the volume of all disassembled components. It should fit within 2mx2mx1m.
- FUN-STRUCT-05: test if the team can carry all the disassembled components in a safe manner (without risk of damage)
- FUN-OPT-02: after some other tests, check if the light source is still focused on the knife edge, by analyzing the image on the detector.
- FUN-STRUCT-04: we check how much heat can the different materials withstand using a lighter.

5.5 Reusability

All parts will be connected in a way that it can be disassembled in the future. Components are either held in place with bolts and screws, or with LEGO connections. The complete system can be reused for other experiments, or the individual components can be reused. The LEGO mounts can be completely disassembled, and all parts can be reused. The mirror mount is specifically tailored to the mirror, and will therefore probably not have any other use. The system could even be adapted with a different detector and a different lens, if needed. If any mechanical part is damaged by the grain, it can be replaced: the mirror cover can be renewed or changed, while the supports can be replaced because they are cheap and mainly made of LEGO or 3D printed parts.

6 Building

In this section, we briefly describe some of the steps that were involved in the building of the Schlieren Imager. For more details, see the "PROCEDURES" document.

Before putting all the components together, different people worked on different parts of the system to make them functional for the final assembly.

LED

A yellow LED has been selected for the system and connected in series with a resistor. To make the electrical system, a breadboard was used from the Arduino building set, to which the LED was connected by 50cm long conducting wires. An Arduino Uno was connected to the breadboard as a controllable powersource (connection to GRND and one of the serial pins, that is controlled with software, as in [Figure 5.1](#)). The Arduino was connected to a laptop on which Arduino IDE was installed. We started with a resistance of $220\ \Omega$ to not burn the LED, but have a bright spot for alignment. After some trial and error we found the $4.7\ k\Omega$ resistor to be the best one to prevent saturating the detector while still creating a clear image. The laptop acts as a power source and as a switch for the LED. Connections between the LED and conducting wires, as well as between the wires and small conducting pins that connect to the breadboard, were soldered and covered with shrinking rubber for safety.

Detector

We install the SpinView program which is used to control the FLIR Blackfly. Moreover, a Python code is also obtained from the open-source directory, which can be used to collect the data easier and in the right format (bitmap).

3D prints

We print the already designed components and try to see if they work as expected. We put the inserts and check if they fit properly without damaging the support significantly. Several tries are required until we achieve the required accuracy and stability. We check if they are compatible with LEGO pieces and if they do not damage any of the components while keeping them stable.

LEGO

We build the LEGO system on a platform. Several tries are needed to acquire the required stability and mobility. It is essential for these components that they move freely in the required directions, but also that they remain stable once the transition ended.

Assembling the system

After the individual components are ready to be used, we start assembling the system. First, we put the mirror on the mount and we fix it to the optical table. Then, we add the lens to its mount using gloves and a soft surface below it in case it drops. We make sure that it is stable, using rubber elastics. The camera, LED, and knife edge with its protective material follow, and we make sure that they are stable in their support. Lastly, we connect the camera to the laptop using its cable, but we make sure that the cable is inserted into its LEGO support so that it does not destabilize the detector. Lastly, we remove the protection from the knife edge, connect the LED and the detector to their specific laptop.

To power up the detector, we first open the SpinView program, then we connect the cable to the laptop, and open the live feed without recording. After this, we remove the protective plastic to check if it is detects any light. In case of the LED, we open its specific Python code and manually turn it on from the terminal.

7 Calibration

After the system is fully built, we have to calibrate it before we can start the scientific observations. The calibration consists of multiple steps which must be made in a specific order, and are presented below.

7.1 System calibration

1. Place the platform with the LED, detector, knife edge and collimating lens at approximately 2.4 m from the parabolic mirror such that the axis from the center of the lens passes exactly in between the LED and knife edge. Doing this very precisely helps making the next steps a lot easier!
2. Put the $220\ \Omega$ resistor in series with the LED.
3. Start the laptops.
4. Start SpinView.
5. Connect the camera.
6. Turn on the camera livestream.
7. Remove the cover of the camera.
8. Turn on the LED (enter 0 on the laptop that controls the LED).
9. Adjust the LED until it points towards the center of the mirror (checking if it passes the mirror edges by holding a white sheet of paper behind it).
10. Move the platform along the x axis until the light appears focused on on the knife edge.
11. Repeat steps 9 and 10 until the LED is pointing towards the center of the mirror and is focused on the knife edge - this is the case if the spot at the knife-edge is round, sharp, and as small as possible.
12. Adjust the position of the knife edge on x axis to better focus the beam on it.
13. Adjust the z position of the knife edge so that it cuts the beam exactly in half.
14. Place the screen in between the knife edge and the lens to check if half of the beam is cut.
15. Move the lens on the y axis until the light beam is centered on it.
16. Move the lens on the z axis until the light beam is centered on it.
17. Move the detector on z and y axis until the light is centered on the detecting area. Use the live stream from the camera to visualize it.
18. Change the resistor from $220\ \Omega$ to $4.7\ k\Omega$ to not saturate the detector.
19. Put an object with sharp features in the position of the sample object.
20. Move the detector on the x axis until the image becomes focused.
21. Test if the camera records using SpinView and the Python code.

7.2 Extra step for better imaging

During the first set of observations, we noticed that the object appears to have two images on the detector, no matter how close we put it to the mirror. This happens because the light passes twice through the observed medium, from different directions. To partially fix this, we moved the LED and the knife edge as close together as we could, and we calibrated the system again. The result was that, at 15 cm from the mirror, the image became sharp and there was only one image (image). However, when we move closer to the mirror the double image appears again (image). Thus, we recommend that the sample system is positioned as close as possible to the mirror, and not more than 1 m away from it. For the results in the following section the double image has a negligible result, visible at most as a blurred contour on a 1-3 pixel scale (compare e.g. [Figure 9.10](#) to [Figure 9.5](#) where sub-mm structures are very clearly visible).



Figure 7.1: The image of an object at 15 cm from the mirror. The image is not doubled and sharp.

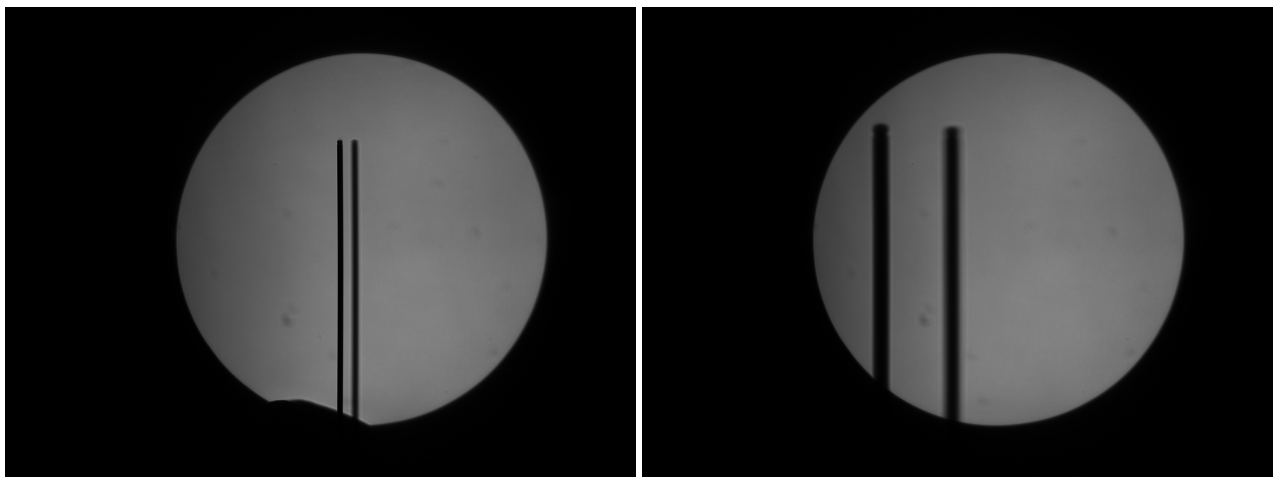


Figure 7.2: Image of an object at 1 m (left) and 2 m (right) from the mirror. We can clearly see that the image is doubled.

8 Test Plan

To verify if the system and its subsystems operate as expected, we performed a series of tests, as described in the testing plan. We use the same structure as presented in [Chapter 5](#), for an easier analogy between the pre-defined tests and the conducted ones.

8.1 For every component:

- FUN-STRUCT-02: we weighted the platform which contains the LED, lens, knife edge, and camera and it has approximately 5 kg. The same approximate weight has been found for the mirror and its mount. We did not weigh the grain, its support, and the aluminum beams yet because the system did not reach the final phase yet, but, considering their dimensions and material, they are well below 10 kg. Thus, we can confirm that the system is lighter than 20 kg.
- FUN-STRUCT-03: we used a ruler to measure the different components. The platform with the LED, knife edge, detector, and lens is approximately 30 cm x 30 cm x 20, and the primary mirror with its support is 10 cm x 20 cm x 20 cm. We did not build the grain platform and the aluminum bars, so we could not measure it, but we know that the grain has the dimensions of 5 cm x 5 cm x 10 cm. Thus, if the sample mechanical system and the aluminum bars respect the presented sizes, the system fits in the 2 m x 2 m x 1 m space.
- FUN-STRUCT-06: we aligned the system and then, perturbed the system with 1 mm in every direction. The images remained sharp and centered on the detector, so the system can sustain small perturbations.

8.2 Platform

- FUN-STRUCT-01: we pressed the components on the z-axis by hand until the string's length diminished by 1 cm. The system remained stable, meaning that it can maintain small loads, larger than the components' weight.
- FUN-STRUCT-01.01: we hit the platform lightly, and we observed that none of the components moved more than 1 mm from their initial positions, meaning that they are stable in their mounts.
- FUN-STRUCT-01.02: we walked past the system and hit the table with our hands, but the system did not move more than 1 mm from their initial positions, meaning that it can withstand small perturbations.
- FUN-STRUCT-03, FUN-STRUCT-05: we measured the platform and we noticed that it is 30 cm x 15 cm. Since it does not fit with the current design, we decided to slightly change the design (see [Appendix B](#)).

8.3 LEGO component mount

For the LED, detector, knife edge and collimating lens.

- FUN-STRUCT-01.01: we hit each component lightly, and we observed that it did not move more than 1 mm from their initial positions, meaning that it is stable in its mount.
- FUN-STRUCT-01.02: we walked past the system and hit the table with our hands, but the component did not move more than 1 mm from their initial positions, meaning that it can withstand small perturbations.
- FUN-OPT-01: we used a ruler and moved each component on all of its axis of freedom. All the movements are smooth and the precision of 1 mm can be easily achieved.
- FUN-STRUCT-07: we checked if the components move on all of their required axis of freedom, presented in the technical requirements and we found out that they all work properly.

8.4 Light Source

- FUN-STRUCT-01.01: we hit the component lightly, and we observed that it did not move more than 1 mm from their initial positions, meaning that it is stable in its mount when connected to the LEGO platform.
- FUN-STRUCT-01.02: we walked past the system and hit the table with our hands, but the component did not move more than 1 mm from their initial positions, meaning that it can withstand small perturbations when connected to the LEGO platform.
- FUN-OPT-02: after we aligned the system, we perturbed the light by slightly touching it. The LED always came back in its initial position, keeping the system focused.

8.5 Sample System

- SH-FUN-PERF-03: we did not do this test because we did not use the propellant when this document has been written.
- FUN-STRUCT-01.01: we did not do this test because we did not use the propellant when this document has been written.
- FUN-STRUCT-01.02: we did not do this test because we did not use the propellant when this document has been written.

8.6 Parabolic Mirror Assembly

- FUN-STRUCT-01.01: we hit the component lightly, and we observed that it did not move more than 1 mm from their initial positions, meaning that it is stable in its mount when connected to the optical table.
- FUN-STRUCT-01.02: we walked past the system and hit the table with our hands, but the component did not move more than 1 mm from their initial positions, meaning that it can withstand small perturbations when connected to the optical table.

8.7 Beam Cutter System

- FUN-STRUCT-01.01: we hit the component lightly, and we observed that it did not move more than 1 mm from their initial positions, meaning that it is stable in its mount when connected to the LEGO platform.
- FUN-STRUCT-01.02: we walked past the system and hit the table with our hands, but the component did not move more than 1 mm from their initial positions, meaning that it can withstand small perturbations when connected to the LEGO platform.

8.8 Collimating System

- FUN-STRUCT-01.01: we hit the component lightly, and we observed that it did not move more than 1 mm from their initial positions, meaning that it is stable in its mount when connected to the LEGO platform.
- FUN-STRUCT-01.02: we walked past the system and hit the table with our hands, but the component did not move more than 1 mm from their initial positions, meaning that it can withstand small perturbations when connected to the LEGO platform.

8.9 Detecting System

- FUN-STRUCT-01.01: we hit the component lightly, and we observed that it did not move more than 1 mm from their initial positions, meaning that it is stable in its mount when connected to the LEGO platform.
- FUN-STRUCT-01.02: we walked past the system and hit the table with our hands, but the component did not move more than 1 mm from their initial positions, meaning that it can withstand small perturbations when connected to the LEGO platform.

8.10 Electronics

- FUN-PERF-05: we measured the distance from the test object to the laptop used to record the data, and found a distance of 2 m, which is a safe distance that makes operating the system easy, without de-calibrating it.

8.11 Software/Computer

- FUN-PERF-02: we observed for 10 seconds and calculated the mean number of images per second that were taken. We found that the detector works at 118 fps, as stated in its manual.
- FUN-PERF-03: we measured the saving time and found out that the images can be accessed a few seconds after the recording stopped, making the accessing time significantly less than 2 minutes.

8.12 System tests

- SH-FUN-PERF-02: we used a compressed air spray at approximately 15 cm from the mirror to check if the system detects disturbances in the air. We tested this without the plastic cover, and with it, we could detect air disturbances in both tests.
- FUN-PERF-01: After we aligned the system, we used the live feed from the SpinView program to observe the light spot. It is easily detected by the detector, meaning that the system detects optical light. We also found no stray light from the LED in our system.
- FUN-PERF-04: we compared the performance with the lights on and with the lights off. In both cases, both with the mirror cover and without it, the system worked properly. We can detect changes in the spectral index with high contrast. The only difference is that the overall image with the lights on is slightly brighter, but it is less bright than the LED.
- FUN-PERF-06, FUN-PERF-07, FUN-PERF-08: we took a couple of test pictures/videos and check if we can easily access them from the laptop. We first used the SpinView program and both images and videos could be recorded and saved directly in a specific folder which can be accessed seconds after the test image/video is acquired. When using Python, we could only save images that are, again, available after a few seconds in a specific folder.
- FUN-STRUCT-01, FUN-STRUCT-06: we slightly hit each component, moved next to the optical table, and hit it with our hands, and we noticed that the image on the detector did not change its location and it was still in focus.
- FUN-STRUCT-02: we calculated the sum of the individual components and their weight is below 10 kg. We did not include the sample system and the aluminum beams, so the total weight is larger, but it does not exceed 20 kg.
- FUN-STRUCT-03: We calculated the volume of the individual components and it does not exceed 1 m x 1 m x 1 m. We did not consider the sample system and the aluminum beams but considering their size and the fact that the aluminum beams can disassemble, we do not expect the total volume to overcome 2 m x 2 m x 1 m.
- FUN-STRUCT-05: we carried the LEGO platform with all the components in the laboratory, and saw that it is easily transportable to the car/bus. We do not think that it is safe to transport it by bike because of all the shocks which will be felt by the lens in its mount. This is the most sensitive component, the mirror mount, aluminum beams, and sample system being easily transportable by any means of transport.
- FUN-OPT-02: We are easily able to use the system for more than 2 hours, without re-aligning it. Putting objects on the table and walking next to the system does not change its alignment.
- FUN-STRUCT-04: We did not test the system using a heat source next to the plastic cover to see possible damage. However, we put a candle at 15 cm from the mirror and everything remained undamaged.

9 Results

9.1 Image Analysis

The images were processed using python code that sorts the raw bitmap files in the correct order and then converts them to FITS image cubes that can be further processed.

We also made use of OpenOpticalFlow (Liu, 2017) to process the images and determine the velocity and vorticity of the flow.

9.2 Cover vs. no cover for the primary mirror

When testing the system, we analyzed the images that result if we remove the cover, or if we keep it on. Keeping it on induces a chessboard-like pattern that is very distinct, while not using the cover gives a smooth, uniform background. For the following tests, we decided to remove the cover for processing the data easier, but the chessboard-like pattern can be removed from future images, by dividing the science images with it (in the same way that we correct for the flat field).

9.3 Spray Up

In order to fulfill the primary science goals we need to show that the system can extract the flow field from images of dynamic, turbulent flow. We used a optical cleaning duster evaporating 1,3,3,3-Tetrafluoropropene (HFO-1234ze(E), R-1234ze) to produce a jet of gas. (GmbH, 2021) 1,3,3,3-Tetrafluoropropene has a refractive index of 1.284 and is thus easily visible when surrounded by air. (Harvey, Paulechka, and Egan, 2018) When a layer of fast flowing medium is adjacent to a layer of slower flowing medium the interaction of the boundary layers at the interface produces sheared vortices, see Figure 9.2. These vortexes grow in size as the length of the interaction increases and under ideal conditions dissipate into smaller eddies down to the Kolmogorov scale.

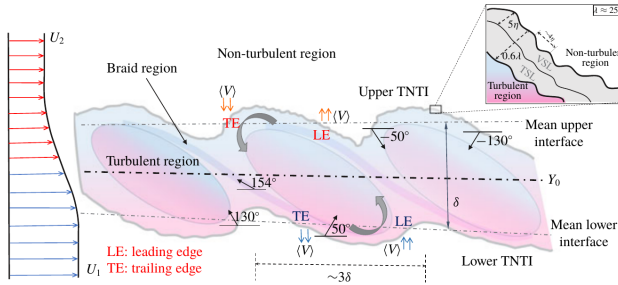


Figure 9.1: Schematic of the turbulent-non-turbulent interface showing the forming vortices. The flow velocity of the two layers is shown on the left as U . (Balamurugan et al., 2020)

Using these differently sized vortices the resolution of the system specifically for vortices can be determined. For high Reynolds number flows these vortices and eddies significantly contribute to mixing of gas as well as energy dissipation from kinetic to thermal and acoustic energy. (Pope and Pope, 2000) Consequently, they contribute and dominantly feature in combustion and transient ignition of solid propellants as they mix burning, hot and cold gas during ignition induction and flame spreading stages of ignition. While the energy transfer from large to small eddies and the dissipation of these small eddies is small compared to heat released by the combustion, the small eddies typically disturb the flame front and thus trigger significant changes in combustion heat release. (Spalding, 1977) For ideal, premixed combustion optimal ignition is reached when the Klimov–Williams criterion is met or exceeded, so the Karlovitz number is smaller than unity. This means that the flame thickness is smaller than the Kolmogorov scale and hence unaffected by the turbulence of the field. (Turns et al., 1996) However, this is generally not the case for solid rocket motor ignition and hence a good test for the system is estimating the Kolmogorov scale and turbulent energy dissipation rate from the integral length scale and assumptions about the fluids. It is noteworthy that the test on which we base the investigation is

1,3,3,3-Tetrafluoropropene injection into a static fluid instead of combustion and hence the result is not fully representative of the actual process and will be in terms of combustion variables.

The turbulent energy dissipation rate can be estimated using [Equation 9.1](#) (Pope and Pope, 2000), where we estimate the RMS of the velocity fluctuations $u'(l_t)$ as 10% of the mean injection velocity¹ and the integral length l_t is found from the images.

$$\varepsilon \approx \frac{u'^2(l_t)}{r/u'(l_t)} = \frac{u'^3(l_t)}{l_t} \approx \frac{(50\text{mm}/\text{s})^3}{4\text{mm}} = 0.03125\text{m}^2/\text{s}^3 \quad (9.1)$$

The result of [Equation 9.1](#) seems reasonable when looking at the divergence of the flow, however it should be noted that it is based on maxing through shear and not combustion.

The Kolmogorov length η_k can then be found using [Equation 9.2](#) (Pope and Pope, 2000), where ν is the kinematic viscosity of the medium, which we estimate for slightly cool 1,3,3,3-Tetrafluoropropene at 1 bar as $\nu = 15.93 \times 10^{-6}\text{m}^2/\text{s}$ (ETB, 2018).

$$\eta_k = \left(\frac{\nu^3}{\varepsilon} \right)^{1/4} \approx 0.6\text{mm} \quad (9.2)$$

The resulting Kolmogorov lengths seems slightly too large since eddies of that size should be resolvable in the images but are not prevalent. However, this could also be due to the cut-off in the image, i.e. they only appear later in the flow or them being lost in the 3D flow field as they are expected to form mostly inside the turbulent 1,3,3,3-Tetrafluoropropene flow. A test was conducted where the injection was significantly faster, which should speed up the breakup of the eddies, which is shown in [Figure 9.3](#).

The largest eddies are roughly on the same scale as for the slower injection, however and recomputing the Kolmogorov length for the faster injection yields $\eta_k \approx 0.36\text{mm}$ which corresponds to the smallest eddies resolved in the turbulent flow and interface.

Since we were unsure weather this faster flow would be sufficient to resolve the eddies inside the FOV of the setup we conducted an even faster injection test, which is shown in [Figure 9.4](#). The structure that is visible in these images is shown magnified in [Figure 9.5](#).

The pattern has the following characteristics:

1. High contrast, alternating regions of bright and dark along the central axis of the flow
 - (a) Bright regions are shaped like convex-convex disks
 - (b) Dark regions are shaped like concave-concave disks
 - (c) The disks are clearly separated near the center axis of the flow but less clearly separated with increasing separation from the center axis
2. The distance between the regions decreases with increasing separation from the outlet
3. The contrast and visibility of the regions decreases with increasing separation from the outlet
4. The diameter (height in the images) of the bright disks decreases with increasing separation from the outlet
5. The pattern is concentric but angled w.r.t. the center axis of the flow
6. The separation between one bright and the next bright region as well as their clarity increases with increasing back-pressure (increasing actuation of the compressed 1,3,3,3-Tetrafluoropropene valve)
7. For steady state there is structure visible inside the disks which look more like peanuts/bubbles inside the flow
8. The pattern is surrounded by unresolved flow

These features are characteristic for a shock train, schematically shown in [Figure 9.6](#). These types of shocks are common in constrained supersonic flow in pipes but also in the overexpanded exhaust plumes of rocket engine operating at sea-level. Interestingly, the shock train develops here without a converging-diverging nozzle and is not in a constant cross section pipe. This means that the flow out of the pipe must be supersonic, cool and choked. (Matsuo, Miyazato, and Kim, 1999) Furthermore, the interface with surrounding air can act like a nozzle (see [Figure 9.7](#)) by creating a parasitic, turbulent boundary layer where the eddies discussed above extract energy from the jet. The more complex shock shape during steady state flow might be a sign of hysteresis as the pressure ratio and shock train length oscillates during the exposure, however this is not clear from the images.

From the images it is not possible to determine if the shock-train develops into a pseudo-shock. It should be highlighted that the systems ability to resolve the shocks is surprising, especially when compared with professional systems such as by M. J. Hargather et al., 2009; Gaweijn et al., 2010; Van Hinsberg and Rösgen, 2014, especially considering the size of the shock train.

¹A common estimate for jet systems (Roekaerts, 2022).

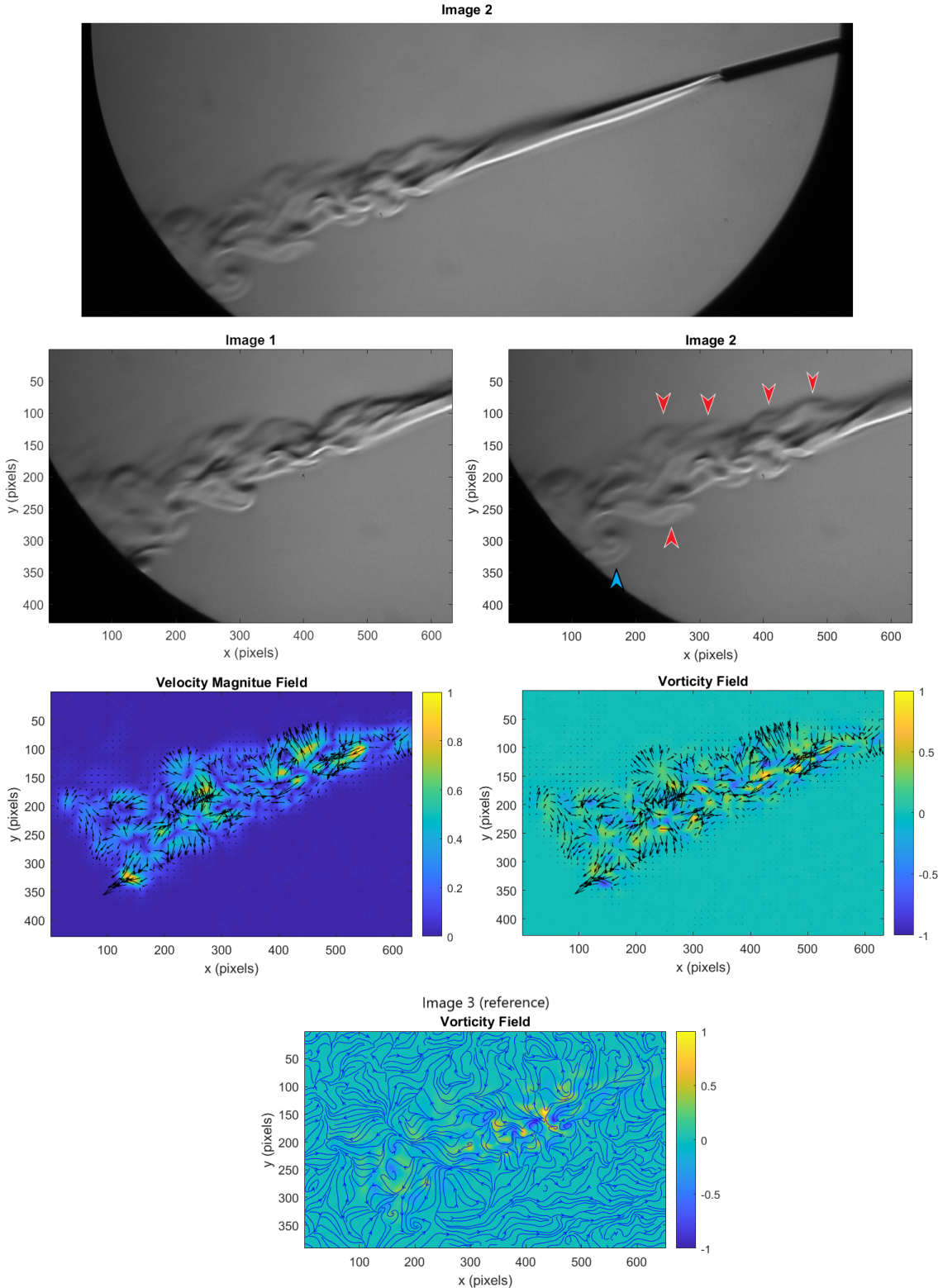


Figure 9.2: Slow injection of cool, compressed 1,3,3,3-Tetrafluoropropene into a static air reservoir. Time 2 is roughly 8.5 ms after time 1. The initial laminar flow shows that the 1,3,3,3-Tetrafluoropropene has almost reached equilibrium pressure with the reservoir when exiting the nozzle. The top image is a magnified image of the entire flow at time 2, showing the laminar flow breaking up into turbulent flow. The second row, left image is a magnified image at time 1, the right image is at time 2. Third row, left shows the normalized velocity field computed between the two images. The third row, right shows the normalized vorticity field computed between the two images. In the bottom row the field at time 2 is compared with the next image at time 3, again 8.5 ms later and the vorticity is shown together with the streamlines. In the bottom row the arrows indicate the flow direction and magnitude. The strong vortex, visible at time 2 in the lower left interface (black-blue arrow), is clearly visible in the vorticity field. The vortices (white-red arrow) that are somewhat visible in the top and bottom interface between the fluids are somewhat recognized by the OpenOpticalFlow. These vortices are near the (laminar-turbulent) transient plane at the top interface are not very well recognized since they are just beginning to separate and form at time 1. Comparing the vorticity fields at 1-2 to 2-3 these vortices are more properly shown as they are mature and actually starting to break up.

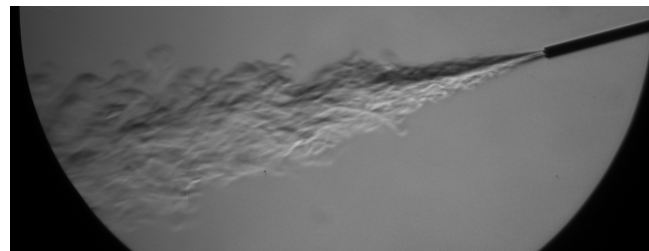


Figure 9.3: Fast injection of cool, compressed 1,3,3,3-Tetrafluoropropene into an static air reservoir. The laminar flow regime out of the pipe is very short and breakup starts around 2-3 mm after the outlet. The largest eddies are of similar sizes as for [Figure 9.2](#), however the faster flow shows more contrast and internal structure of the injected flow.

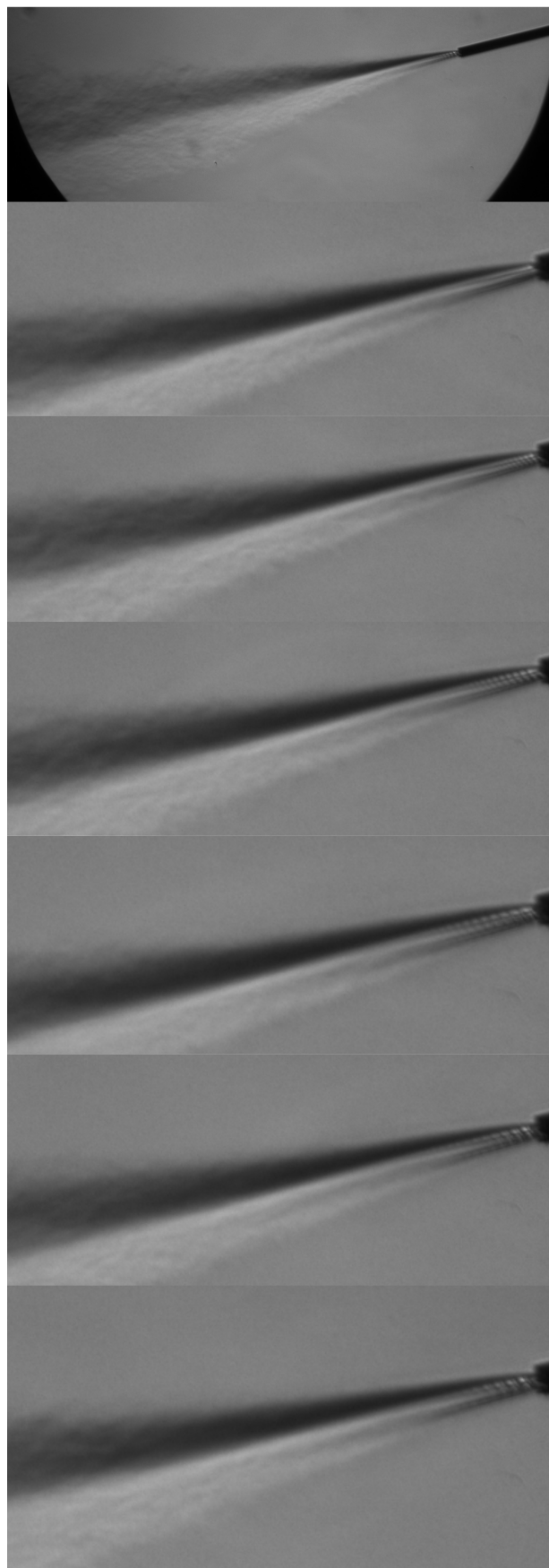


Figure 9.4: Very fast injection of cool, compressed 1,3,3,3-Tetrafluoropropene into a static air reservoir. Shock wave like structures are visible near the outlet. As the back pressure increases the distance between each structure, the number of visible structure and the total distance the structures that are visible increase. The reverse is visible as the back pressure is decreasing. The images are adjusted so that the red line is at the same position as the tube moves during the test.

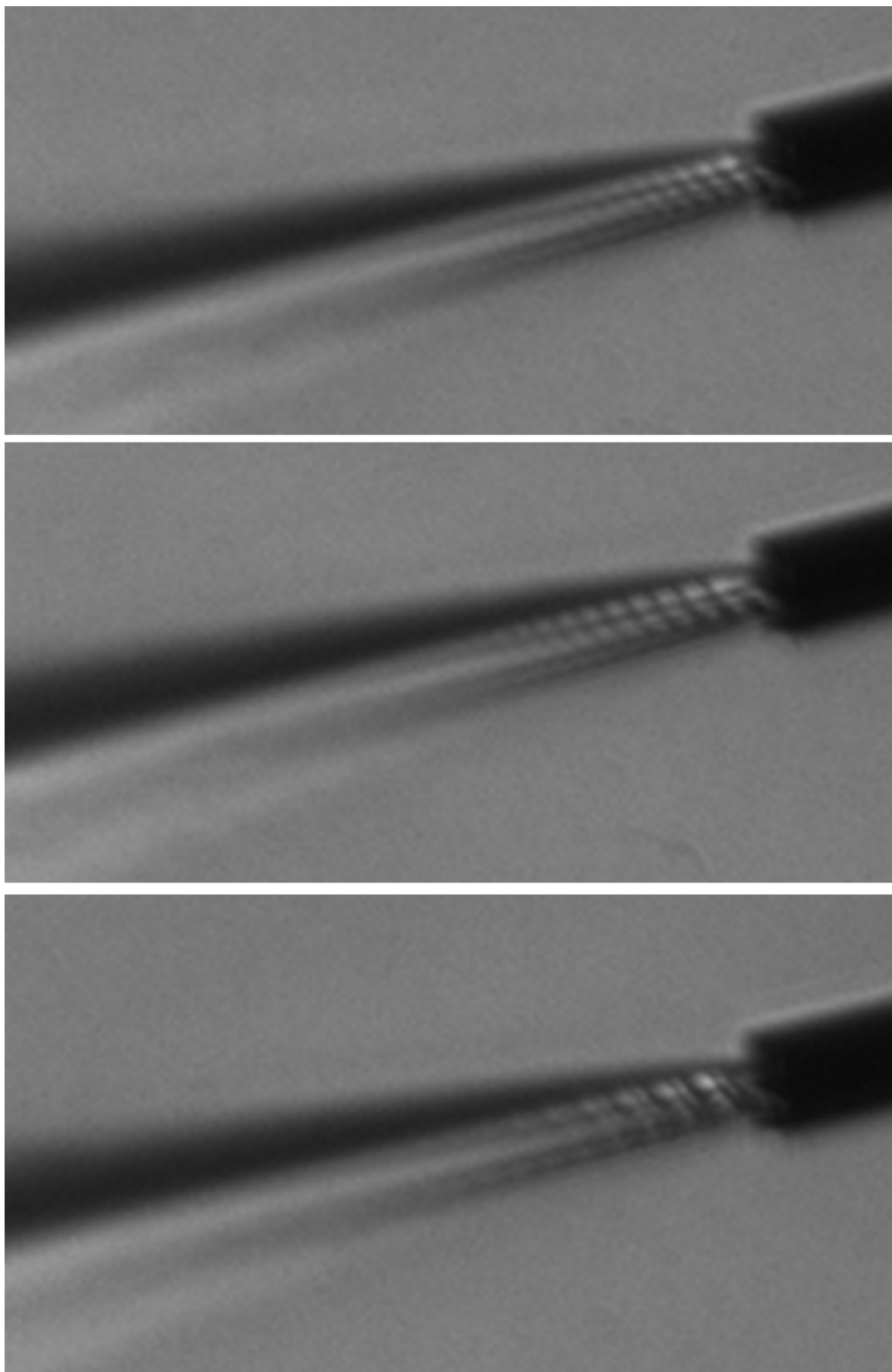


Figure 9.5: Magnified figures of the shock train during development (top figure is the first image with shocks visible, middle is 8.5 ms later) and during steady state (bottom).

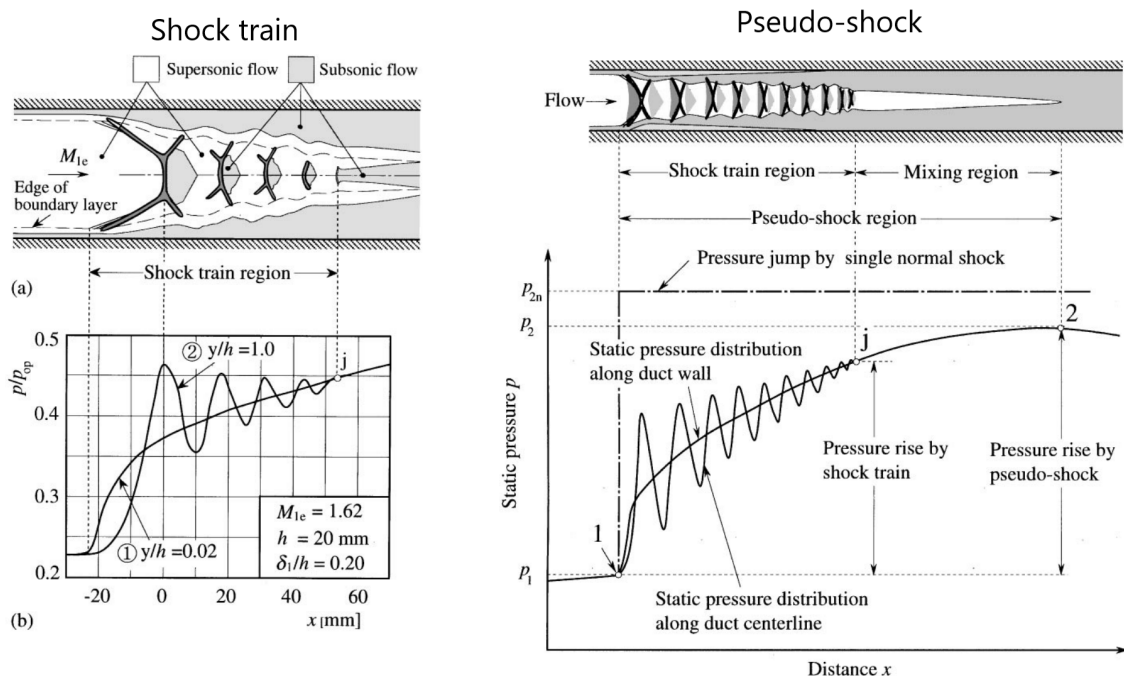


Figure 9.6: Left: Schematic of shock train structure for constant cross section flows (a) and a representative static pressure distribution over a shock train. Right: Schematic of a pseudo-shock. (Matsuo, Miyazato, and Kim, 1999)

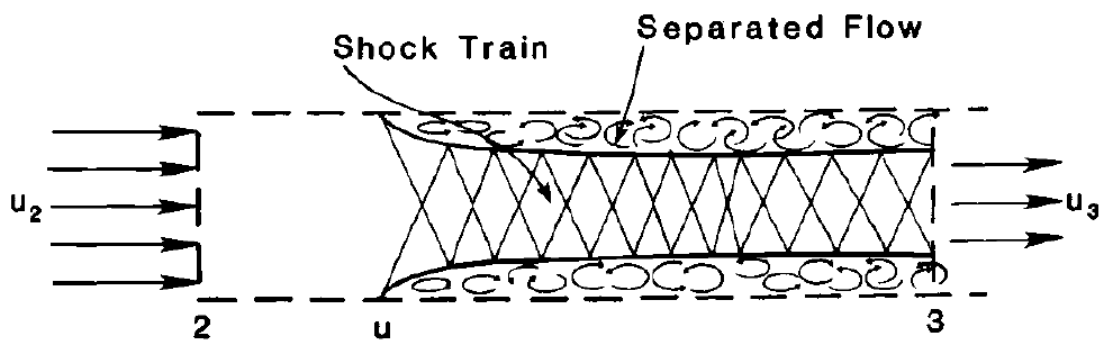


Figure 9.7: Schematic of the interaction of a turbulent boundary layer with a shock train in a supersonic jet. (Heiser, Pratt, and Daley, 1994)

9.4 Spray Down

In order to verify that sputter and molten propellant droplets can be imaged by the system, the flow out of an overturned pressurized canister was imaged. In this way liquid pressurant is forced out of the reservoir creating droplets that vaporize in the warm ambient air, shown in [Figure 9.8](#).

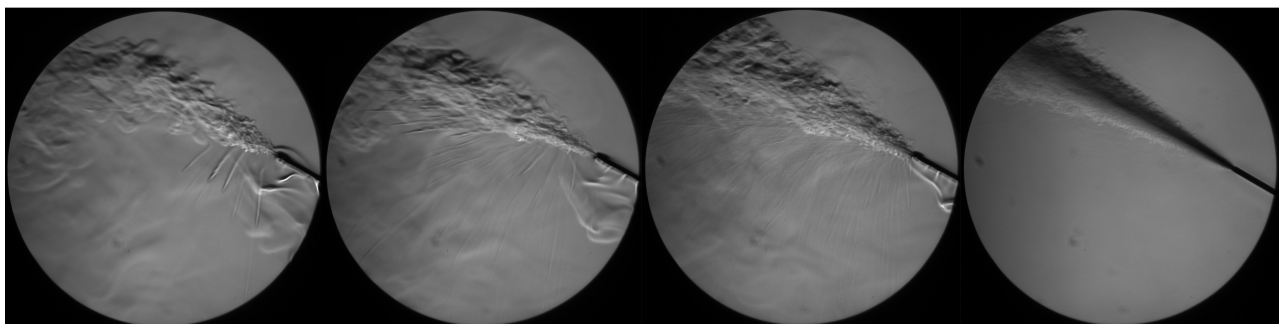


Figure 9.8: Pressurant droplet size varying over the exit velocity of the 1,3,3,3-Tetrafluoropropene spray. The evaporation trails of the pressurant droplets can be used as a tracer for otherwise invisible droplets, where larger droplets leave longer lasting and larger trails.

While it was not possible to image the droplets themselves the trails themselves show that the setup can be used to track small, evaporating or burning particles using their trails. This is not only useful for solid rocket motor ignition where squib igniters spray cellulose acetate to the initiation sites but could also be used for liquid rocketry to characterize liquid-liquid or gas-liquid atomizing injectors. In order to extract quantitative data from non-resolved droplets convective and/or evaporative models need to be used that do not fit the scope of this project. ([Lefebvre and McDonell, 2017](#))

9.5 Candles

In this section, we determine the laminar-turbulent transition for different types of candles, and we try to say something about their Reynolds number. The transition between the laminar and turbulent flow takes place when the hot air emitted from the candle cools down enough so that its motion is heavily influenced by the random motion in the surrounding air currents and not by its upward force (Atcheson, 2007). This corresponds to a specific measure called the Reynolds number: low Reynolds numbers suggest that the flow is laminar, while high Reynolds numbers suggest that it is turbulent.

For this particular analysis, we cannot use the flat field to correct for the detection efficiency of each pixel. This is because, before taking the images, one of the stakeholders moved the whole platform, de-aligning the system. Moreover, after we aligned the system again, we forgot to take another set of flat fields. We cannot use the old flat fields because the image on the camera is not positioned in the same place.

9.5.1 Standard white candle

The first candle that is analyzed is a common small candle made of white candle wax. In an ideal case, the airflow is vertical and a transition between the laminar and turbulent flow is visible. However, in the case of a perfectly vertical flow, the FOV of the system is not large enough and we cannot see the transition (Figure 9.9). Knowing that the candle is 15 cm from the mirror and that the diameter of the mirror is 20 cm, we can say that the transition between laminar and turbulent flow happens at more than 14.4 cm from the candle flame. We also note that the flame saturates the detector, but we do not see any banding effects.

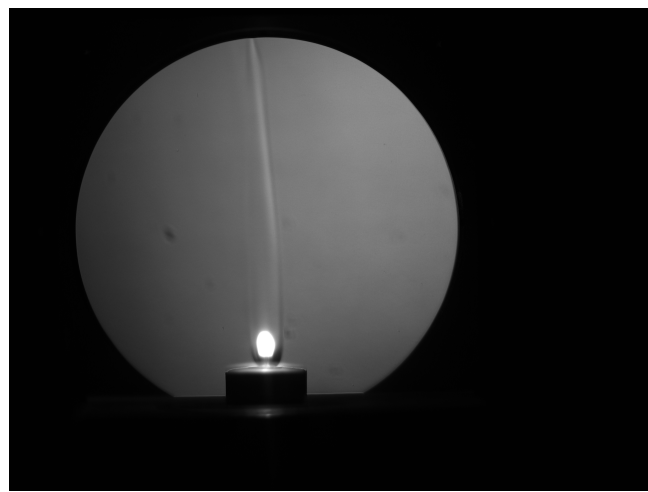


Figure 9.9: Laminar flow of the white candle when the air next to it is unperturbed.

For most of the observations, the burning of the candle is not ideal and there is an incoming air stream from the right of the camera, which deviates the air to the left of the detector. In this case, we can see the transition between the laminar and turbulent flow. Moreover, we note that the stronger the perturbation, the shorter the laminar flow becomes (Figure 9.10).

Combining all of the above, we see that the more perturbed the airflow of the candle is, the faster it cools down. Because of this faster cooling, the laminar flow is shorter and thus, the Reynolds number increases significantly. The turbulent air which affects the candle originates, most likely, from the people standing in the lab, breathing and moving.

Nevertheless, estimate the Reynolds number of the flow from the location of the laminar-turbulent transition using Equation 9.3.

$$2.30Re = \frac{\nu L}{\nu} \approx \frac{590\text{mm}/\text{s} \times 170\text{mm}}{12.2 \times 10^{-6}\text{m}^2/\text{s}} = 8276, \quad (9.3)$$

where ν is the flow velocity, L is the characteristic transition length and ν is the kinematic viscosity of the fluid. The result is as expected for late onset turbulence, which where the fluid is prone to oscillate between turbulent and laminar flow.

9.5.2 Scented candle

The second analyzed candle is a scented candle that contains paraffin wax. The ideal case with a perfectly vertical flow was difficult to observe for this test object and the transition from laminar to turbulent flow, in this

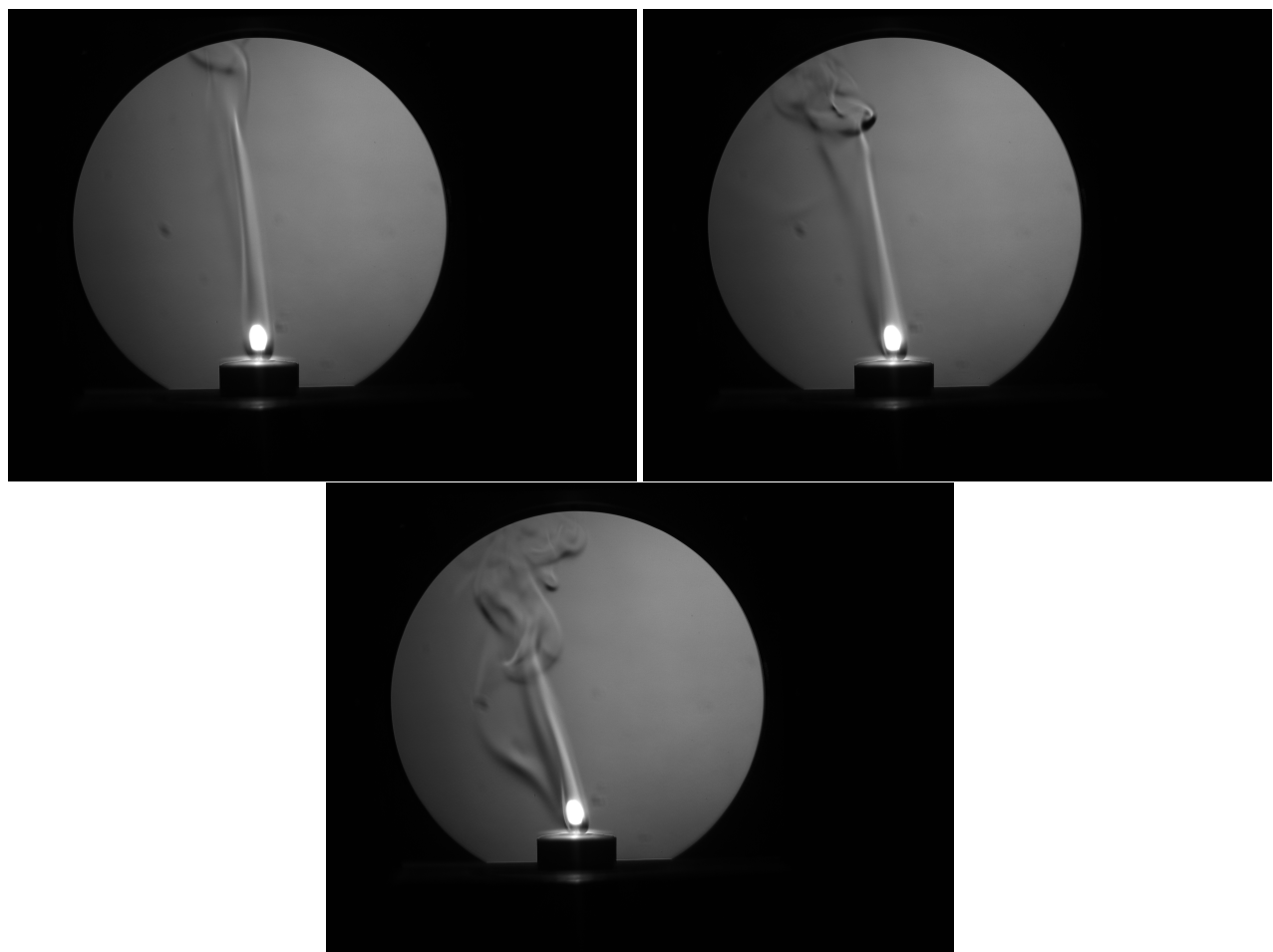


Figure 9.10: Turbulent flow of the hot air of the white candle. We see that the more it deviated from perfectly vertical flow, the faster it becomes turbulent.

case, is, again, not visible ([Figure 9.11](#)), meaning that the laminar flow is longer than 11.1 cm. To calculate this number, we use the fact that the mirror has a diameter of 20 cm and the candle is 15 cm from the mirror. The flame saturates the detector, but there appear to be no sign of banding, which suggests that the flux is not extremely large in comparison to the detector limit.

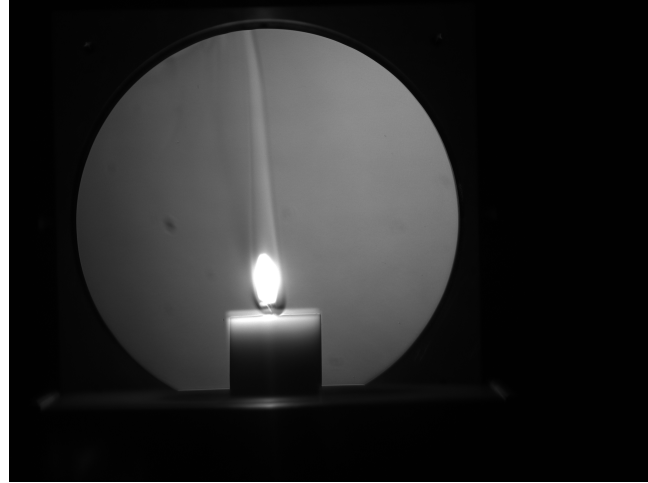


Figure 9.11: Laminar flow of the scented candle when the air next to it is unperturbed.

For most of the observations, we see the same pattern as for the white candle: the flow becomes significantly more turbulent the more it is perturbed by the air flows in the room. However, the intensity of this effect is significantly stronger than for the white candle, and we discuss possible implications of this in the next subsection. The different intensities of the turbulence can be observed in [Figure 9.12](#) and we believe that the cause of the air currents is the people breathing and moving in the laboratory.

After this experiment, we note, again, that the perturbation in the airflow cools the hot air from the candle faster, making the laminar flow shorter, and thus, increasing its Reynolds number significantly.

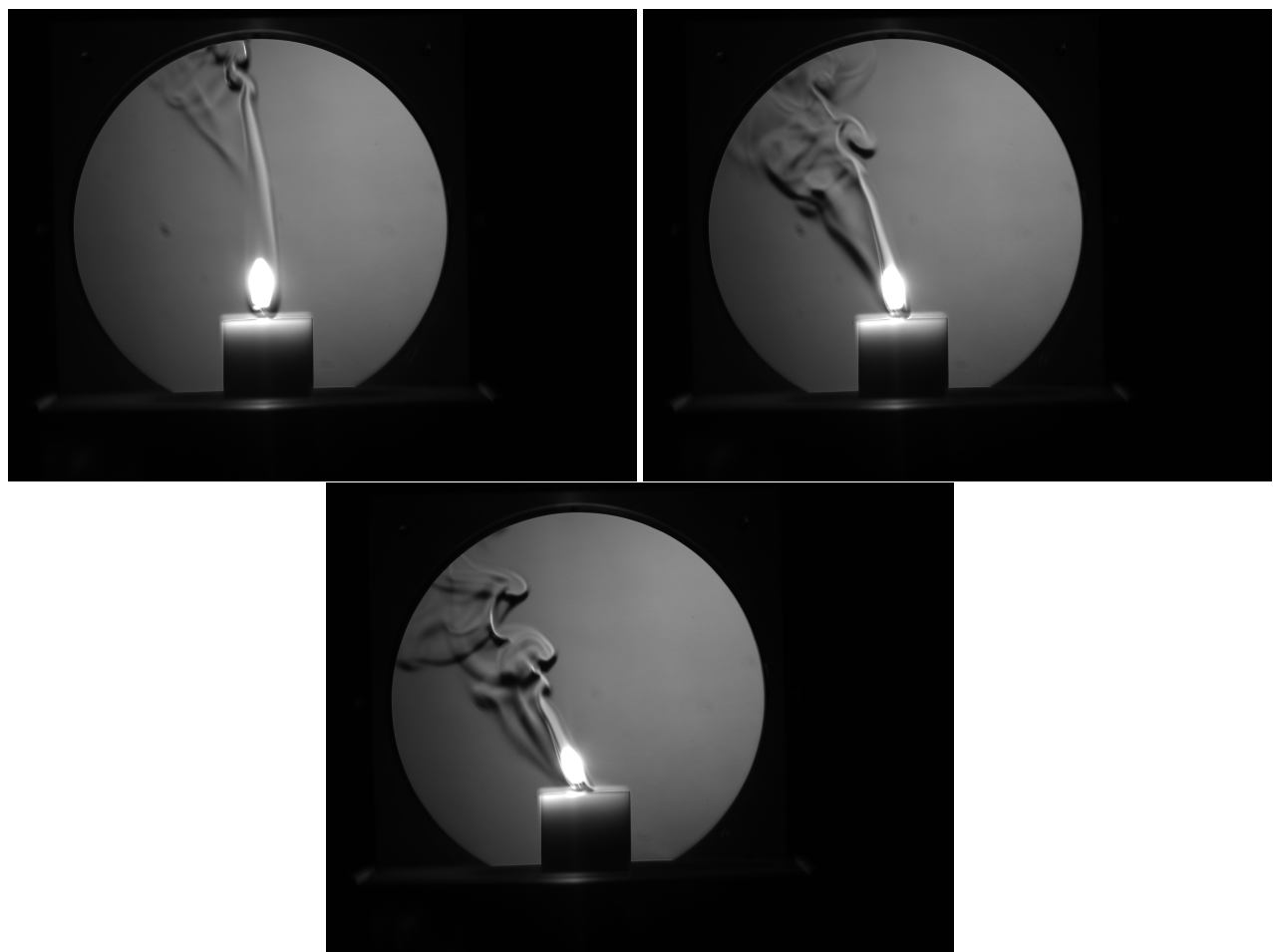


Figure 9.12: Turbulent flow of the hot air of the scented candle. We see that the more it deviated from perfectly vertical flow, the faster it becomes turbulent.

9.5.3 Comparison between candles

In this section, we discuss the implications of the fact that the scented candle has a significantly more perturbed flow than the white candle, but first, it is critical to mention that the surrounding conditions have not been changed between the experiments. The experiments has been performed within 10 minutes, one after the other, and the people in the lab have been stationary during the recording of the data at approximately the same location for both measurements. Thus, we can approximate the surrounding conditions as being identical for the two observations.

We note that the scented candle has its flow deviated much easier from the ideal vertical trajectory. This suggests that the upward force for the scented candle is significantly less than for the white candle, and it cannot withstand small environmental perturbations. Assuming that the surrounding conditions are identical in both experiments we can say that the temperature of the flame of the scented candle is significantly lower than for the white candle. Thus, candles that contain paraffin wax burn at a lower temperature than the ones made purely of the candle was, and are much easier perturbed by the surrounding environment.

9.6 Results Summary

In the above section we believe that we have demonstrated that the system is partially compliant with the goals set out for the project. The system exceeds the required mechanical and optical precision and can image diverse, multi-scale flow phenomena, such as laminar-turbulence transition, eddy cascades, normal shock waves and trains on a sub-mm size and droplet traces. Nevertheless, the system has not been tested in its intended environment to image solid rocket motor grain ignitions, however based on the results we find the this design can serve as an excellent starting point for further development and use.

10 Future work

The final form of this system is supposed to detect the density changes induced by an SRM grain in daylight, and it should be easy to transport and calibrate. Due to time shortages, we were not able to detect the SRM grain, but we made sure that everything will function properly for this observation. As proven in this report, the system can be calibrated relatively fast, in under 30 minutes, and it is stable and small, making its transportation to the rocket field by train or car relatively easy. Moreover, we tested it in daylight and confirmed that it can still operate well in these conditions. We also performed several tests, and analyzed different airflows, from an air-pressurized tube or candles. All of these helped us to create software that will be used in the future analysis of the SRM grain. An attempt could be made to calibrate the system in such a way as to measure refractive indices quantitatively.

The remaining steps are to buy the aluminum beams, make the platforms that connect them to the components, and move the system outside to observe the SRM grain. For outside conditions another important alteration may be shielding from wind. We believe that these steps will not be problematic, the only changes that might appear is in the design of the platforms, in case they do not fit with our existing system. Some additional changes could be made to shield the system from too much bright sunlight, by blocking the area between the camera and the lens from above and the sides, or by covering the whole setup in some way. The system can be finished, and the SRM grain analyzed in 1 or 2 weeks, depending on the delivery time of the aluminum beams.

Bibliography

- anonymous (2019). ‘Resistance’ of an LED. Ed. by LEDnique. url: <http://lednique.com/current-voltage-relationships/resistance-of-an-led/>.
- Atcheson, Bradley (2007). “Schlieren-based flow imaging”. PhD thesis. Citeseer.
- Balamurugan, G et al. (2020). “Characteristics of the turbulent non-turbulent interface in a spatially evolving turbulent mixing layer”. In: *Journal of Fluid Mechanics* 894.
- Ciucci, A, WINFRED FOSTER JR, and RHONALD JENKINS (1992). “Results of an experimental investigation of the flow field in the head-end star slot section of a solid rocket motor”. In: *28th Joint Propulsion Conference and Exhibit*, p. 3048.
- Coultas-McKenney, Caralyn, Kyle Winter, and Michael Hargather (Nov. 2016). “High-speed schlieren imaging of rocket exhaust plumes”. In: *APS Division of Fluid Dynamics Meeting Abstracts*. APS Meeting Abstracts, L31.004, p. L31.004.
- Crowell, Gary (2019). *The Forward Voltages of Different LEDs*. Ed. by CircuitBread. url: <https://www.circuitbread.com/ee-faq/the-forward-voltages-of-different-leds>.
- ETB (Jan. 2018). *Nitrogen - Dynamic and Kinematic Viscosity vs. Temperature and Pressure*. Online. Available online: https://www.engineeringtoolbox.com/nitrogen-N2-dynamic-kinematic-viscosity-temperature-pressure-d_2067.html[Accessed 29.5.2022]..
- Gawehn, Thomas et al. (2010). “Experimental and numerical analysis of the structure of pseudo-shock systems in laval nozzles with parallel side walls”. In: *Shock Waves* 20.4, pp. 297–306.
- GmbH, Thorlabs (Aug. 2021). *Thorlabs - CA6-EU Ultra Pure Duster 400 ml*. Safety Data Sheet 1,04,24. Thorlabs GmbH.
- Gojani, Ardian B., Kamishi, Burim, and Obayashi, Shigeru (2013). “Review of background oriented schlieren and development for ballistic range applications”. In: *EPJ Web of Conferences* 45, p. 01034. doi: <10.1051/epjconf/20134501034>. url: <https://doi.org/10.1051/epjconf/20134501034>.
- Goldstein, Richard J and TH Kuehn (1996). “SHADOWGRAPH, SCHLIEREN, AND INTERFEROMETRIC TECHNIQUES”. In: *Fluid Mechanics Measurements*, p. 451.
- Hargather, Michael J et al. (2009). “Focusing-schlieren PIV measurements of a supersonic turbulent boundary layer”. In: *47th AIAA Aerospace Sciences Meeting, Paper AIAA-2009-69*.
- Harvey, Allan H, Eugene Paulechka, and Patrick F Egan (2018). “Candidates to replace R-12 as a radiator gas in Cherenkov detectors”. In: *Nuclear Instruments and Methods in Physics Research Section B: Beam Interactions with Materials and Atoms* 425, pp. 38–42.
- Heiser, William H, David T Pratt, and Daniel H Daley (1994). *Hypersonic airbreathing propulsion*. Aiaa.
- Hooke, R. (1665). *Micrographia*. London: J. Martyn J. Allestry.
- Hu, Bowen, Bing Wang, and Xiaotao Tian (2016). “Numerical modeling and studies of ignition transients in end-burning-grain solid rocket motors”. In: *Journal of Propulsion and Power* 32.6, pp. 1333–1342.
- Kirchheck, Daniel, Dominik Saile, and Ali Gühan (2019). “Spectral Analysis of Rocket Wake Flow-Jet Interaction by Means of High-speed Schlieren Imaging”. In: *8th European Conference for Aeronautics and Space Sciences (EUCASS)*, pp. 1–15. url: <https://elib.dlr.de/135502/>.
- Kleine, H. and H. Grönig (1991). “Color schlieren methods in shock wave research”. In: doi: <10.1007/BF01414868>. url: <https://doi.org/10.1007/BF01414868>.
- Lefebvre, Arthur H and Vincent G McDonell (2017). *Atomization and sprays*. CRC press.
- Liu, Tianshu (2017). “OpenOpticalFlow: An open source program for extraction of velocity fields from flow visualization images”. In: *Journal of Open Research Software* 5.1.
- Matsuo, Kazuyasu, Yoshiaki Miyazato, and Heuy-Dong Kim (1999). “Shock train and pseudo-shock phenomena in internal gas flows”. In: *Progress in aerospace sciences* 35.1, pp. 33–100.
- Morales, Rudy, Julio Peguero, and Michael Hargather (Nov. 2017). “Schlieren image velocimetry measurements in a rocket engine exhaust plume”. In: *APS Division of Fluid Dynamics Meeting Abstracts*. APS Meeting Abstracts, G25.004, G25.004.
- Neil, M. A. A., M. J. Booth, and T. Wilson (Aug. 2000). “Closed-loop aberration correction by use of a modal Zernike wave-front sensor”. In: *Opt. Lett.* 25.15, pp. 1083–1085. doi: <10.1364/OL.25.001083>. url: <http://opg.optica.org/ol/abstract.cfm?URI=ol-25-15-1083>.
- Olde, Martin (2019). “Potassium Nitrate Sorbitol Propellant: Experimental Investigation of Solid Propellant Characteristics”. In.
- Pandya, Brian H., Gary S. Settles, and James D. Miller (2003). “Schlieren imaging of shock waves from a trumpet”. In: *The Journal of the Acoustical Society of America* 114.6, pp. 3363–3367. doi: <10.1121/1.1628682>. eprint: <https://doi.org/10.1121/1.1628682>. url: <https://doi.org/10.1121/1.1628682>.

- Pope, Stephen B and Stephen B Pope (2000). *Turbulent flows*. Cambridge university press.
- Por, Emiel H. (Jan. 2020). "Phase-apodized-pupil Lyot Coronagraphs for Arbitrary Telescope Pupils". In: *The Astrophysical Journal* 888.2, p. 127. doi: [10.3847/1538-4357/ab3857](https://doi.org/10.3847/1538-4357/ab3857). url: <https://doi.org/10.3847/1538-4357/ab3857>.
- Raffel, M. (Mar. 2015). "Background-oriented schlieren (BOS) techniques". In: *Experiments in Fluids* 56, pp. 1–17. doi: [10.1007/s00348-015-1927-5](https://doi.org/10.1007/s00348-015-1927-5).
- Roekaerts, Dirk (Feb. 2022). *Lecture: Laminar and turbulent transport processes*. Course: TUD AE4-262 Combustion for Propulsion & Power Technologies.
- Schmidt, Bryan (2014). *Schlieren Visualization*. Online: shepherd.caltech.edu/T5/Ae104/Ae104b_handout2015.pdf.
- Scully, Taylor (2019). *How Does a 5mm LED Work?* Ed. by LED Supply. url: <https://www.ledsupply.com/blog/how-does-a-5mm-led-work/>.
- Settles, G.S. (2001a). "Schlieren and Shadowgraph Techniques". In: Springer. Chap. Historical Background. – (2001b). *Schlieren and Shadowgraph Techniques*. Springer.
- Spalding, D Brian (1977). "Development of the eddy-break-up model of turbulent combustion". In: *Symposium (International) on Combustion*. Vol. 16. 1. Elsevier, pp. 1657–1663.
- Tanda, Giovanni, Marco Fossa, and Mario Misale (2014). "Heat transfer measurements in water using a schlieren technique". In: *International Journal of Heat and Mass Transfer* 71, pp. 451–458. issn: 0017-9310. doi: <https://doi.org/10.1016/j.ijheatmasstransfer.2013.12.022>. url: <https://www.sciencedirect.com/science/article/pii/S0017931013010661>.
- TAYLOR, LESLIE L. and LEONARD S. THOMPSON (1969). "Analysis of turbulence by schlieren photography". In: *AIAA Journal* 7.10, pp. 2030–2031. doi: [10.2514/3.5505](https://doi.org/10.2514/3.5505). eprint: <https://doi.org/10.2514/3.5505>. url: <https://doi.org/10.2514/3.5505>.
- Toscano, Angelica Maria et al. (2022). "Optical Diagnostics for Solid Rocket Plumes Characterization: A Review". In: *Energies* 15.4, p. 1470.
- Turns, Stephen R et al. (1996). *Introduction to combustion*. Vol. 287. McGraw-Hill Companies New York, NY, USA.
- Van Hinsberg, Nils Paul and Thomas Rösgen (2014). "Density measurements using near-field background-oriented schlieren". In: *Experiments in fluids* 55.4, pp. 1–11.
- Wallace, J. Kent et al. (2011). "Phase-shifting Zernike interferometer wavefront sensor". In: *Optical Manufacturing and Testing IX*. Ed. by James H. Burge, Oliver W. Fähnle, and Ray Williamson. Vol. 8126. International Society for Optics and Photonics. SPIE, pp. 110–120. doi: [10.1117/12.892843](https://doi.org/10.1117/12.892843). url: <https://doi.org/10.1117/12.892843>.

Appendix

A.1 Photon budget calculations

For each individual system presented before in [Table 3.8](#), we calculate the photon budget at different wavelengths. For this, it is important to know the transmission, reflection and absorption characteristics of all the optical components. In this comparison, we assume that the used detector is the same, and does not affect our photon budget comparison.

The characteristics of the mirrors bought from ThorLabs (the plane and parabolic mirrors) are presented in [Figure A.1](#). Moreover, the beam splitter would have a 50-50 coefficient, the lenses are known to transmit 80% of the light, and the knife edge stops 50% of the light. By knowing this, we calculate the percentage of the initial light which reaches the detector and we present it in [Table A.2](#).

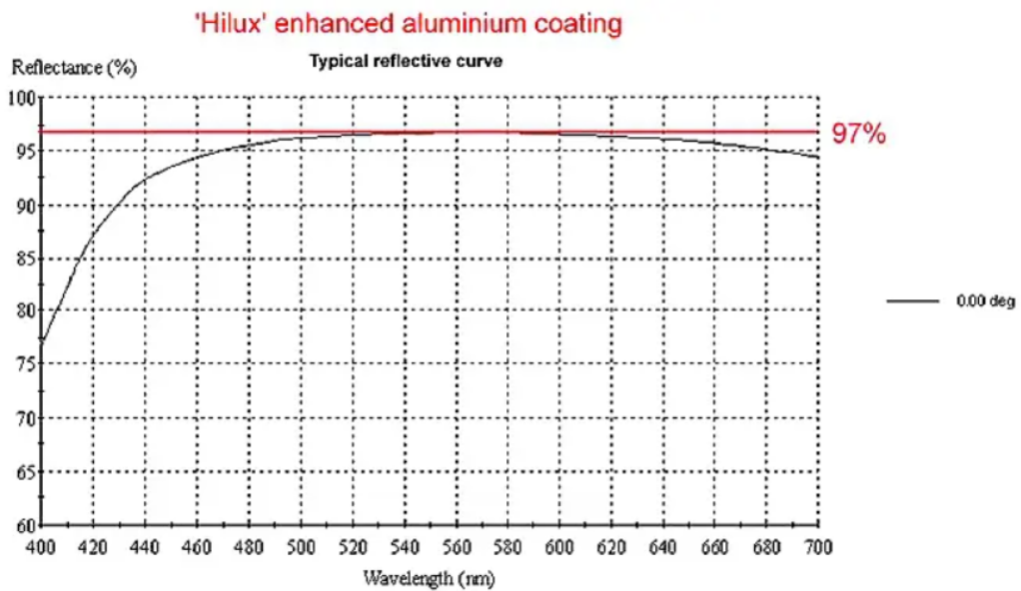


Figure A.1: Reflection percentages of a mirror bought from ThorLabs.

System	Transmission			
	400 nm	500 nm	560 nm	700 nm
A	34%	48%	49%	48%
B	30%	46	47%	45%
C	19%	24%	24%	24%
D	36%	36%	36%	36%

Table A.1: Photon budget for all the designs for different wavelengths.

A.2 Wave front error (WFE)

The precise wave front error is extremely complicated to calculate analytically, and it is not needed for a Schlieren Imager. Here, we calculate a rough approximation of the WFE, considering only the aberrations from the imperfection of the optical components. Other effects, like inclination of the beam on the mirror and its location on it are not considered for this comparison.

According to the ThorLabs official website, the parabolic mirror and the plane one have a WFE of $\lambda/6$, while the beam splitter, of $\lambda/10$. For the lenses, we assume a WFE of $\lambda/4$. Since they deform the beam independently, the total WFE if calculated using the following formula:

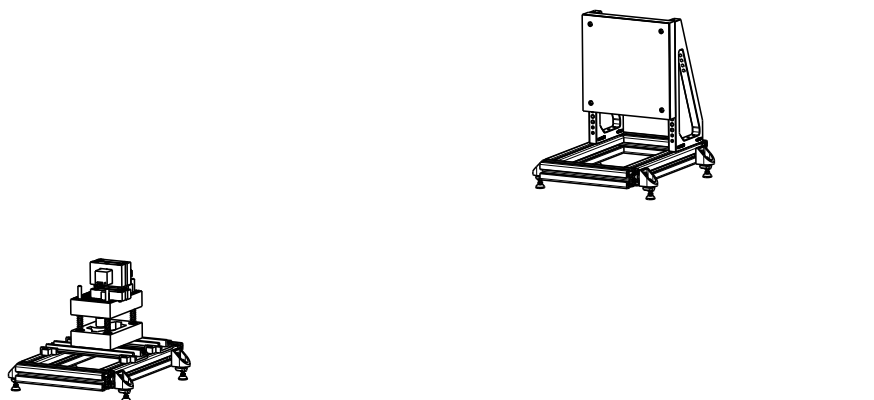
$$\text{WFE}_{\text{total}} = \sum_i (\text{WFE}_i^2) \quad (\text{A.1})$$

The values for the individual designs at different wavelengths is presented in:

System	Transmission			
	400 nm	500 nm	560 nm	700 nm
A	67 nm	83 nm	93 nm	117 nm
B	95 nm	117 nm	132 nm	167 nm
C	166 nm	208 nm	233 nm	291 nm
D	141 nm	177 nm	198 nm	248 nm

Table A.2: WFE for all the designs for different wavelengths.

A.3 BOM



Bill of Material: STRIA_ASSEMBLY

Quantity	Part Number	Type	Nomenclature	Revision
1	OPTICS_ASSEMBLY	Assembly		
1	MIRROR_ASSEMBLY	Assembly		
1	MIRROR_ASSEMBLY_SAMP LE	Assembly		

Bill of Material: OPTICS_ASSEMBLY

Quantity	Part Number	Type	Nomenclature	Revision
1	SUPPORT	Assembly		
4	PF-rail-slides	Part		
1	KE-assembly	Assembly		
1	TS-vertical	Assembly		
1	LED-assembly	Assembly		
1	LENS_ASSEMBLY_1IN	Assembly		
1	CAMERA_ASSEMBLY	Assembly		

Bill of Material: SUPPORT

Quantity	Part Number	Type	Nomenclature	Revision
2	item_7000009_Profile 8 40x40 E_L=220	Part		
2	item_7000009_Profile 8 40x40 E_L=300	Part		
4	item_0045776_Angle Hinge Bracket 8	Part		
4	Foot-M5x45	Assembly		

Bill of Material: Foot-M5x45

Quantity	Part Number	Type	Nomenclature	Revision
1	item_0046475_Knuckle Foot D20, M5x45_A=0_h=20_2	Part	item_0046475_Knuckl e Foot D20, M5x45_A=0_h=20_2	
1	item_0046475_Knuckle Foot D20, M5x45_A=0_h=20_1	Part	item_0046475_Knuckl e Foot D20, M5x45_A=0_h=20_1	
1	item_0046475_Knuckle Foot D20, M5x45_A=0_h=20	Part	item_0046475_Knuckl e Foot D20, M5x45_A=0_h=20	

Figure A.2: BOM page 9

A.4 BOM

Bill of Material: KE-assembly

Quantity	Part Number	Type	Nomenclature	Revision
1	KE-base	Part		
1	KE-holder	Part		
1	KE-razor-blade-model	Part		
1	94180A333_HS_M3	Part	94180A333_HS_M3	ANY
1	91292A022_18-8SS_SH_M3	Part	91292A022_18-8SS_SH_M3	ANY
1	92095A321_BH_HEX_M1.6	Part	92095A321_BH_HEX_M1.6	ANY
2	98689A112_WAS_M3	Part	98689A112_WAS_M3	ANY
1	8969T384_316SS_Spring_21.5-12.5_0.15	Part	8969T384_316SS_Spring_21.5-12.5_0.15	ANY

Bill of Material: TS-vertical

Quantity	Part Number	Type	Nomenclature	Revision
1	TS-vertical-base	Part		
1	TS-vertical-top	Part		
8	TS-vertical-guides	Part		
4	TS-vertical-rails	Part		
4	2006N425_302_SS_COMP_SPRING	Part	COMP_SPRING	ANY
8	TS-vertical-washers	Part		
1	97171A370_Heat-Set_Insert	Part	97171A370_Brass Heat-Set Inserts for Plastic	ANY
1	92217A626_18-8SS-ASME_washer_soft	Part	92217A626_18-8SS-ASME_washer_soft	ANY
1	91290A209_M6_80mm_SocketHead	Part	91290A209_M6_80mm_SocketHead	ANY
2	PF-rail-insert	Part		

Bill of Material: LED-assembly

Quantity	Part Number	Type	Nomenclature	Revision
1	KE-base	Part		
1	LED-holder	Part		
1	94180A333_HS_M3	Part	94180A333_HS_M3	ANY
1	91292A022_18-8SS_SH_M3	Part	91292A022_18-8SS_SH_M3	ANY
2	98689A112_WAS_M3	Part	98689A112_WAS_M3	ANY
1	8969T384_316SS_Spring_21.5-12.5_0.15	Part	8969T384_316SS_Spring_21.5-12.5_0.15	ANY

Figure A.3: BOM page 10

A.5 BOM

Bill of Material: LED-assembly

Quantity	Part Number	Type	Nomenclature	Revision
1	2779K123_Panel Light	Part	2779K123_Panel Light	ANY

Bill of Material: LENS_ASSEMBLY_1IN

Quantity	Part Number	Type	Nomenclature	Revision
1	LENS-mount-base_1IN	Part		
1	LENS-mount_1IN	Part		
2	91292A203_18-8 Stainless Steel Socket Head Screw	Part	91292A203_18-8 Stainless Steel Socket Head Screw	ANY
2	94180A373_HSI_M6	Part	94180A373_Tapered Heat-Set Inserts for Plastic	ANY
2	8969T553_SSS_M6_12	Part	8969T553_316 Stainless Steel Corrosion-Resistant Compression Springs	ANY
1	LENS-lego-stage	Part		
1	20526-EOW	Part	20526-EOW	ANY

Bill of Material: CAMERA_ASSEMBLY

Quantity	Part Number	Type	Nomenclature	Revision
1	CAMERA-mount-base_1IN	Part		
1	CAMERA-mount_1IN	Part		
2	91292A203_18-8 Stainless Steel Socket Head Screw	Part	91292A203_18-8 Stainless Steel Socket Head Screw	ANY
2	94180A373_HSI_M6	Part	94180A373_Tapered Heat-Set Inserts for Plastic	ANY
2	8969T553_SSS_M6_12	Part	8969T553_316 Stainless Steel Corrosion-Resistant Compression Springs	ANY
1	CAMERA-lego-stage	Part		
1	CAMERA_PLACEHOLDER	Part		
1	94180A331_Tapered Heat-Set Inserts for Plastic	Part	94180A331_Tapered Heat-Set Inserts for Plastic	ANY
1	91292A114_18-8 Stainless Steel Socket Head Screw	Part	91292A114_18-8 Stainless Steel Socket Head Screw	ANY

Figure A.4: BOM page 11

A.6 BOM

Bill of Material: MIRROR_ASSEMBLY

Quantity	Part Number	Type	Nomenclature	Revision
1	Mirror_Unit	Assembly		
1	SUPPORT	Assembly		

Bill of Material: Mirror_Unit

Quantity	Part Number	Type	Nomenclature	Revision
1	Mirror_Placeholder	Part		
1	Mirror-mount	Part		
1	Mirror-Screen	Part		
2	1085-EOW	Part	1085-EOW	ANY

Bill of Material: MIRROR_ASSEMBLY_SAMPLE

Quantity	Part Number	Type	Nomenclature	Revision
1	MIRROR_ASSEMBLY	Assembly		
2	SAMPLE-rail-slides	Part		
1	SAMPLE HOLDER	Assembly		

Bill of Material: SAMPLE HOLDER

Quantity	Part Number	Type	Nomenclature	Revision
1	SAMPLE_SUPPORT	Part		
1	SAMPLE_PLACEHOLDER	Part		
1	SAMPLE-insert	Part		
1	SAMPLE-bottom_shield	Part		

Recapitulation of:

STRIA_ASSEMBLY

Different parts: 49

Total parts: 150

Quantity	Part Number
6	item_700009_Profile 8 40x40 E L=220
6	item_700009_Profile 8 40x40 E L=300
12	item_0045776_Angle Hinge Bracket 8
12	item_0046475_Knuckle Foot D20, M5x45 A=0 h=20_2
12	item_0046475_Knuckle Foot D20, M5x45 A=0 h=20_1
12	item_0046475_Knuckle Foot D20, M5x45 A=0 h=20
4	PF-rail-slides
2	KE-base
1	KE-holder
1	KE-razor-blade-model

Figure A.5: BOM page 12

A.7 BOM

Recapitulation of:

STRIA_ASSEMBLY

Different parts: 49

Total parts: 150

Quantity	Part Number
2	94180A333_HS_M3
2	91292A022_18-8SS_SH_M3
1	92095A321_BH_HEX_M1.6
4	98689A112_WAS_M3
2	8969T384_316SS_Spring_21.5-12.5_0.15
1	TS-vertical-base
1	TS-vertical-top
8	TS-vertical-guides
4	TS-vertical-rails
4	2006N425_302_SS_COMP_SPRING
8	TS-vertical-washers
1	97171A370_Heat-Set Insert
1	92217A626_18-8SS-ASME_washer_soft
1	91290A209_M6_80mm_SocketHead
2	PF-rail-insert
1	LED-holder
1	2779K123_Panel Light
1	LENS-mount-base_1IN
1	LENS-mount_1IN
4	91292A203_18-8 Stainless Steel Socket Head Screw
4	94180A373_HSI_M6
4	8969T553_SSS_M6_12
1	LENS-lego-stage
1	20526-EOW
1	CAMERA-mount-base_1IN
1	CAMERA-mount_1IN
1	CAMERA-lego-stage
1	CAMERA_PLACEHOLDER
1	94180A331_Tapered Heat-Set Inserts for Plastic
1	91292A114_18-8 Stainless Steel Socket Head Screw
2	Mirror_Placeholder
2	Mirror-mount
2	Mirror-Screen
4	1085-EOW

Figure A.6: BOM page 13

A.8 BOM

Recapitulation of:

STRIA_ASSEMBLY

Different parts: 49

Total parts: 150

Quantity	Part Number
2	SAMPLE-rail-slides
1	SAMPLE_SUPPORT
1	SAMPLE_PLACEHOLDER
1	SAMPLE-insert
1	SAMPLE-bottom_shield

Figure A.7: BOM page 14

Design Changes & Iterations

B.1 Platform dimensions

In the initial design, we state that the platform on which we mount the LED, collimating lens, detector and knife edge should have a dimension of maximum 10 cm x 15 cm. However, when building the LEGO mount, we found that the minimum dimensions for making it stable and precise are 15 cm x 30 cm. Thus, considering that the 3D printer can only print platforms of 18 cm x 18 cm, we decide to print two platforms of 15 cm x 15 cm put them next to each other on the x-axis.